Estimation of Option-Implied Risk Measures – An Arbitrage-Free RND-Based Smile Construction Approach

Faculty of Social Sciences, Economics and Business Administration

University of Bamberg

A thesis presented for the degree of

– doctor rerum politicarum –

Submitted by

Pascal Dietmar Albert

Primary reviewer: Prof. Dr. Matthias Muck

Secondary reviewer: Prof. Dr. Markus Rudolf

Submission date: December 19, 2024

Oral examination date: May 21, 2025

Bamberg 2025

The thesis has been submitted to the Faculty of Social Sciences, Economics, and Business Administration of the University of Bamberg as a dissertation.

1st Reviewer: Prof. Dr. Matthias Muck

2nd Reviewer: Prof. Dr. Markus Rudolf

Date of Defense: May 21, 2025

URN: urn:nbn:de:bvb:473-irb-108650x
DOI: https://doi.org/10.20378/irb-108650

Contents

List of Abbreviations

AAPL	Apple
AMZN	Amazon
a.s.	Almost surely
ATM	At-the-money
BKM	Bakshi, Kapadia, and Madan
CBOE	Chicago Board Options Exchange
CDF	Cumulative distribution function
CIR	Cox, Ingersoll, and Ross
EndPoint	Endpoint volatility
FAANG	Facebook, Amazon, Apple, Netflix, Google
FB	Facebook (Meta)
FX	Foreign exchange
GEV	Generalized Extreme Value
GOOG	Google (Alphabet)
i.i.d	Independent and identically distributed
ITM	In-the-money
LinReg	Linear regression
MGF	Moment-generating function
NFLX	Netflix
OTM	Out-of-the-money
PDE	Partial differential equation
PDF	Probability density function
RMSE	Root mean squared error

RND	Risk-neutral probability density function or risk-neutral distribution
RRMSE	Relative root mean squared error
SKEW	Skewness
S&P	Standard & Poor's
SVCJ	Stochastic volatility with contemporaneous jumps
UK	United Kingdom

List of Symbols

The following list contains symbols used in this thesis based on their order of appearance. Symbols used frequently across several chapters are assigned to common symbols, whereas those specific to individual chapters are defined separately within those chapters. Superscripts and subscripts in parentheses are optional. Bold capital letters denote matrices and bold small letters vectors. All vectors are defined as column vectors. Elements of matrices and vectors are represented by the same but not bold symbols with suitable subscripts.

Common Symbols

t, τ, T	Time
Ω	State space
$\mathcal{F}$	Sigma-algebra
$\mathbb{P}$	Probability measure
$\mathcal{F}_t$	Sub-sigma-algebra of $\mathcal{F}$ at time t
$\{\mathcal{F}_t\}$	Filtration
$\mu(.,.)$	Drift
$\sigma(.,.)$	Dispersion
$W, (W_t)_t$	Brownian motion
$\mathbb{E}(.)$	Expectation
$\mathbb{E}(. \mid \mathcal{F}_t)$	Conditional expectation with respect to $\mathcal{F}_t$
i, j, k, l, n, N	Integers
$\mathcal{N}(.,.)$	Normal distribution
$\mathbb{R}$	Real numbers

μ	Drift parameter
σ	Dispersion parameter
$(\mu_t)_t$	(Adapted) drift process
$(\sigma_t)_t$	(Adapted) dispersion process
$N, (N_t)_t$	Poisson process
λ	Intensity
$\mathbb{N}$	Natural numbers
$\mathbb{1}$	Indicator function
$\mathbb{N}_0$	Natural numbers including zero
Exp(.)	Exponential distribution
$[.,.]_T^{(c)}$	Quadratic variation of a (continuous) stochastic process up to time T
Δ	Difference operator
A	Set
$\mathcal{J}_{(.)}(.,.)$	Jump measure
$S, (S_t)_t$	Stock price process
K	Strike price
$\mathbb{Q}$	Risk-neutral probability measure
$\mathbb{E}^{\mathbb{Q}}(. \mid \mathcal{F}_t)$,	Conditional expectation under $\mathbb{Q}$ with respect to $\mathcal{F}_t$
r	Risk-free interest rate
$(r_t)_t$	Short rate process
$C(.,.;.)$	Call option value
$P(.,.;.)$	Put option value
$q(.)$	Risk-neutral probability density function
$f(.,.)$	Real-valued function
i	Imaginary unit
ΔK	Strike spacing
$Q(.)$	Risk-neutral cumulative distribution function
$\hat{Q}(.)$	Estimate of $Q(.)$ using finite differences
$\hat{q}(.)$	Estimate of $q(.)$ using finite differences
$\mathrm{Var}^{\mathbb{Q}}$	Risk-neutral variance of the holding period log-return

$\text{Skew}^{\mathbb{Q}}$	Risk-neutral skewness of the holding period log-return
$\text{Kurt}^{\mathbb{Q}}$	Risk-neutral kurtosis of the holding period log-return
$\mathbb{VIX}$	Volatility index
$\mathbb{JTIX}$	Jump and tail index
$\mathbb{RIX}$	Rare disaster concern index
$\mathbb{V}$	Risk-neutral second moment of the holding period log-return
$\mathbb{IV}$	$\mathbb{VIX}$-type integrated variance of the holding period log-return
$\mathbb{V}^-$	Downside version of $\mathbb{V}$
$\mathbb{IV}^-$	Downside version of $\mathbb{IV}$
$\tilde{N}$	Number of observable option contracts
$\tilde{K}_i$	Strike price of the i'th option observed at the market
$\tilde{\sigma}_{i,(\text{Put/Call})}$	Implied volatility of the i'th option observed at the market

Symbols Chapter 2

$s, u, \mathcal{T}$	Time
$X, (X_t)_t$	Stochastic Process
$g(.), h(.)$	Borel-measurable functions
h, ϵ	Arbitrary small positive number
Y	Jump size
$B, (B_t)_t$	Brownian motion
$\mathbb{C}ov(.,.)$	Covariance
$\mathbb{V}ar(.)$	Variance
$Z, (Z_t)_t$	Exponential martingale process of Brownian motion
$f(.)$	Probability density function of the normal distribution
$\mathbb{R}^+$	Positive real numbers
$M_.(.)$	Moment-generating function
$\Gamma(.)$	Gamma distribution
$f_\Gamma(.)$	Probability density function of $\Gamma(.)$

$\hat{N}, (\hat{N}_t)_t$	Compensated Poisson process
$J, (J_t)_t$	Compound Poisson process
μ_Y	Expected value of jump size Y
$\hat{J}, (\hat{J}_t)_t$	Compensated Poisson process
Π_n	Partition
$\|\Pi_n\|$	Mesh of the partition Π_n
$FV_X(.)$	Sampled first-order variation
FV_X	First-order variation
$V_X(.)$	Sampled quadratic variation
$\mathcal{L}^2$	Space of square-integrable functions
$(\sigma_{(n,t)})_t$	Simple (piecewise constant) stochastic process
R_t	Riemann integral with upper limit t
I_t	Itô integral with upper limit t
$\delta(.,.)$	Dirac measure

Symbols Chapter 3

$P_{\text{Call/Put}}(.)$	Payoff function of a European-style call/put option
H	Contingent claim
$\Pi(.;.)$	Price of a contingent claim
$C_{BS}(.)$	Call option price in the Black and Scholes (1973) model
$P_{BS}(.)$	Put option price in the Black and Scholes (1973) model
$\Phi(.)$	Cumulative distribution function of the standard normal distribution
d_1, d_2	Auxiliary variables in the Black and Scholes (1973) model
$\alpha, \mu, \tilde{\sigma}$	Auxiliary variables
I_1, I_2	Auxiliary integrals
$\lambda(.)$	Auxiliary function
$\tilde{X}$	Normally distributed random variable
$\hat{\sigma}_{imp}$	Implied volatility plug-in estimate

$C^*(.,.;.)$	Quoted call option price
$\mathbb{R}_0$	Real numbers excluding zero
X_t	Normally distributed random variable determining the jump size at time t
μ_X	Expected (relative) jump size
σ_X	(Relative) jump size standard deviation of X_t
u	Input for the charateristic function
$\varphi(.)$	Characteristic function
$\alpha(.;.)$	Auxiliary function
Π_1, Π_2	Conditional probabilities
$\Re(.)$	Real part of a complex number
$V, (V_t)_t$	Variance process
$W^S, (W_t^S)_t$	Brownian motion driving the stock price process S
$W^V, (W_t^V)_t$	Brownian motion driving the variance process V
κ	Mean reversion speed
θ	Long-term mean
y	Variance rate jump size
μ_y	Mean of y
ρ	Correlation between Brownian motions
ρ_J	Correlation between jump sizes
$\beta(.;.)$	Auxiliary function
d, g, a	Auxiliary parameters

Symbols Chapter 4

S	Abbreviation for S_T
$\bar{S}$	Fixed positive value
$H(.)$	Payoff function
$\mathcal{C}^2$	Class of twice-continuously differentiable functions
$R(.,.)$	Log-return
$\mathcal{V}(.,.)$	Volatility contract

$\mathcal{W}(.,.)$	Cubic contract
$\mathcal{X}(.,.)$	Quartic contract
$\mathcal{M}(.,.)$	Expected value of the τ-period log-return under $\mathbb{Q}$
$\mathcal{O}$	Landau symbol
$Q(.)$	Out-of-the-money option price
F	Forward price
$S^c, (S^c_t)_t$	Continuous stock price process

Symbols Chapter 5

$F_{GEV}(.)$	Cumulative distribution function of the GEV distribution
$f_{GEV}(.)$	Probability density function of the GEV distribution
μ, σ, ξ	Parameters of the GEV distribution
$t(.)$	Auxiliary function
supp(.)	Support
M_n	Block maximum
a_n, b_n	Real constants
X^*	Random variable
$C_{GEV}(.,.;.)$	Call option price recovered from the GEV distribution
$P_{GEV}(.,.;.)$	Put option price recovered from the GEV distribution
$g(.)$	(Smoothing) spline function
a_i, b_i, c_i, d_i	Piecewise polynomial coefficients
$g_i, \boldsymbol{g}$	Value of the spline function and corresponding vector
$\gamma_i, \boldsymbol{\gamma}$	Second derivative value of the spline function and corresponding vector
h_i	Spacing between adjacent strikes
λ	Smoothing parameter
$\boldsymbol{Q}, q_{i,j}$	Matrix with corresponding entries
$\boldsymbol{R}, r_{i,j}$	Matrix with corresponding entries
$\boldsymbol{y}, \boldsymbol{x}$	Vectors

$\boldsymbol{I}$	Identity matrix
$\mathbf{0}$	Zero matrix
ρ	Weighting coefficient
$\tilde{\sigma}_{\text{blend}}$	Blended implied volatility
υ	Weighting coefficient
$\tilde{K}_{\text{high}}, \tilde{K}_{\text{low}}$	Highest and lowest strike price

Symbols Chapter 6

$\mathcal{Y}$	Placeholder for $\mathbb{V}$, $\mathbb{IV}$, $\mathbb{RIX}$
$\widehat{\mathcal{Y}}$	Estimate of $\mathcal{Y}$
$\mathcal{Y}_{\text{dense}}$	Benchmark value of $\mathcal{Y}$
$\tilde{\sigma}_{\text{noisy},i}$	Perturbed implied volatility
η	Standard normally distributed random variable
θ	Scaling coefficient

Symbols Appendix

$I_{t,n}$	Itô integral of a simple process with upper limit t
$\mathbb{C}$	Complex numbers
$\mathcal{C}^{1,2}$	Class of functions that are once (twice) continuously differentiable in the first (second) variable
$\varphi_X(.)$	Characteristic function
$f_X(.)$	Probability density function
$F_X(.)$	Cumulative distribution function
$\delta(.)$	Dirac delta function
$\widetilde{\mathbb{Q}}$	Risk-neutral probability measure
$\widetilde{q}(.)$	Risk-neutral density function

List of Figures

List of Tables

Chapter 1

Introduction

In financial markets, risk management is of paramount importance for investors, financial institutions, and regulators. The main task in managing identified risks is to accurately measure the associated exposures by selecting a suitable risk metric, before implementing strategies to mitigate or transfer those risks. Traditional risk measures, like historical volatility, Value-at-Risk, and Expected Shortfall, are either retrospective in nature or typically estimated based on historical data. These approaches implicitly assume that past price movements and volatility patterns are reliable indicators of future market behavior. However, during periods of market stress, they often fall short in capturing the full spectrum of risk. To address these limitations, one often resorts to so-called *option-implied risk measures*. These measures extract information embedded in option prices to infer market participants' expectations about future stock return characteristics and are inherently forward-looking. While there exist various option-implied risk measures, they all share a common assumption for computation, i.e. the availability of a continuum of out-of-the-money put and call option prices. Since this prerequisite is commonly not fulfilled in the market, a procedure known as *volatility smile construction* is required. This method enables the computation of missing implied volatilities, which are then used as plug-in estimates for the Black and Scholes (1973) model to calculate corresponding option prices, thereby providing the required continuum. Consequently, the accuracy of smile modeling is critical for reliable risk measure estimation, particularly when raw options data is either sparse, subject to microstructure noise, or both.

In the domain of smile modeling, one typically distinguishes between smile interpolation, including smoothing, and smile extrapolation. While interpolation techniques aim to estimate implied volatilities within the range of observed market data, extrapolation methods extend beyond this range. Although numerous sophisticated interpolation methods, such as kernel regression and smoothing splines, exist, the techniques for extrapolation are comparatively simpler. In the context of equity options, the standard approaches are flat and linear extrapolation, known as endpoint volatility and linear regression. Considering the tails of the risk-neutral distribution (RND) derived from extrapolated options, both of these methods do not comply with the principle of no-arbitrage, though. Their application can therefore lead to pronounced errors in the estimation of option-implied risk measures, as various studies demonstrate. Especially for tail risk metrics, which are per se highly prone to extrapolation inaccuracies, these errors are even amplified. Thus, for limited raw data where a high degree of extrapolation is required, neither endpoint volatility nor linear regression are qualified for accurate risk measure estimation.

In this thesis, we tackle this challenge by introducing an advanced volatility smile construction technique, known as the *arbitrage-free RND-based smile construction approach*. Before detailing this approach, we first address the risk measures relevant to this thesis. Subsequently, we provide a comprehensive presentation of this innovative approach, originating from my paper Albert et al. (2023), recently published in the Journal of Futures Markets. This smile construction technique combines arbitrage-free RND tail modeling for smile extrapolation with a convexity-preserving cubic smoothing spline for smile interpolation. In addition, we present a refined version of this smile construction technique that accommodates the modeling of potentially bimodal RNDs. Building directly on my previous work, we then analyze the robustness of the original smile construction technique in comparison to standard methods through a two-stage analysis. First, a numerical analysis is conducted using a benchmark option pricing model to address various sources of implementation errors. Then, an empirical application is performed using real-world financial data. Both analyses will confirm that the advanced RND-based smile construction approach is superior to standard techniques, ensuring accurate risk measure estimation.

The three main contributions of this thesis can thus be summarized as follows: First, after establishing the necessary foundations of stochastic processes and option pricing theory, we provide – to the best of our knowledge – the most comprehensive overview of option-implied risk measures in the literature to date. This overview includes not only the theoretical derivations of the respective measures but also the construction of replication portfolios for estimation, along with a critical examination of the underlying assumptions regarding stock price dynamics and their related deficiencies. Second, we deliver an innovative smile construction approach that unifies techniques from RND tail modeling with those from volatility smile construction in a modified and sophisticated manner. This arbitrage-free RND-based smile construction approach is primarily characterized by its accurate extrapolation performance and its robustness with respect to sparse and distorted data. Furthermore, it can be augmented in interpolation to capture potential bimodality in RND modeling. Third, we present an extensive analysis in which the original technique is benchmarked against standard methods within a model-based environment for error tractability, as well as in a practical setting utilizing financial data, to confirm its superiority. The three contributions of this thesis are elaborated upon in the following chapters:

Chapter 2 provides an introduction to stochastic processes, establishing the necessary foundation for the subsequent chapters. Starting with fundamental definitions, various classes of stochastic processes are presented, encompassing diffusion, jump, and jump-diffusion processes. Next, two processes are examined in detail, which constitute the foundation of modern asset pricing: Brownian motion and Poisson processes. The former is utilized for modeling diffusive dynamics, while the latter is employed to incorporate jump risk. In both cases, special emphasis is put on transformations satisfying the definition of a martingale, as such processes are qualified for derivatives pricing. Thereafter, the concept of quadratic variation is introduced and applied to the aforementioned classes of processes, which is essential for understanding option-implied risk measures.

Chapter 3 deals with option pricing theory. First, fundamental definitions and theorems pertinant to pricing options under the so-called *risk-neutral (probability) measure* are estab-

lished. Then, the celebrated Black and Scholes (1973) model is presented and examined with respect to its empirical limitations, which provides the motivation for exploring more advanced models discussed subsequently. Thereafter, the perspective is reversed: rather than making assumptions about stock return dynamics under the risk-neutral measure, the focus shifts to the extraction of the risk-neutral probability density function (RND) from observed option prices.[1] The mathematical relation between option prices and the RND, as outlined in Breeden and Litzenberger (1978), is elucidated, and practical issues encountered when working with real financial data are also addressed.

Chapter 4 presents the option-implied risk measures integral to this thesis: the risk-neutral moments of Bakshi et al. (2003) (BKM), the volatility index ($\mathbb{VIX}$) of the Chicago Board Options Exchange (CBOE), and the rare disaster concern index ($\mathbb{RIX}$) of Gao et al. (2018). The underlying methodology of these measures, commonly referred to as *generic spanning*, is outlined first. Each risk metric is then discussed individually, including its mathematical derivation and the presentation of the corresponding replication portfolio. The chapter concludes with the estimation of these measures via volatility smile construction, including a concise review of various smile modeling techniques and an examination of the deficiencies inherent in contemporary standard approaches.

Chapter 5 addresses the central component of this thesis: the arbitrage-free RND-based volatility smile construction technique. Starting with smile extrapolation, relevant results from extreme value theory are presented first, before the explicit RND tail modeling approach is discussed in detail. The chapter then covers smile interpolation and smoothing, focusing primarily on the convexity-preserving cubic smoothing spline method, which ensures robust extrapolation through its additional constraints. For practitioners and researchers interested in bimodal RNDs, the chapter also provides a brief overview of a quintic smoothing spline as an alternative interpolation and smoothing technique that remains compatible with the extrapolation methodology.

[1] If there is no ambiguity, the abbreviation RND may either refer to the risk-neutral probability density function or to the risk-neutral distribution in general.

Chapter 6 presents a comprehensive two-stage analysis, which corroborates the superiority of the proposed RND-based smile construction technique in comparison to standard methodologies. In the first stage, a benchmark option pricing model is employed to numerically assess the robustness of the respective smile construction methods in the presence of various implementation errors. The numerical analysis is conducted for two distinct scenarios to simulate both a normal trading day and a volatile trading day. In addition, the limitations of the RND tail modeling approach of Birru and Figlewski (2012), similar yet distinct to our innovative approach, are addressed within this model-based setting. In the second stage, the RND-based smile construction technique is empirically applied to options written on the set of *FAANG* stocks.[2] Analogously to the numerical analysis, a normal and a volatile trading day are considered, indicated by different levels of the $\mathbb{VIX}$. Then, for three narrowed moneyness ranges, volatility smiles are constructed according to the RND-based technique and the considered standard methodologies. This allows not only the estimation of the $\mathbb{RIX}$, which, by construction, partially encompasses the estimation of the BKM variance and $\mathbb{VIX}$, but also the computation of the root mean squared error (RMSE) resulting from the discrepancy between the discarded and the extrapolated implied volatilities.

Chapter 7 concludes this thesis and offers an outlook for potential future research. Throughout Chapters 2 to 6, proofs and derivations essential for understanding are presented within the respective chapters. Basics of stochastic calculus, including the Itô integral and Itô's formulae, and option pricing via Fourier transform are deferred to Appendix A and B.

[2] *FAANG* stands for the stocks of Facebook (Meta), Amazon, Apple, Netflix, and Google (Alphabet).

Chapter 2

Stochastic Processes

In risk management, understanding asset price dynamics is crucial for regulatory risk assessment, market analysis, and strategic decision-making regarding the risk-return trade-off. The mathematical tools for modeling these dynamics are stochastic processes, which capture the randomness inherent in financial markets and facilitate both the valuation of derivative contracts, including options, and the derivation of option-implied risk measures. Key processes include Brownian motion, which models diffusive price movements, and Poisson processes, which account for sudden jumps. These processes are often combined to create sophisticated models that mimic real price movements. A profound understanding of stochastic processes is, therefore, indispensable for option pricing theory and the derivation of option-implied risk measures.

This chapter is organized as follows: Section 2.1 provides all the necessary definitions and classes of processes required for the remainder of this thesis. Sections 2.2 and 2.3 are dedicated to the backbone of modern asset pricing, i.e. Brownian motion and Poisson processes. Besides their definitions, main properties and common transformations are presented. Special emphasize is put on those transformations satisfying the definition of a martingale, introduced in the preceding Section 2.1, since these are qualified for applications in option pricing. Next, an entire section is devoted to the concept of quadratic variation, which serves as the continuous counterpart to the more commonly term used in finance, i.e. realized variance. This topic is thoroughly examined due to its relevance to three risk metrics discussed

in this thesis: the risk-neutral return variance of BKM, the widely recognized $\mathbb{VIX}$, and the tail metric $\mathbb{RIX}$. While the former two metrics represent measures of expected quadratic variation itself, the latter isolates the higher-order impact of jumps on expected quadratic variation by exploiting the difference between them. It is important to emphasize that this chapter is focused exclusively on topics integral to this thesis. For a more thorough examination of the subject matter, which forms the basis of the entire chapter, please refer to the foundational works of Cont (2001), Shreve (2004), Björk (2009), and Frey (2017).

2.1 Basic Notion and Classes of Processes

In this section we present fundamental definitions pertinent to stochastic processes. First, a stochastic process is defined as follows:

Definition 1 ((Adapted) Stochastic Process)**.** *Let $(\Omega, \mathcal{F}, \mathbb{P})$ be a probability space, T some fixed point in time, and $\{\mathcal{F}_t\}$ a filtration of sub-sigma-algebras of $\mathcal{F}$, $t \in [0, T]$. Let $(X_t)_t$ denote a collection of random variables X_t. Then, $X = (X_t)_t$ is a stochastic process. X is called adapted, if for all t the random variable X_t is $\mathcal{F}_t$-measurable.*

This definition also encompasses the concept of adaptivity with respect to $\mathcal{F}$ which informally indicates that the value of X_t is observable at time t. It is important to note that stock price processes are considered adapted, given that they are observable at any time t due to their listing on an exchange. Furthermore, for the pricing of derivatives under the risk-neutral measure, as discussed in the subsequent chapter, the employed processes are required to be martingales, as characterized by the following definition:

Definition 2 (Martingale)**.** *Let $(\Omega, \mathcal{F}, \mathbb{P})$ be a probability space equipped with filtration $\{\mathcal{F}_t\}$, $t \in [0, T]$. An adapted stochastic process X, with $\mathbb{E}(|X_t|) < \infty$ for all t, is called a martingale if*

$$\mathbb{E}(X_t \mid \mathcal{F}_s) = X_s \quad \forall\, s, t \text{ with } t > s. \tag{2.1}$$

Hence, for a process that is a martingale, the best estimate of its future value, given all current information, is its present value. To accurately replicate the price dynamics observed

in financial markets, it is essential that the processes are not only martingales but also include a diffusive pattern. Thus, so-called *diffusion processes* are widely applied in financial mathematics for modeling price dynamics. Since diffusion processes are a special type of so-called *Markov processes*, we give the corresponding definition first:[3]

Definition 3 (Markov Process)**.** *Let $(\Omega, \mathcal{F}, \mathbb{P})$ be a probability space equipped with filtration $\{\mathcal{F}_t\}$, $t \in [0,T]$. An adapted process X is called Markov process if for every non-negative or integrable Borel-measurable function g, there is another Borel-measurable function h such that*

$$\mathbb{E}\left(g(X_t) \mid \mathcal{F}_s\right) = h(X_s) \quad \forall\, s,t \text{ with } t > s. \tag{2.2}$$

If (2.2) holds not only for deterministic s,t, but also for (stochastic) stopping times, then X is called strong Markov process.

A Markov process is thus characterized by a lack of memory, meaning future dynamics depend only on the current value.[4] Hence, diffusion processes, as a distinct subclass of Markov processes, are specified as follows:

Definition 4 (Diffusion Process)**.** *Let $(\Omega, \mathcal{F}, \mathbb{P})$ be a probability space equipped with filtration $\{\mathcal{F}_t\}$, $t \in [0,T]$. A strong Markov process X is called diffusion process if X exhibits continuous trajectories, i.e. the limits*

$$\mu(t,x) = \lim_{h\to 0} \frac{1}{h}\mathbb{E}\left(X_{t+h} - X_t \mid X_t = x\right) \tag{2.3}$$

$$\sigma^2(t,x) = \lim_{h\to 0} \frac{1}{h}\mathbb{E}\left(\left(X_{t+h} - X_t\right)^2 \mid X_t = x\right) \tag{2.4}$$

exist for all (t,x). In that case $\mu(x,t)$ denotes the drift and $\sigma(x,t)$ the diffusion.

The most commonly used processes in finance for modeling diffusive dynamics are so-called *Itô processes*. In fact, diffusion processes are a special type of Itô processes, which are driven by Brownian motion. For completeness, we provide the definition of Itô processes at the

[3] The following definition includes the notion of a *stopping time*. A random variable τ is called a *stopping time* with respect to $\{\mathcal{F}_t\}$, if for all $t \in [0,T]$ it holds that $\{\tau \leq t\} \in \mathcal{F}_t$.

[4] Therefore, Markov processes cannot be used for pricing path-dependent derivatives.

end of our discussion of Brownian motion to ensure a thorough understanding. Another important class of processes in finance, particularly for modeling discontinuities in asset price dynamics, are *jump processes*, which are defined as follows:

Definition 5 (Jump Process)**.** *Let* $(\Omega, \mathcal{F}, \mathbb{P})$ *be a probability space equipped with filtration* $\{\mathcal{F}_t\}$, $t \in [0, T]$. *An adapted process* X *is called jump process if*

(i) there exists a non-negative, increasing sequence $(\mathcal{T}_n)_{n\geq 1}$ *where* $\mathcal{T}_n \in [0, T]$ *represents the time of the n'th jump.*

(ii) there exists a corresponding sequence of jump sizes $(Y_n)_{n\geq 1}$ *such that* $X_{\mathcal{T}_n} = X_{\mathcal{T}_n -} + Y_n$ *where* Y_n *represents the jump size of the n'th jump at time* $\mathcal{T}_n$.

(iii) X *exhibits continuous sample paths for all* $t \in (\mathcal{T}_n, \mathcal{T}_{n+1})_{n\geq 1}$.

(iv) X *has independent increments, i.e. for* $0 = t_0 < t_1 < \ldots < t_n$ *the increments* $X_{t_1} - X_{t_0}, X_{t_2} - X_{t_1}, \ldots, X_{t_n} - X_{t_{n-1}}$ *are independent.*

If $X_0 = 0$ *and* X *is constant for all* $t \in (\mathcal{T}_n, \mathcal{T}_{n+1})_{n\geq 1}$, *then* X *is called pure jump process.*

The most prominent example of jump processes is the *Poisson process*, which is discussed in detail in Section 2.3. To accurately emulate the price dynamics observed in financial markets, it is essential to consider processes that incorporate both continuous and discrete components. *Jump-diffusion processes* are commonly employed for this purpose. As the name suggests, jump-diffusion processes are stochastic processes that integrate a diffusion component, usually driven by Brownian motion, with a jump component, typically modeled by a Poisson process.[5] In financial applications, these processes are frequently modeled in form of so-called *Lévy processes*, which exhibit desirable mathematical properties.[6] These are defined as follows:

[5]Since both processes are discussed in detail in the subsequent sections, a rigorous mathematical definition of jump-diffusion processes is not provided here.

[6]For Lévy processes, the characteristic function is determined according to the Lévy-Khintchine theorem. Utilizing the characteristic function enables the computation of option prices through simple integral evaluation. Appendix B provides comprehensive information on characteristic functions and the methodology for applying them in option pricing.

Definition 6 (Lévy Process)**.** *Let* $(\Omega, \mathcal{F}, \mathbb{P})$ *be a probability space equipped with filtration* $\{\mathcal{F}_t\}$, $t \in [0, T]$, *and* X *be an adapted process which has right-continuous sample paths with left limits (càdlàg) and* $X_0 = 0$. *Then,* X *is called Lévy process if*

(i) X *has independent increments, i.e. for* $0 = t_0 < t_1 < \ldots < t_n$ *the increments* $X_{t_1} - X_{t_0}, X_{t_2} - X_{t_1}, \ldots, X_{t_n} - X_{t_{n-1}}$ *are independent.*

(ii) X *has stationary increments, i.e. the distribution of* $X_{t+h} - X_t$ *does not depend on* t.

(iii) X *is stochastically continuous, i.e.* $\lim_{h \to \infty} \mathbb{P}(|X_{t+h} - X_t| \geq \epsilon) = 0$, $\forall \epsilon > 0$.

Therefore, jump-diffusion processes that satisfy the definition of a Lévy process are primarily characterized by having stationary and independent increments. Consequently, processes with a stochastic volatility term $\sigma(t, x)$ in their diffusive component generally do not qualify as Lévy processes, as the presence of $\sigma(t, x)$ being stochastic typically leads to non-stationary increments. This distinction will become important later in this thesis. Having covered all the necessary definitions, we now turn our attention to one of the most important processes in financial mathematics, namely, Brownian motion.

2.2 Brownian Motion

Brownian motion is regarded as one of the two principal building blocks of asset pricing. Discovered by the Scottish botanist R. Brown and rigorously formalized by the mathematician N. Wiener, Brownian motion is employed for modeling random events across various scientific disciplines. In finance, Brownian motion is specifically utilized to emulate the diffusive pattern of price dynamics by means of Itô processes. In the one-dimensional case, Brownian motion is defined as follows:

Definition 7 (Brownian Motion)**.** *Let* $(\Omega, \mathcal{F}, \mathbb{P})$ *be a probability space and* X *be a stochastic process. Then* X *is a one-dimensional Brownian Motion if*

(i) $X_0 = 0$ *a.s.*

(ii) X *has continuous sample paths.*

(iii) X *has independent increments that are stationary and normally distributed, i.e.* $X_{t+u} - X_t \sim \mathcal{N}(0, u)$ *is independent of* X_s *with* $u \geq 0$, $t \geq s$, *and* $t + u, t, s \in [0, T]$.

In recognition of Brown and Wiener, Brownian motion $(X_t)_t$ is commonly referred to as $(B_t)_t$ or $(W_t)_t$.

It is important to note that Brownian motion is not merely a theoretical construct but an actual phenomenon, as established by the following theorem:

Theorem 8. *A stochastic process as described in Definition 7 exists.*

Proof. See Karatzas and Shreve (1998). □

Graphically, the properties of Brownian motion, as described in Definition 7, translate into a continuous, diffusive process that is nowhere differentiable, as illustrated by the following sample path:[7]

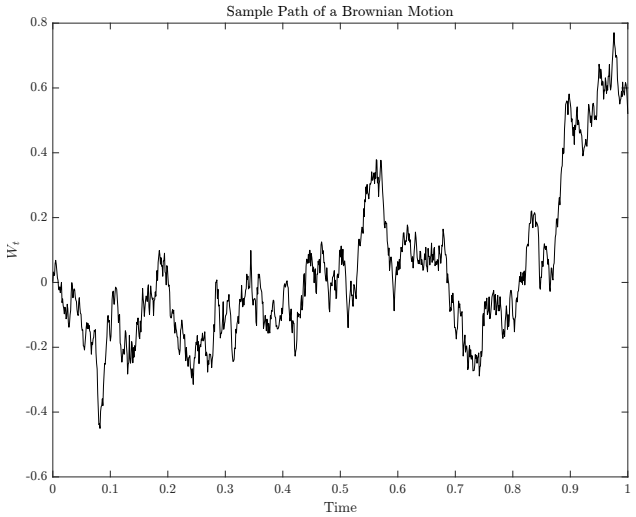

Figure 2.1: Brownian Motion – The figure plots a sample path of Brownian motion.

Comparing the diffusive pattern depicted in Figure 2.1 with asset price dynamics observed in financial markets suggests that Brownian motion is indeed suitable for modeling the diffusive components, while potential issues related to negative values are disregarded at this stage. Two fundamental properties of Brownian motion that are widely recognized are specified in the following proposition:

[7]The non-differentiability of Brownian motion follows directly from the properties specified in Definition 7 and is therefore omitted from the current discussion.

Proposition 9. *Let $(W_t)_t$ be a Brownian motion. Then,*

(i) $W_t = W_t - W_0$ follows a normal distribution with mean 0 and variance t.

(ii) for $t > s$, the covariance between W_t and W_s is given by $\mathbb{C}ov(W_t, W_s) = s$.

Proof. (i) is an immediate consequence of Definition 7, (iii), and implies that $\mathbb{E}(W_t) = \mathbb{E}(W_s) = 0$. (ii) follows by straightforward computation

$$\begin{aligned}\mathbb{C}ov(W_t, W_s) &= \mathbb{E}(W_t W_s) \\ &= \mathbb{E}((W_t - W_s)W_s + W_s^2) \\ &= \mathbb{E}(W_t - W_s)\mathbb{E}(W_s) + \mathbb{E}(W_s^2) \\ &= 0 + \mathbb{V}ar(W_s) = s. \end{aligned} \tag{2.5}$$

□

Having established the definition and fundamental properties of Brownian motion, the next question is which processes relative to Brownian motion are suitable for derivatives pricing. As previously noted, such processes must be martingales under the risk-neutral measure. While the details of pricing under this measure will be discussed in Chapter 3, we now present processes driven by Brownian motion that are martingales. First Brownian motion itself is a martingale, as stated in the following theorem:

Theorem 10. *Brownian motion is a martingale.*

Proof. Let $0 \leq s \leq t$ be given. Then,

$$\begin{aligned}\mathbb{E}(W_t \mid \mathcal{F}_s) &= \mathbb{E}((W_t - W_s) + W_s \mid \mathcal{F}_s) \\ &= \mathbb{E}(W_t - W_s \mid \mathcal{F}_s) + \mathbb{E}(W_s \mid \mathcal{F}_s) \\ &= \mathbb{E}(W_t - W_s) + W_s \\ &= W_s. \end{aligned} \tag{2.6}$$

Thus, by Definition 2, (i), $(W_t)_t$ is a martingale. □

Although Brownian motion is a martingale and thus mathematically suitable for describing asset price dynamics, it is not economically appropriate for modeling stock prices, which are non-negative.[8] As shown in Figure 2.1, Brownian motion can take negative values, which conflicts with the non-negativity requirement for stock prices. To address this issue, the exponential of Brownian motion is commonly used to model stock prices, as demonstrated by Black and Scholes (1973) in their renowned option pricing model, discussed in Subsection 3.1.2. For the exponential of Brownian motion to maintain the martingale property, an additional correction term is required, as summarized in the following theorem:

Theorem 11 (Exponential Martingale)**.** *Let $(W_t)_t$ be a Brownian motion with filtration $\{\mathcal{F}_t\}$, $t \in [0,T]$, and σ be a constant. Then, the process $Z = (Z_t)_t$ with Z_t defined as*

$$Z_t = \exp\left\{\sigma W_t - \frac{1}{2}\sigma^2 t\right\} \tag{2.7}$$

is a martingale.

Proof. Let $0 \leq s \leq t$ be given. Then,

$$\begin{aligned}
\mathbb{E}(Z_t \mid \mathcal{F}_s) &= \mathbb{E}\left(\exp\left\{\sigma W_t - \frac{1}{2}\sigma^2 t\right\}\middle|\mathcal{F}_s\right) \\
&= \mathbb{E}\left(\exp\left\{\sigma(W_t - W_s)\right\} \cdot \exp\left\{\sigma W_s - \frac{1}{2}\sigma^2 t\right\}\middle|\mathcal{F}_s\right) \\
&= \mathbb{E}\left(\exp\left\{\sigma(W_t - W_s)\middle|\mathcal{F}_s\right\}\right) \cdot \mathbb{E}\left(\exp\left\{\sigma W_s - \frac{1}{2}\sigma^2 t\right\}\middle|\mathcal{F}_s\right) \\
&= \mathbb{E}\Big(\exp\left\{\sigma(W_t - W_s)\right\}\Big) \cdot \exp\left\{\sigma W_s - \frac{1}{2}\sigma^2 t\right\} \\
&= \exp\left\{\frac{1}{2}\sigma^2(t-s)\right\} \cdot \exp\left\{\sigma W_s - \frac{1}{2}\sigma^2 t\right\} \\
&= \exp\left\{\sigma W_s - \frac{1}{2}\sigma^2 s\right\} = Z_s,
\end{aligned} \tag{2.8}$$

[8] For underlying assets where negative values are reasonable, dynamics are typically modeled not by Brownian motion itself, but by arithmetic Brownian motion. Arithmetic Brownian motion is presented at the end of this section.

where we used in the fourth step that for $X \equiv W_t - W_s \sim \mathcal{N}(0, t-s)$ it holds

$$\begin{aligned}
\mathbb{E}\left(e^{\sigma X}\right) &= \int_{-\infty}^{\infty} e^{\sigma x} f(x) \mathrm{d}x \\
&= \frac{1}{\sqrt{2\pi(t-s)}} \int_{-\infty}^{\infty} \exp\{\sigma x\} \exp\left\{-\frac{x^2}{2(t-s)}\right\} \mathrm{d}x \\
&= \frac{1}{\sqrt{2\pi(t-s)}} \int_{-\infty}^{\infty} \exp\left\{\sigma x - \frac{x^2}{2(t-s)}\right\} \mathrm{d}x \\
&= \frac{1}{\sqrt{2\pi(t-s)}} \int_{-\infty}^{\infty} \exp\left\{-\frac{x^2 - 2x\sigma(t-s)}{2(t-s)}\right\} \mathrm{d}x \\
&= e^{\frac{1}{2}\sigma^2(t-s)} \frac{1}{\sqrt{2\pi(t-s)}} \int_{-\infty}^{\infty} \exp\left\{-\frac{(x-\sigma(t-s))^2}{2(t-s)}\right\} \mathrm{d}x \\
&= e^{\frac{1}{2}\sigma^2(t-s)}. \qquad (2.9)
\end{aligned}$$

□

In Subsection 3.1.2, we will utilize this theorem to demonstrate that the stock price process is indeed a martingale within the framework of the Black and Scholes (1973) model. Finally, after Brownian motion is covered to a sufficient extend, we now come to Itô processes which constitute the most important diffusion process in finance:[9]

Definition 12 (Itô Process)**.** *Let W be a Brownian motion, $t_0 \in [0, T]$, $X_{t_0} \in \mathbb{R}$, and functions $\mu : \mathbb{R}^+ \times \mathbb{R} \to \mathbb{R}$ and $\sigma : \mathbb{R}^+ \times \mathbb{R} \to \mathbb{R}$. Then the process X is called an Itô process with initial value X_{t_0}, drift μ and dispersion σ, if X satisfies the SDE*

$$X_{\bar{t}} = X_{t_0} + \int_{t_0}^{\bar{t}} \mu(t, X_t) \mathrm{d}t + \int_{t_0}^{\bar{t}} \sigma(t, X_t) \mathrm{d}W_t. \qquad (2.10)$$

for all $\bar{t} \in [t_0, T]$. In differential notation, Equation (2.10) can be written as

$$\mathrm{d}X_t = \mu(t, X_t)\mathrm{d}t + \sigma(t, X_t)\mathrm{d}W_t. \qquad (2.11)$$

[9] Precisely, the given definition refers to a standard Itô process. In general, Itô processes require that the drift μ_t and the dispersion σ_t be adapted processes, but they are not necessarily Markovian. To satisfy the definition of a diffusion process as specified in Definition 4, only the standard version is presented here.

In finance, it is common to restrict σ to be positive and set t_0 to 0. For the remainder of this thesis, we comply with this convention. Moreover, it is crucial to note that the integral with respect to Brownian motion in (2.10) is not an ordinary Lebesgue integral, but an Itô integral. The rigorous definition of the Itô integral is provided in Appendix A.1. We conclude this section by presenting two fundamental, yet frequently utilized Itô processes in finance: arithmetic Brownian motion and geometric Brownian motion.

X is called an *arithmetic* Brownian motion, if for some $\mu \in \mathbb{R}$ and $\sigma \in \mathbb{R}^+$, $X_{\bar{t}}$ is defined as

$$X_{\bar{t}} = X_0 + \int_0^{\bar{t}} \mu \mathrm{d}t + \int_0^{\bar{t}} \sigma \mathrm{d}W_t, \quad \bar{t} \in [0, T], \tag{2.12}$$

which simplifies to

$$X_{\bar{t}} = X_0 + \mu\bar{t} + \sigma W_{\bar{t}} \tag{2.13}$$

by the definition of the Itô integral. Therefore, $X_{\bar{t}} \sim \mathcal{N}\left(X_0 + \mu\bar{t}, \sigma^2\bar{t}\right)$. In the notation of an Itô process, we have $\mu(t, X_t) = \mu$ and $\sigma(t, X_t) = \sigma$. It should be emphasized that, by construction, an arithmetic Brownian motion is a martingale if and only if its drift μ is zero.

X is called a *geometric* Brownian motion, if for some $\mu \in \mathbb{R}$ and $\sigma \in \mathbb{R}^+$, $X_{\bar{t}}$ is defined as

$$X_{\bar{t}} = X_0 + \int_0^{\bar{t}} \mu X_t \mathrm{d}t + \int_0^{\bar{t}} \sigma X_t \mathrm{d}W_t, \quad \bar{t} \in [0, T], \tag{2.14}$$

which simplifies to

$$X_{\bar{t}} = X_0 \exp\left\{\left(\mu - \frac{1}{2}\sigma^2\right)\bar{t} + \sigma W_{\bar{t}}\right\}, \tag{2.15}$$

as demonstrated in Subsection 3.1.2. It is important to note that in the notation of an Itô process $\mu(t, X_t) = \mu X_t$, where $\mu(.)$ denotes drift and μ is simply a parameter. The same applies to $\sigma(.)$ and σ. For the geometric Brownian motion to be a martingale, only μ must be adjusted due to the exponential martingale property.

2.3 Poisson Processes

The second principal building block of modern asset pricing are Poisson processes. These processes enable the incorporation of jumps into price dynamics, allowing for the modeling of idiosyncratic risk or market crashes. While the basic Poisson process is a pure counting process, with its compensated version serving as the martingale equivalent, the augmented compound Poisson process incorporates stochastic jump sizes, providing a more realistic representation of financial data. The compensated version of this process is widely regarded as the standard approach for modeling jumps in asset price dynamics. Due to their increasing complexity, we begin with the definition of the standard Poisson process, which reads:

Definition 13 (Poisson Process)**.** *Let $(\tau_i)_{i\geq 1}$ be a sequence of independent exponential random variables with intensity λ. Let $\mathcal{T}_n = \sum_{i=1}^{n} \tau_i$ be the time of the n'th jump. Then, the process $N = (N_t)_t$ with N_t defined as*

$$N_t = \sum_{n\geq 1} \mathbb{1}_{t\geq \mathcal{T}_n} = \begin{cases} 0 \text{ if } 0 \leq t < \mathcal{T}_1, \\ 1 \text{ if } \mathcal{T}_1 \leq t < \mathcal{T}_2, \\ \vdots \\ n \text{ if } \mathcal{T}_n \leq t < \mathcal{T}_{n+1}, \\ \vdots \end{cases} \tag{2.16}$$

is a Poisson process with intensity λ.

As evident from the definition, N_t can only take integer values, classifying it as a pure counting process. As indicated by its declaration, the Poisson process is closely related to the Poisson distribution. To elucidate this interdependence, the main properties of the Poisson process, which can be partially anticipated from Figure 2.2, are summarized in the following proposition:

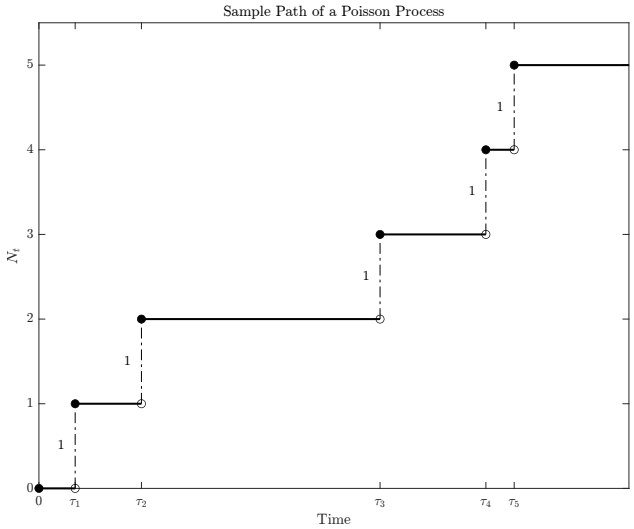

Figure 2.2: Poisson Process – The figure plots a sample path of a Poisson process, where the number of jumps N_t is restricted to five and the inter-arrival times τ_i are exponentially distributed: $\tau_i \overset{\text{i.i.d}}{\sim} \text{Exp}(1)$, $i = 1, \ldots, 5$.

Proposition 14. *Let N be a Poisson process with intensity λ. Then,*

(i) for any $t > 0$, N_t is finite a.s.

(ii) N has piecewise constant samples paths which increase by jumps of size 1.

(iii) N has right-continuous sample paths with left limits (càdlàg).

(iv) for any $t > 0$, N_t follows a Poisson distribution with parameter λt, i.e.

$$\mathbb{P}(N_t = n) = \frac{(\lambda t)^n}{n!} e^{-\lambda t} \quad \forall\, n \in \mathbb{N}_0. \tag{2.17}$$

(v) N has stationary and independent increments, i.e. for $0 = t_0 < t_1 < \ldots < t_n$ the increments $N_{t_1} - N_{t_0}, N_{t_2} - N_{t_1}, \ldots, N_{t_n} - N_{t_{n-1}}$ are independent and

$$\mathbb{P}(N_{t_{j+1}} - N_{t_j} = n) = \frac{\lambda^n (t_{j+1} - t_j)^n}{n!} e^{-\lambda(t_{j+1} - t_j)} \quad \forall\, n \in \mathbb{N}_0. \tag{2.18}$$

(vi) N has homogeneous increments, i.e. for any $t > s$, $N_t - N_s$ has the same distribution as N_{t-s}.

Partial Proof. Since the Poisson distribution is eponymous for the process itself, property (iv) is proved in the following. For the other properties, please refer to Cont (2004), Proposition 2.12. To prove (iv), the distribution of $\mathcal{T}_n$ is determined first using the moment-generating function (MGF) approach. Recall $\mathcal{T}_n = \sum_{i=1}^{n} \tau_i$, where $\tau_i \overset{\text{i.i.d}}{\sim} \text{Exp}(\lambda)$. Then the MGF M of $\mathcal{T}_n$ is given by

$$\begin{aligned} M_{\mathcal{T}_n}(t) &= \mathbb{E}\left(\exp\left\{\mathcal{T}_n \cdot t\right\}\right) \\ &= \mathbb{E}\left(\exp\left\{\left(\sum_{i=1}^{n} \tau_i\right) t\right\}\right) \\ &= \mathbb{E}\left(\prod_{i=1}^{n} \exp\left\{\tau_i \cdot t\right\}\right) \\ &= \prod_{i=1}^{n} \mathbb{E}\left(\exp\left\{\tau_i \cdot t\right\}\right) \\ &= \prod_{i=1}^{n} \left(1 - \frac{1}{\lambda} \cdot t\right)^{-1} \\ &= \left(1 - \frac{1}{\lambda} \cdot t\right)^{-n}, \end{aligned} \tag{2.19}$$

which is the MGF of a Gamma distribution with shape parameter n and rate paramter λ. Thus, for $n \geq 1$, $\mathcal{T}_n \sim \Gamma(n, \lambda)$ with density

$$f_\Gamma(s) = \frac{(\lambda s)^{n-1}}{(n-1)!} \lambda e^{-\lambda s}, \quad s \geq 0. \tag{2.20}$$

For $n \geq 1$, note that $N_t \geq n$ if and only if the time of the n'th jump is less than or equal to t. Hence, $N_t \geq n$ is equivalent to $\mathcal{T}_n \leq t$ such that

$$\mathbb{P}(N_t \geq n) = \mathbb{P}(\mathcal{T}_n \leq t) = \int_0^t \frac{(\lambda s)^{n-1}}{(n-1)!} \lambda e^{-\lambda s} \mathrm{d}s. \tag{2.21}$$

Analogously,

$$\mathbb{P}(N_t \geq n+1) = \mathbb{P}(\mathcal{T}_{n+1} \leq t) = \int_0^t \frac{(\lambda s)^{n}}{n!} \lambda e^{-\lambda s} \mathrm{d}s. \tag{2.22}$$

Using integration by parts, the latter expression can be rewritten as

$$\begin{aligned}\mathbb{P}(N_t \geq n+1) &= -\left[\frac{(\lambda s)^n}{n!}e^{-\lambda t}\right]_{s=0}^{s=t} + \int_0^t \frac{(\lambda s)^{n-1}}{(n-1)!}\lambda e^{-\lambda s}\mathrm{d}s \\ &= -\frac{(\lambda t)^n}{n!}e^{-\lambda t} + \mathbb{P}(N_t \geq n). \end{aligned} \tag{2.23}$$

Therefore, $\mathbb{P}(N_t = n)$ results from the following difference

$$\mathbb{P}(N_t = n) = \mathbb{P}(N_t \geq n) - \mathbb{P}(N_t \geq n+1) = \frac{(\lambda t)^n}{n!}e^{-\lambda t}. \tag{2.24}$$

For $n = 0$, $N_t = 0$ is equivalent to $\mathcal{T}_1 > t$ which means no jump occurred up to time t. So,

$$\mathbb{P}(N_t = 0) = \mathbb{P}(\mathcal{T}_1 > t) = \mathbb{P}(\tau_1 > 1) = e^{-\lambda t}, \tag{2.25}$$

which corresponds to (2.17) with $n = 0$. □

As previously mentioned, to apply the Poisson process in derivatives pricing, it must be compensated for its drift to satisfy the martingale property. The resulting *compensated Poisson process* is defined as follows:

Definition 15 (Compensated Poisson Process)**.** *Let N be a Poisson process with intensity λ. Then, $\hat{N} = (\hat{N}_t)_t$ with $\hat{N}_t$ defined as*

$$\hat{N}_t = N_t - \lambda t \tag{2.26}$$

is called compensated Poisson process.

Therefore, according to the basic properties of the Poisson distribution, the compensated Poisson process is essentially a Poisson process adjusted by subtracting its expectation. Its visual representation is illustrated in the figure on the next page.

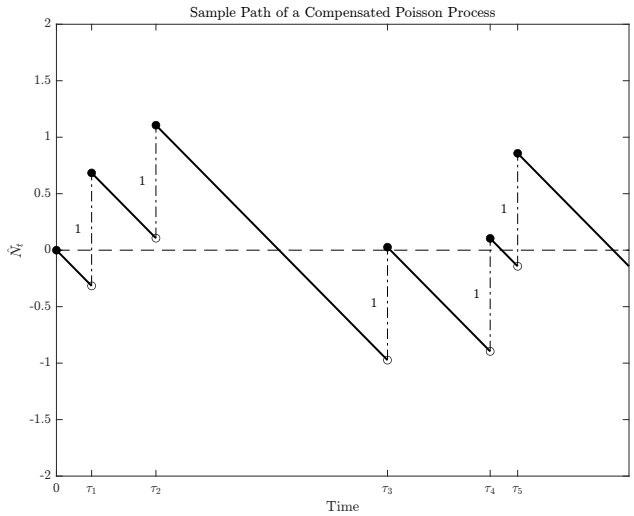

Figure 2.3: Compensated Poisson Process – The figure plots a sample path of a compensated Poisson process, where the number of jumps N_t is restricted to five and the inter-arrival times τ_i are exponentially distributed: $\tau_i \overset{\text{i.i.d}}{\sim} \text{Exp}(1)$, $i = 1, \ldots, 5$.

Comparing Figures 2.2 and 2.3, it is apparent that the compensation de-trends the Poisson process, thereby disqualifying the compensated version from being classified as a pure jump process. The proof that subtracting its expectation transforms the Poisson process into a martingale is provided by the following theorem:

Theorem 16. *The compensated Poisson process is a martingale.*

Proof. Let $0 \leq s < t$ be given. Since $N_t - N_s$ is independent of $\mathcal{F}_s$, it holds

$$\begin{aligned}
\mathbb{E}\left(\hat{N}_t \mid \mathcal{F}_s\right) &= \mathbb{E}\left(\hat{N}_t - \hat{N}_s + \hat{N}_s \mid \mathcal{F}_s\right) \\
&= \mathbb{E}\left(\hat{N}_t - \hat{N}_s \mid \mathcal{F}_s\right) + \mathbb{E}\left(\hat{N}_s \mid \mathcal{F}_s\right) \\
&= \mathbb{E}\left(N_t - N_s - \lambda(t-s) \mid \mathcal{F}_s\right) + \hat{N}_s \\
&= \mathbb{E}\left(N_t - N_s \mid \mathcal{F}_s\right) - \lambda(t-s) + \hat{N}_s \\
&= \mathbb{E}\left(N_t - N_s\right) - \lambda(t-s) + \hat{N}_s \\
&= \hat{N}_s, \qquad (2.27)
\end{aligned}$$

where we used Proposition 14, (v) to determine

$$\begin{aligned}\mathbb{E}(N_t - N_s) &= \sum_{n=0}^{\infty} n \frac{\lambda^n (t-s)^n}{n!} e^{-\lambda(t-s)} \\ &= \lambda(t-s) \cdot e^{-\lambda(t-s)} \sum_{n=1}^{\infty} \frac{\lambda^{n-1}(t-s)^{n-1}}{(n-1)!} \\ &= \lambda(t-s) \cdot e^{-\lambda(t-s)} \cdot e^{\lambda(t-s)} \\ &= \lambda(t-s). \end{aligned} \tag{2.28}$$

□

Although the compensated Poisson process satisfies the martingale property, it remains unsuitable for financial applications due to its constant jump size of one. In financial markets, asset values typically exhibit jumps of random sizes, often with a negative sign. The so-called *compound Poisson process* accommodates the randomness in jump sizes, as specified in the definition below:

Definition 17 (Compound Poisson Process)**.** *Let N be a Poisson process with intensity λ. Let $Y_1, Y_2, \ldots$ be independent and identically distributed random variables independent of $(N_t)_t$. Then, $J = (J_t)_t$ with J_t defined as*

$$J_t = \sum_{i=1}^{N_t} Y_i, \quad t \geq 0, \tag{2.29}$$

is called compound Poisson process.

According to this definition, the distribution of the jump size Y_i is not restricted to any specific family of distribution functions. In financial applications, however, it is common to model jump sizes as normally or log-normally distributed random variables. The normal distribution is typically employed for additive models, whereas the log-normal distribution is preferred in multiplicative models where jumps are modeled relative to the current asset value.

An illustration of the compound Poisson process with normally-distributed jump sizes is provided in the figure below:

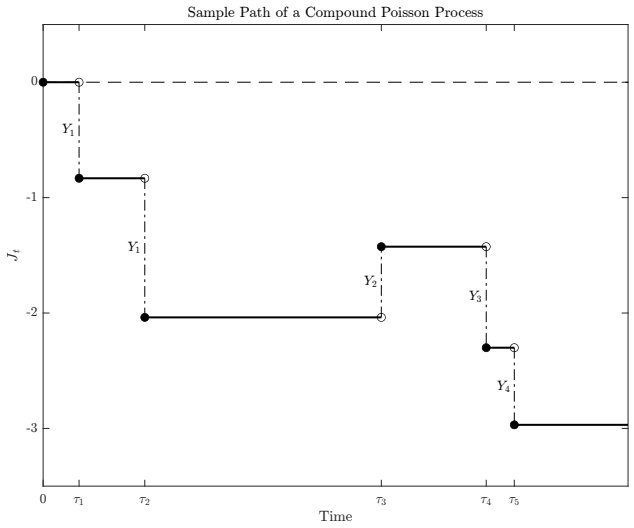

Figure 2.4: Compound Poisson Process – The figure plots a sample path of a compound Poisson process, where the number of jumps N_t is restricted to five, the inter-arrival times τ_i are exponentially distributed, and jump sizes Y_i are normally distributed: $\tau_i \overset{\text{i.i.d}}{\sim} \text{Exp}(1)$ and $Y_i \overset{\text{i.i.d}}{\sim} \mathcal{N}(-0.5, 1)$, $i = 1, \ldots, 5$.

Similar to the Poisson process, the compound Poisson process exhibits certain properties regarding its increments, which are summarized in the following proposition:

Proposition 18. *Let J be a compound Poisson process with intensity λ and independent and identically distributed jump sizes Y_i, $i \in \mathbb{N}$, with expected value μ_Y. Then,*

(i) The expected value of the compound Poisson process is given by $\mathbb{E}(J_t) = \mu_Y \lambda t$.

(ii) J has stationary and independent increments, i.e. for $0 = t_0 < t_1 < \ldots < t_n$ the increments $J_{t_1} - J_{t_0}, J_{t_2} - J_{t_1}, \ldots, J_{t_n} - J_{t_{n-1}}$ are independent and stationary. In particular, the increments are identically distributed.

(iii) J has homogeneous increments, i.e. for any $t > s$, $J_t - J_s$ has the same distribution as J_{t-s}.

Partial Proof. We only prove (i) since (ii) and (iii) are immediate consequences of Proposition 14, (v) in conjunction with the assumption that Y_i's are i.i.d. To prove (i) recall that the jump sizes Y_i are not only mutual independent, but also independent with respect to N_t such

that $\mathbb{E}(J_t)$ is given by

$$\begin{aligned}
\mathbb{E}(J_t) &= \mathbb{E}\left(\sum_{i=1}^{N_t} Y_i,\right) \\
&= \sum_{n=0}^{\infty} \mathbb{E}\left(\sum_{i=1}^{n} Y_i \mid N_t = n\right) \cdot \mathbb{P}\left(N_t = n\right) \\
&= \sum_{n=0}^{\infty} \sum_{i=1}^{n} \mathbb{E}\left(Y_i \mid N_t = n\right) \cdot \mathbb{P}\left(N_t = n\right) \\
&= \sum_{n=0}^{\infty} \sum_{i=1}^{n} \mathbb{E}(Y_i) \cdot \mathbb{P}\left(N_t = n\right) \\
&= \sum_{n=0}^{\infty} \mu_Y \cdot n \cdot \frac{(\lambda t)^n}{n!} e^{-\lambda t} \\
&= \mu_Y \lambda t \, e^{-\lambda t} \sum_{n=1}^{\infty} \frac{(\lambda t)^{n-1}}{(n-1)!} \\
&= \mu_Y \lambda t \, e^{-\lambda t} e^{\lambda t} \\
&= \mu_Y \lambda t. \qquad (2.30)
\end{aligned}$$

□

Analogous to the de-trending of the Poisson process, the compound Poisson process must be compensated by some correction term to be a martingale. This leads to the definition of the *compensated compound Poisson process*, which reads:

Definition 19. *Let J be a compound Poisson process as defined above and let μ_Y be the expected value of Y_i, $i \in \mathbb{N}$. Then, $\hat{J} = (\hat{J}_t)_t$ with $\hat{J}_t$ defined as*

$$\hat{J}_t = J_t - \mu_Y \lambda t \qquad (2.31)$$

is called compensated compound Poisson process.

An illustration of such a process is provided by the figure on the following page.

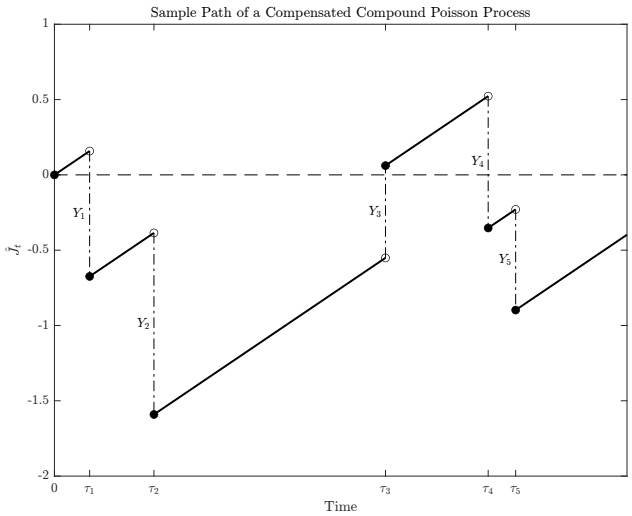

Figure 2.5: Compensated Compound Poisson Process – The figure plots a sample path of a Compensated Compound Poisson Process, where the number of jumps N_t is restricted to five, the inter-arrival times τ_i are exponentially distributed, and jump sizes Y_i are normally distributed: $\tau_i \overset{\text{i.i.d}}{\sim} \text{Exp}(1)$ and $Y_i \overset{\text{i.i.d}}{\sim} \mathcal{N}(-0.5, 1)$, $i = 1, \ldots, 5$

As indicated by Figure 2.5, subtracting its expectation $\mu_Y \lambda t$ from the initial compound Poisson process results in de-trending. The verification that this adjustment term transforms the compound poisson process into a martingale is provided by the following theorem:

Theorem 20. *The compensated compound Poisson process is a martingale.*

Proof. Let $0 \leq s < t$ be given. Since $J_t - J_s$ is independent of $\mathcal{F}_s$ with expectation $\mu_Y \lambda (t-s)$ as a consequence of Proposition 18, (iii), it holds

$$\begin{aligned}
\mathbb{E}\left(\hat{J}_t \mid \mathcal{F}_s\right) &= \mathbb{E}\left(J_t - \mu_Y \lambda t \mid \mathcal{F}_s\right) \\
&= \mathbb{E}\left(J_t - J_s \mid F_s\right) + \mathbb{E}(J_s \mid \mathcal{F}_s) - \mu_Y \lambda t \\
&= \mathbb{E}\left(J_t - J_s\right) + J_s - \mu_Y \lambda t \\
&= \mu_Y \lambda (t-s) + J_s - \mu_Y \lambda t \\
&= J_s - \mu_Y \lambda s \\
&= \hat{J}_s. \qquad (2.32)
\end{aligned}$$

□

Thus, the compensated compound Poisson process accommodates both a random number of jumps and random jump sizes while preserving the martingale property, making it an optimal choice for modeling jumps in asset price dynamics.

2.4 Quadratic Variation

We now turn to a concept that is not only integral to stochastic calculus, but also essential to this thesis on option-implied risk measures: quadratic variation. From an economic perspective, quadratic variation measures the variability of a process over time, serving as the continuous counterpart to realized variance. As outlined in the chapter's introduction, almost all of the option-implied risk measures in this thesis are related to this concept.[10]

To gain a comprehensive understanding of quadratic variation, including its application to the stochastic processes discussed in the preceding sections, we organize this section as follows: Subsection 2.4.1 introduces fundamental definitions pertinent to the field of quadratic variation. In Subsection 2.4.2, we begin with the quadratic variation of (scaled) Brownian motion and the Itô integral, before addressing the quadratic variation of Itô processes. Following this, we elucidate the quadratic variation of Poisson processes in Subsection 2.4.3. Then, we combine results in Subsection 2.4.4, which covers the quadratic variation of jump-diffusion processes.

2.4.1 Basic Definitions and Properties

We begin this subsection with the definition of a partition, which is given by:

Definition 21 (Partition)**.** *A partition* Π_n *of a time interval* $[0, T]$ *is a set of time points* $\{t_0, t_1, \ldots, t_n\}$ *with* $0 = t_0 < t_1 < \ldots < t_n = T$. $\|\Pi_n\|$ *denotes the mesh of the partition* Π_n *and is defined as the largest subinterval , i.e.* $\|\Pi_n\| = \sup_{0 \leq i \leq n-1} \left| t_{i+1} - t_i \right|$.

[10] For the higher-order risk-neutral moments of BKM, only the variance is related to quadratic variation, as explained in Subsection 4.4.1.

Building on this foundational concept, we introduce the notion of first-order variation and quadratic variation in the following. First-order variation, a distinct yet pertinent concept in the context of quadratic variation, is defined as follows:[11]

Definition 22 (First-Order Variation)**.** *Let $X : [0,T] \to \mathbb{R}$ be a function and $(\Pi_n)_n$ be a sequence of partitions of the time interval $[0,T]$ such that $\|\Pi_n\| \to 0$ as $n \to \infty$. For a partition Π_n, define $FV_X(\Pi_n)$ as*

$$FV_X(\Pi_n) = \sum_{i=0}^{n-1} |X(t_{i+1}) - X(t_i)|. \tag{2.33}$$

Then, provided the limit of $FV_X(\Pi_n)$ exists, FV_X specified by

$$FV_X = \lim_{n\to\infty} FV_X(\Pi_n) \tag{2.34}$$

is called first-order variation of X. If $FV_X < \infty$, then X has finite variation.

$FV_X(\Pi_n)$ is commonly referred to as sampled first-order variation. In financial terminology, the first-order variation can be regarded as the cumulative magnitude of price fluctuations. However, the more pertinent measure of price fluctuations is quadratic variation, which offers a more nuanced understanding of volatility and variance. This concept is specified as follows:

Definition 23 (Quadratic Variation)**.** *Let X be a stochastic process defined on a probability space $(\Omega, \mathcal{F}, \mathbb{P})$. Let $(\Pi_n)_n$ be a sequence of partitions of a time interval $[0,T]$ such that $\|\Pi_n\| \to 0$ as $n \to \infty$. For a given partition Π_n, define $V_X(\Pi_n)$ as follows*

$$V_X(\Pi_n) = \sum_{i=0}^{n-1} \left(X_{t_{i+1}} - X_{t_i}\right)^2. \tag{2.35}$$

Then, provided the limit of $V_X(\Pi_n)$ exists, $[X,X]_T$ specified as

$$[X,X]_T = \lim_{n\to\infty} V_X(\Pi_n) \tag{2.36}$$

is called quadratic variation of X.

[11] Sometimes, first-order variation is defined as $FV_X \equiv \sup\left\{\sum_{t_i\in\Pi} |X(t_{i+1}) - X(t_i)| : \Pi \text{ is a partition of } [0,T]\right\}$, which is mathematically equivalent to (2.34).

In a financial context, $V_X(\Pi_n)$ is commonly referred to as realized variance or sampled quadratic variation. Fundamental properties of quadratic variation are summarized in the proposition below:[12]

Proposition 24 (Properties of Quadratic Variation)**.**

(i) *The existence of* $[X,X]_T$ *implies that* $[X,X]_t$ *is defined for all* $t \in [0,T]$*.*

(ii) $[X,X]_t$ *is an increasing process in* $t \in [0,T]$*.*

(iii) *The jumps of* $[X,X]_t$ *are related to the jumps of* X *by:* $\Delta[X,X]_t = |\Delta X_t|^2$*. In particular,* $[X,X]_t$ *has continuous sample paths if and only if* X *does.*

(iv) *If* X *is continuous and has paths of finite variation, then* $[X,X]_t = 0$ *for all* $t \in [0,T]$*.*

(v) *If* X *is a martingale and* $[X,X]_T = 0$*, then* $X = X_0$ *almost surely.*

Proof. (i) follows from Definition 23 with appropriate adjustments, i.e. $[X,X]_t \equiv \lim_{n\to\infty} V_X(\Pi_n, t)$ where $V_X(\Pi_n, t) \equiv \sum_{t_{i+1}\in\Pi_n; t_{i+1}<t} \left(X_{t_{i+1}} - X_{t_i}\right)^2$. (ii) and (iii) follow by construction. For (iv) note that if X is continuous, then $\sup_i \left|W_{t_{i+1}} - W_{t_i}\right| \to 0$ as $\|\Pi_n\| \to 0$ for $n \to \infty$. Therefore, in case of $[X,X]_T$, one obtains

$$\begin{aligned}
[X,X]_T &= \lim_{n\to\infty} \sum_{i=0}^{n-1} \left(X_{t_{i+1}} - X_{t_i}\right)^2 \\
&\leq \lim_{n\to\infty} \left(\sup_i \left|X_{t_{i+1}} - X_{t_i}\right| \sum_{i=0}^{n-1} \left(X_{t_{i+1}} - X_{t_i}\right) \right) \\
&= \lim_{n\to\infty} \sup_i \left|X_{t_{i+1}} - X_{t_i}\right| \cdot \lim_{n\to\infty} \sum_{i=0}^{n-1} \left(X_{t_{i+1}} - X_{t_i}\right) \\
&= \lim_{n\to\infty} \sup_i \left|X_{t_{i+1}} - X_{t_i}\right| \cdot FV_X \\
&= 0, \qquad (2.37)
\end{aligned}$$

since X is assumed to be of finite variation. As $[X,X]_t$ is non-negative and increasing in $t \in [0,T]$, the general result holds. For (v) we refer to in Jacod and Shiryaev (2013), Propositions 4.13 and 4.50. □

[12]The Δ-operator in Proposition 24 is defined as $\Delta X_t \equiv X_t - X_{t-}$, where X_{t-} denotes the left-limit of X at time t. For $\Delta[X,X]_t$ the analogous definition applies, where $\Delta[X,X]_t \equiv [X,X]_t - [X,X]_{t-}$.

Having established the fundamental definitions relevant to quadratic variation, we now proceed to examine the quadratic variation of stochastic processes relevant to modeling asset price dynamics. In particular, we focus on quadratic variation of Itô processes, Poisson processes, and certain jump-diffusion processes.

2.4.2 Quadratic Variation of Itô Processes

As previously discussed, Itô processes are conventionally employed for modeling diffusive dynamics. According to Definition 12, these processes are driven by Brownian motion. Consequently, to analyze the quadratic variation of Itô processes, it is imperative first to establish the properties of quadratic variation with respect to Brownian motion. This includes not only standard Brownian motion but also scaled Brownian motion, encompassing both constant and time-varying scaling. To begin, the quadratic variation of standard Brownian motion is detailed in the following theorem:

Theorem 25. *Let W be a Brownian motion. Then $[W,W]_T = T$ for all $T \geq 0$ a.s.*

Proof. Let Π_n be a partition of $[0,T]$. Then $V_W(\Pi_n)$ is given by

$$V_W(\Pi_n) = \sum_{i=0}^{n-1} (W_{t_{i+1}} - W_{t_i})^2. \tag{2.38}$$

According to Definition 7, $W_{t_{i+1}} - W_{t_i} \sim N(0, t_{i+1} - t_i)$ and the increments are independent. Therefore,

$$\mathbb{E}\left((W_{t_{i+1}} - W_{t_i})^2\right) = \mathbb{V}ar(W_{t_{i+1}} - W_{t_i}) = t_{i+1} - t_i, \tag{2.39}$$

and by independence

$$\mathbb{E}\left(V_W(\Pi_n)\right) = \sum_{i=0}^{n-1} \mathbb{E}\left((W_{t_{i+1}} - W_{t_i})^2\right) = \sum_{i=0}^{n-1} (t_{i+1} - t_i) = T. \tag{2.40}$$

Further, the variance of $(W_{t_{i+1}} - W_{t_i})^2$ is given by

$$\begin{aligned}\mathbb{V}ar\left((W_{t_{i+1}} - W_{t_i})^2\right) &= \mathbb{E}\left(\left((W_{t_{i+1}} - W_{t_i})^2\right)^2\right) - \mathbb{E}\left((W_{t_{i+1}} - W_{t_i})^2\right)^2 \\ &= \mathbb{E}\left((W_{t_{i+1}} - W_{t_i})^4\right) - (t_{i+1} - t_i)^2 \\ &= 3\,(t_{i+1} - t_i)^2 - (t_{i+1} - t_i)^2 \\ &= 2\,(t_{i+1} - t_i)^2\,, \end{aligned} \tag{2.41}$$

where we used in the second step that the fourth moment of a normal random variable with zero mean is three times its variance squared. Then, again by independence, it follows

$$\begin{aligned}\mathbb{V}ar\left(V_W(\Pi_n)\right) &= \mathbb{V}ar\left(\sum_{i=0}^{n-1}(W_{t_{i+1}} - W_{t_i})^2\right) = \sum_{i=0}^{n-1}\mathbb{V}ar\left((W_{t_{i+1}} - W_{t_i})^2\right) \\ &= \sum_{i=0}^{n-1} 2\,(t_{i+1} - t_i)^2 \leq \sum_{i=0}^{n-1} 2||\Pi_n||\,(t_{i+1} - t_i) = 2||\Pi_n||T. \end{aligned} \tag{2.42}$$

Since $\|\Pi_n\| \to 0$ as $n \to \infty$, it holds $\mathbb{V}ar\left(V_W(\Pi_n)\right) \to 0$. Thus, in conjunction with (2.40), we have proved that $V_W(\Pi_n)$ converges in mean square to T.[13] Mean square convergence implies convergence in probability. Furthermore, every sequence of random variables that converges in probability has a subsequence that converges almost surely. Therefore,

$$[W, W]_T = \lim_{n\to\infty} V_W(\Pi_n) = \mathbb{E}\left(V_W(\Pi_n)\right) = T \tag{2.43}$$

a.s. for a subsequence of $(\Pi_n)_{n\in\mathbb{N}}$. By convention, this subsequence is considered. □

In finance, Brownian motion is frequently scaled to account for various factors such as volatility adjustments and different time horizons. This scaling is crucial for accurately modeling the dynamics of financial processes. With a constant scaling factor applied to Brownian motion, the following result can be directly deduced from Theorem 25:

[13] Convergence in mean square is also called $\mathcal{L}^2$-convergence.

Corollary 26. *Let $X_t = \sigma W_t$ where σ is a constant and W is a Brownian motion. Then $[X, X]_T = \sigma^2 T$.*

Proof. The proof follows the same logic as the proof of Theorem 25. Since σ is a constant, conducting the individual steps is straightforward and thus omitted here. □

Given that volatility varies over time, the scaling of Brownian motion is frequently modeled as a time-dependent stochastic process. This time-varying scaling facilitates a more precise representation of the dynamic risk and uncertainty inherent in financial markets. The quadratic variation of such time-dependent scaling processes is characterized by the following proposition:[14]

Proposition 27. *Let X be a stochastic process defined as $X_{\bar{t}} \equiv \int_0^{\bar{t}} \sigma_t \mathrm{d}W_t$, $\bar{t} \in [0, T]$, where $(\sigma_t)_t$ is an adapted process and assume $\mathbb{E}\int_0^T \sigma_t^2 \mathrm{d}t < \infty$. Then the quadratic variation of X accumulated up to time T is*

$$[X, X]_T = \int_0^T \sigma_t^2 \mathrm{d}t. \tag{2.44}$$

Proof. Let Π_n be a partition of $[0, T]$ and let $X_{n,t}$ denote the Itô integral of the simple process $(\sigma_{(n,t)})_t$, i.e.

$$X_{n,T} = \int_0^T \sigma_{n,t} \mathrm{d}W_t, \tag{2.45}$$

where $\sigma_{(n,t)}$ is chosen such that[15]

$$\lim_{n\to\infty} \mathbb{E} \int_0^T \left|\sigma_{n,t} - \sigma_t\right|^2 \mathrm{d}t = 0. \tag{2.46}$$

Then, for the subinterval $[t_i, t_{i+1}]$ with $\sigma_{(n,t)}$ constant, denoted by σ_{t_i}, apply the following

[14]The process described in Proposition 27 is, in fact, a general Itô process with a drift of zero.

[15]Note that the assumption $\mathbb{E}\int_0^T \sigma_t^2 \mathrm{d}t < \infty$ ensures not only the quadratic variation of X to be finite, but also it is a necessary condition for the mean square convergence of the simple process $\sigma_{(n,t)}$. Readers unfamiliar with simple processes are referred to Appendix A.1, in which these processes are introduced in the context of the Itô integral.

subpartition $t_i = s_0 < s_1 < \ldots < s_m = t_{i+1}$ such that

$$\sum_{j=0}^{m-1} \left(X_{n,s_{j+1}} - X_{n,s_j}\right)^2 = \sum_{j=0}^{m-1} \left(\sigma_{t_i}\left(W_{s_{j+1}} - W_{s_j}\right)\right)^2 = \sigma_{t_i}^2 \sum_{j=0}^{m-1} \left(W_{s_{j+1}} - W_{s_j}\right)^2. \tag{2.47}$$

According to Corollary 26, this converges to $\sigma_{t_i}^2 (t_{i+1} - t_i)$ for $\max_j (s_{j+1} - s_j) \to 0$ as $m \to \infty$. Thus, in the limit, we can write

$$\lim_{m\to\infty} \sigma_{t_i}^2 \sum_{j=0}^{m-1} \left(W_{s_{j+1}} - W_{s_j}\right)^2 = \sigma_{t_i}^2 (t_{i+1} - t_i) = \int_{t_i}^{t_i+1} \sigma_{t_i}^2 \mathrm{d}t. \tag{2.48}$$

Since $\|\Pi_n\| \to 0$ as $n \to \infty$ implies $\max_j (s_{j+1} - s_j) \to 0$ for all subintervals $[t_i, t_{i+1}]$, the quadratic variation of X follows by concatenation of all subintervals and is given by

$$[X, X]_T = \int_0^T \sigma_t^2 \mathrm{d}t. \tag{2.49}$$

□

Finally, having established the quadratic variation for various processes driven by Brownian motion, ranging from basic to more complex processes, we now turn our attention to the quadratic variation of (general) Itô processes, stated in the proposition below:[16]

Proposition 28. *Let X be a (general) Itô process defined as $X_{\bar{t}} = X_0 + \int_0^{\bar{t}} \mu_t \mathrm{d}t + \int_0^{\bar{t}} \sigma_t \mathrm{d}W_t$, where $(\mu_t)_t$ and $(\sigma_t)_t$ are adapted processes with $\int_0^T \left|\mu_t\right| \mathrm{d}t < \infty$ and $\mathbb{E}\int_0^T \sigma_t^2 \mathrm{d}t < \infty$. Then, the quadratic variation of X accumulated up to time T is*

$$[X, X]_T = \int_0^T \sigma_t^2 \mathrm{d}t. \tag{2.50}$$

Proof. To ease notation, let $R_{\bar{t}} = \int_0^{\bar{t}} \mu_t \mathrm{d}t$ and $I_{\bar{t}} = \int_0^{\bar{t}} \sigma_t \mathrm{d}W_t$ for $\bar{t} \in [0, T]$. Note that both $R_{\bar{t}}$ and $I_{\bar{t}}$ are continuous in $\bar{t}$ as their upper limit of integration. Further, let Π_n be a partition

[16] In the remainder of this chapter, the general definition of Itô processes, as utilized in Proposition 28, is employed, where $(\mu_t)_t$ and $(\sigma_t)_t$ are simply adapted processes. This approach is intentional to demonstrate the generality of the results. However, within the context of diffusion processes commonly applied in finance, one should consider $\mu(t, X_t)$ as the drift term and $\sigma(t, X_t)$ as the diffusion term instead.

of $[0,T]$. Then, for $\bar{t}=T$, the sampled quadratic variation is given by

$$\begin{aligned}\sum_{i=0}^{n-1}\left(X_{t_{i+1}}-X_{t_i}\right)^2 &= \sum_{i=0}^{n-1}\left(\left(R_{t_{i+1}}+I_{t_{i+1}}\right)-\left(R_{t_i}+I_{t_i}\right)\right)^2\\ &= \sum_{i=0}^{n-1}\left(\left(R_{t_{i+1}}-R_{t_i}\right)+\left(I_{t_{i+1}}-I_{t_i}\right)\right)^2\\ &= \sum_{i=0}^{n-1}\left(\left(R_{t_{i+1}}-R_{t_i}\right)^2+\left(I_{t_{i+1}}-I_{t_i}\right)^2+2\left(R_{t_{i+1}}-R_{t_i}\right)\left(I_{t_{i+1}}-I_{t_i}\right)\right)\\ &= \sum_{i=0}^{n-1}\left(R_{t_{i+1}}-R_{t_i}\right)^2+\sum_{i=0}^{n-1}\left(I_{t_{i+1}}-I_{t_i}\right)^2+2\sum_{i=0}^{n-1}\left(R_{t_{i+1}}-R_{t_i}\right)\left(I_{t_{i+1}}-I_{t_i}\right).\end{aligned} \tag{2.51}$$

This decomposition allows us to compute the quadratic variation by taking the limit operator at each sum individually. According to Proposition 27, the second summation term converges to $\int_0^T \sigma_t \mathrm{d}t$ as $n\to\infty$. The first sum is bounded below by 0 and bounded above by

$$\begin{aligned}\sum_{i=0}^{n-1}\left(R_{t_{i+1}}-R_{t_i}\right)^2 &\le \max_i\left|R_{t_{i+1}}-R_{t_i}\right|\cdot\sum_{i=0}^{n-1}\left|R_{t_{i+1}}-R_{t_i}\right|\\ &= \max_i\left|R_{t_{i+1}}-R_{t_i}\right|\cdot\sum_{i=0}^{n-1}\left|\int_{t_i}^{t_{i+1}}\mu_t\mathrm{d}t\right|\\ &\le \max_i\left|R_{t_{i+1}}-R_{t_i}\right|\cdot\sum_{i=0}^{n-1}\int_{t_i}^{t_{i+1}}\left|\mu_t\right|\mathrm{d}t\\ &= \max_i\left|R_{t_{i+1}}-R_{t_i}\right|\cdot\int_0^T\left|\mu_t\right|\mathrm{d}t.\end{aligned} \tag{2.52}$$

Since $R_{\bar{t}}$ is continuous, $\max_i\left|R_{t_{i+1}}-R_{t_i}\right|$ converges to 0 as $n\to\infty$ and so the entire term does as the integral is assumed to be finite. The third sum is also bounded, i.e.

$$\begin{aligned}\left|\sum_{i=0}^{n-1}\left(R_{t_{i+1}}-R_{t_i}\right)\left(I_{t_{i+1}}-I_{t_i}\right)\right| &\le \max_i\left|I_{t_{i+1}}-I_{t_i}\right|\cdot\sum_{i=0}^{n-1}\left|R_{t_{i+1}}-R_{t_i}\right|\\ &= \max_i\left|I_{t_{i+1}}-I_{t_i}\right|\cdot\sum_{i=0}^{n-1}\left|\int_{t_i}^{t_{i+1}}\mu_t\mathrm{d}t\right|\\ &\le \max_i\left|I_{t_{i+1}}-I_{t_i}\right|\cdot\sum_{i=0}^{n-1}\int_{t_i}^{t_{i+1}}\left|\mu_t\right|\mathrm{d}t\\ &= \max_i\left|I_{t_{i+1}}-I_{t_i}\right|\cdot\int_0^T\left|\mu_t\right|\mathrm{d}t.\end{aligned} \tag{2.53}$$

Again, since $I_{\bar{t}}$ is continuous, $\max_i \left|I_{t_{i+1}} - I_{t_i}\right|$ converges to 0 as $n \to \infty$ and so the total term does as the integral is assumed to be finite. □

2.4.3 Quadratic Variation of Poisson Processes

Having established the quadratic variation of Itô processes, which are employed for modeling the diffusive dynamics of asset prices, we now focus on examining the quadratic variation within the framework of jump processes used in finance, specifically Poisson processes and compound Poisson processes. The analysis of the compensated versions of these processes is deferred to the subsequent section on jump-diffusion processes, as the compensation is incorporated into the drift component. To commence with the pure counting process, namely the standard Poisson process, its quadratic variation is described by the following proposition:

Proposition 29 (Quadratic Variation of a Poisson Process)**.** *Let N be a Poisson process. Then, the quadratic variation of N accumulated up to time T is given by*

$$[N, N]_T = N_T \tag{2.54}$$

Proof. The result is an immediate consequence of Definition 13. □

Building on this result, the quadratic variation of the compound Poisson process is addressed in the subsequent proposition. This proposition also introduces the concept of a jump measure, whose definition is provided within the corresponding proof.

Proposition 30 (Quadratic Variation of a Compound Poisson Process)**.** *Let J be a compound Poisson process according to Definition 17. Then, the quadratic variation of J accumulated up to time T is given by*

$$[J, J]_T = \sum_{t\in[0,T]}^{\Delta J_t \neq 0} \left|\Delta J_t\right|^2 = \sum_{i=1}^{N_T} \left|Y_i\right|^2 = \int_0^T \int_{\mathbb{R}} y^2 \mathcal{J}_J(\mathrm{d}y, \mathrm{d}t) \tag{2.55}$$

where $\Delta J_t = J_t - J_{t-}$, and $\mathcal{J}_J$ is the jump measure of the associated process J.

Proof. First note that the compound Poisson process is a pure jump process. Thus, J is constant for all $t \in (\mathcal{T}_i, \mathcal{T}_{i+1})_{i\geq 1}$ which implies $\Delta J_t = 0$ for those t. Therefore, only pure

jumps ($\Delta J_t \neq 0$) contribute to quadratic variation as indicated by the first equality. The second equality follows from definition of the compound Poisson process with N_t denoting the random but finite number of jumps between $[0, T]$ and Y_i the amplitude of the i'th jump. For the third equality, we first introduce the jump measure $\mathcal{J}_X$ of an associated process X (in our case J) in a general context:[17]

$$\mathcal{J}_X(\omega, .) = \sum_{i \geq 1} \delta_{(Y_i(\omega), \mathcal{T}_i(\omega))} = \sum_{t \in [0,T]}^{\Delta X_t \neq 0} \delta_{(\Delta X_t, t)}, \tag{2.56}$$

where $\delta_{(Y_i(\omega), \mathcal{T}_i(\omega))}$ denotes the Dirac measure, which is 1 if a jump of size $Y_i(\omega)$ occurs at time $\mathcal{T}_i(\omega)$ and zero otherwise. Since $\Delta X_t \neq 0$ at jump times only, we can also use the Dirac measure with respect to ΔX_t and t such that for $A \subseteq \mathbb{R}$, we can define

$$\mathcal{J}_X(A \times [0, T]) \equiv \text{number of jumps of } X \text{ whose amplitude belongs to } A$$
$$\text{and which occur between 0 and } T.$$

Consequently, it holds

$$\sum_{i=1}^{N_T} \left| Y_i \right|^2 = \int_0^T \int_{\mathbb{R}} y^2 \mathcal{J}_X(\mathrm{d}y, \mathrm{d}t), \tag{2.57}$$

which completes the proof.[18] □

2.4.4 Quadratic Variation of Jump-Diffusion Processes

After dealing with quadratic variation of Itô processes and Poisson processes, we now turn our attention to jump-diffusion processes, which integrate the characteristics of both types of processes. The quadratic variation of such jump-diffusion processes is given by the following proposition:[19]

[17] Since this is a general definition, we do not restrict ourselves to the specific process J and thus use X as the associated process.

[18] Please note that Cont (2004) defined the product measure J_X on the product space $[0, T] \times A$. To preserve the desired order of integration in (2.57), we flipped the product space and the corresponding Dirac measure, which is innocuous as integrability is implicitly assumed.

[19] Jump-diffusion processes are not restricted to a combination of Itô processes with compound Poisson processes. However, these two processes are the common choice in financial applications.

Proposition 31 (Quadratic Variation of a Jump-Diffusion Process)**.** *Let X be defined as*

$$X_{\bar{t}} = X_0 + \int_0^{\bar{t}} \mu_t \mathrm{d}t + \int_0^{\bar{t}} \sigma_t \mathrm{d}W_t + \sum_{t \in [0,\bar{t}]}^{\Delta J_t \neq 0} \Delta J_t, \tag{2.58}$$

where $(\mu_t)_t$ and $(\sigma_t)_t$ are adapted processes and $(J_t)_t$ a compound Poisson process. Further, let

$$X^c_{\bar{t}} = X_0 + \int_0^{\bar{t}} \mu_t \mathrm{d}t + \int_0^{\bar{t}} \sigma_t \mathrm{d}W_t \tag{2.59}$$

denote the continuous part of X with $\int_0^T \left|\mu_t\right| \mathrm{d}t < \infty$. Then the quadratic variation of X accumulated up to time T is

$$[X,X]_T = [X,X]^c_T + [J,J]_T = \int_0^T \sigma_t^2 \mathrm{d}t + \int_0^T \int_{\mathbb{R}} y^2 \mathcal{J}_J(\mathrm{d}y, \mathrm{d}t), \tag{2.60}$$

where $[X,X]^c_T = \int_0^T \sigma_t^2 \mathrm{d}t$ denotes the quadratic variation of the continuous part of X and $\mathcal{J}_J$ is the jump measure of the associated compound Poisson process.

Proof. Note that we have already established $[X,X]^c_T$ and $[J,J]_T$ in Propositions 28 and 30, respectively. For the remaining but tedious steps, we refer to the proof of Theorem 11.4.7 in Shreve (2004). □

It is crucial to note that the jump-diffusion process in Proposition 31 also includes the compensated compound Poisson process, as the adapted process $(\mu_t)_t$ absorbs not only the drift of the Itô process, but also the compensation of the compound Poisson process. Thus, according to this proposition, the drift term of a jump-diffusion process does not contribute to its quadratic variation.[20]

Having established the mathematical foundations of stochastic processes, we now turn our focus to their economic applications within derivatives pricing. The subsequent chapter will delve into the realm of option pricing theory.

[20]To qualify as a jump-diffusion process, the drift term μ_t in Proposition 31 must not only be adapted but also Markovian. If the continuous part $X^c_{\bar{t}}$ is not Markovian, it is not considered a diffusion process according to Definition 4. However, the result concerning its quadratic variation remains valid.

Chapter 3

Option Pricing Theory

In the past, option pricing theory was almost exclusively associated with mathematical models, where pricing is based on the so-called *risk-neutral (probability) measure*. The world-renowned option pricing model of Black and Scholes (1973) served as a catalyst in the mid-seventies such that numerous and by far more sophisticated models were developed in the following years, e.g. the jump-diffusion model of Merton (1976) or the stochastic volatility model of Heston (1993). Almost concurrently with the development of this parametric strand of the literature, a second, non-parametric strand of option pricing theory emerged. This approach focused on the extraction and modeling of the *risk-neutral density* from traded option prices, building on the foundational work of Breeden and Litzenberger (1978). Over the years, this second branch has gained in importance through the works of Jackwerth (2004), Figlewski (2010), Birru and Figlewski (2012), and many more.

Corresponding to the two strands of the literature, this chapter is structured as follows: Section 3.1 presents fundamental definitions and theorems of option pricing theory, along with explicit pricing models, beginning with the renowned Black and Scholes (1973) model and progressing to more advanced models. Section 3.2 is devoted to the derivation of the RND from observable option prices. In particular, it exposes the relation between option prices and the underlying RND, as described in Breeden and Litzenberger (1978), and briefly discusses prevalent techniques for RND modeling.

3.1 Option Pricing under the Risk-Neutral Measure

In contrast to obligatory claims such as forwards or futures, options are classified as contingent claims. Contingent claims are derivatives whose future payoffs, both in terms of amount and occurrence, depend on the evolution of the underlying asset's price. The pricing of these instruments is typically not conducted under the physical probability measure, which would involve incorporating a utility function to account for risk aversion. Instead, the no-arbitrage principle is employed to construct an equivalent martingale measure, commonly referred to as the risk-neutral measure. Under this probability measure, a hypothetical investor is assumed to be risk-neutral, eliminating the need to explicitly account for utility functions and individual risk preferences, which are often challenging or impractical to quantify. Instead, pricing relies on discounted expected future payoffs, highlighting the strength and widespread adoption of the risk-neutral measure in derivatives pricing, commonly known as risk-neutral pricing.

To gain a comprehensive understanding about options and risk-neutral pricing, we organize this section as follows: First, we recall the basic definitions and fundamental theorems in Subsection 3.1.1. Then, we proceed to the renowned Black and Scholes (1973) model, the first closed-form option pricing model. In this Subsection 3.1.2, we do not only derive the pricing formula, but also address the empirical deficiencies arising from the model's assumptions. Additionally, terminologies such as *implied volatility*, which are pertinent for price communication within the marketplace, are introduced. Finally, we discuss more elaborate option pricing models in Subsection 3.1.3. Due to their relevance in the remaining sections, we opt to present the jump-diffusion model of Merton (1976) and the affine jump-diffusion model with stochastic volatility and contemporaneous jumps (SVCJ) of Duffie et al. (2000) in more detail.[21]

[21] As this thesis focuses on the robust estimation of option-implied risk measures rather than on pricing models per se, we confine our discussion to the fundamental terminology pertinent to this objective. Consequently, we do not delve into the construction of the risk-neutral measure from the physical measure, nor do we address other mathematical aspects such as partial differential equations (PDEs), the Feynman-Kac theorem, and related topics.

3.1.1 Basic Definitions and Theorems

Options represent some of the most actively traded derivative securities, both on exchange and in over-the-counter markets. Despite the seemingly countless contractual variations of call and put options – the two general types of options – a fundamental distinction is often made based on exercise style, namely between European and American options. In the context of option-implied risk measures, our focus is specifically on (plain vanilla) options with European exercise style, which are defined as follows:[22]

Definition 32 (European-Style Call and Put Options)**.** *A European-style call (put) option securitizes the right to buy (sell) the underlying asset at a prespecified price at an agreed-upon future date. The price is called strike price or more briefly strike, while the future point in time is referred to as expiration or maturity date. At option expiry, the options' payoffs are respectively*

$$P_{Call}(S_T) = \max(S_T - K, 0) \qquad \textit{and} \qquad P_{Put}(S_T) = \max(K - S_T, 0), \tag{3.1}$$

where K denotes the strike price and S_T the underlying asset value at option expiry T.

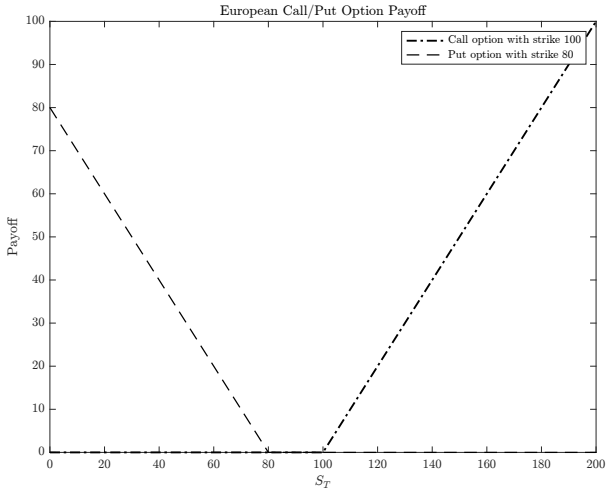

Figure 3.1: Payoffs of a European Call and Put Option – This figure plots the payoff functions of a European-style call option with strike 100 and a European-style put option with strike 80 at maturity T.

[22] As an alternative to the payoff functions in (3.1), one frequently encounters the abbreviated notations $(S_T - K)^+$ and $(K - S_T)^+$. At this stage, it is pertinent to emphasize that underlying asset S in Definition 32 will consistently refer to a stock for the remainder of this thesis, as the focus is exclusively on equity options. Moreover, American-style options will not be addressed due to their lack of relevance to option-implied risk measures, as outlined in the following section.

Since the future payoff of a long position in an option will always be non-negative, with $\mathbb{P}(P_{\cdot}(S_T) > 0) > 0$, no-arbitrage necessitates the upfront price paid to the underwriter, referred to as the *option price* or *premium*, to be strictly positive. As previously mentioned, such prices are determined under the risk-neutral measure, which is specified as follows:

Definition 33 (Risk-Neutral Measure)**.** *A probability measure $\mathbb{Q}$ on $(\Omega, \mathcal{F})$ is called risk-neutral measure if*

(i) $\mathbb{Q} \sim \mathbb{P}$*, i.e. for all* $A \in \mathcal{F}$ *it holds* $\mathbb{Q}(A) = 0 \Leftrightarrow \mathbb{P}(A) = 0$.

(ii) under $\mathbb{Q}$, the discounted stock price is a martingale, i.e. $e^{-rt}S_t = \mathbb{E}^{\mathbb{Q}}\left(e^{-rT}S_T \mid \mathcal{F}_t\right)$.

From a technical standpoint, the measure equivalence in condition (i), combined with the martingale property in condition (ii), establishes the risk-neutral measure $\mathbb{Q}$ as an equivalent martingale measure to $\mathbb{P}$.[23] The economic reason for pricing derivatives under such a measure stems from no one other than the first fundamental theorem of asset pricing, which links the existence of a risk-neutral measure with the principle of no-arbitrage, as described below:

Theorem 34 (First Fundamental Theorem of Asset Pricing)**.** *A security market model is arbitrage-free if and only if there exists at least one risk-neutral measure $\mathbb{Q}$.*

Proof. This rigorous formulation of the theorem applies exclusively in discrete-time. In a continuous-time setting, additional technical conditions must be assumed. For further details, we refer to Bingham and Kiesel (2004) and explicitly to Delbaen and Schachermayer (1994). □

It is imperative to emphasize that this theorem refers only to the existence and not to the uniqueness of a risk-neutral measure. The uniqueness of such a measure is related to market's completeness, posited in the second fundamental theorem of asset pricing:

Theorem 35 (Second Fundamental Theorem of Asset Pricing)**.** *Consider a security market model that admits (at least) one risk-neutral measure $\mathbb{Q}$. Then the market is complete if and only if $\mathbb{Q}$ is unique.*

Proof. Again, we refer to Bingham and Kiesel (2004). □

[23] In condition (ii), the money market account serves as the numéraire asset.

In the presence of jump risk, it is crucial to note that contingent claims are not perfectly replicable, thus they are classified as not attainable. This implies market incompleteness, leading to non-uniqueness of the risk-neutral measure $\mathbb{Q}$. However, practitioners utilize advanced hedging strategies to achieve close approximations, resulting in contingent claim prices that are nearly unique.[24] Consequently, financial markets are regarded as being close to complete. This perspective further asserts that the RND extracted from option prices, as describe in Section 3.2, is considered (almost) unique, even in the presence of jumps.

After introducing the necessary definitions and theorems, we now present the risk-neutral pricing formula employed in option pricing, stated in the following theorem:[25]

Theorem 36 (Risk-Neutral Pricing Formula)**.** *Let $(\Omega, \mathcal{F}, \mathbb{P})$ be a probability space equipped with filtration $\{\mathcal{F}_t\}_{t\in[0,T]}$ and $\mathbb{Q}$ be a risk-neutral measure equivalent to $\mathbb{P}$. Then, the time-t price Π of a contingent claim H with payoff at time T, is given by*

$$\Pi(t; H) = \mathbb{E}^{\mathbb{Q}}\left(e^{-\int_t^T r_s \mathrm{d}s} H \mid \mathcal{F}_t\right), \tag{3.2}$$

where r_s is the time-s short rate.

Proof. For the rigorous proof we refer to Harrison and Pliska (1981). □

The application of Theorem 36 to a European-style call option C with strike K and expiry T yields the following pricing formula:

$$\begin{aligned} C(t, \tau; K) &= e^{-r\tau}\mathbb{E}^{\mathbb{Q}}\left((S_T - K)^+ \mid \mathcal{F}_t\right) \\ &= e^{-r\tau}\int_{-\infty}^{\infty} (S_T - K)^+ \, q\left(S_T\right) \mathrm{d}S_T \\ &= e^{-r\tau}\int_{K}^{\infty} (S_T - K) \, q\left(S_T\right) \mathrm{d}S_T, \end{aligned} \tag{3.3}$$

where r denotes the constant risk-free rate, $\tau = T - t$ represents the time to option expiry,

[24] For pricing and hedging in incomplete markets, we refer to Cont (2004) or Privault (2013).

[25] In the context of non-attainable claims, prices may vary under different risk-neutral measures $\mathbb{Q}$. However, for attainable claims, prices are constrained to align with the value of the replication portfolio. Therefore, for these claims, the symbol Π in (3.2) is often substituted with V, which denotes the value of the replication portfolio.

and $q(.)$ denotes the (time-t conditional) risk-neutral density. Similarly, the pricing formula for a put option P reads

$$P(t,\tau;K) = e^{-r\tau}\int_0^K (K - S_T)\, q\,(S_T)\,\mathrm{d}S_T, \tag{3.4}$$

where in both cases the existence of the density $q(.)$ is assumed. The price of an option is typically decomposed into two distinct components, namely the *intrinsic value* and the *time value*. Additionally, in this context, one frequently encounters the term *moneyness*.[26] The definitions of these terms are as follows:

Definition 37 (Intrinsic Value, Time Value and Moneyness of an Option)**.** *For a call option C with underlying S, strike price K, and option expiry T, the intrinsic value, if the option were exercised immediately, is defined as* $\max(S_t - K, 0)$*. The difference between the call option price $C(t,\tau;K)$ and its intrinsic value is called the time value. Further, a call option is said to be in-the-money (ITM) if $S_t > K$, at-the-money (ATM) if $S_t = K$, and out-of-the money (OTM) if $S_t < K$. For put options, the analogous definitions apply.*

We conclude this section with a fundamental and exceedingly useful principle in option pricing, namely, the put-call parity:[27]

Theorem 38 (Put-Call Parity)**.** *Let C denote a European-style call option, and P denote a European-style put option, both written on the same underlying asset S with strike price K and option expiry T. Then, under the assumption of no-arbitrage, it holds*

$$C(t,\tau;K) - P(t,\tau;K) = S_t - e^{-r\tau}K, \tag{3.5}$$

where r denotes the constant risk-free rate and $\tau = T - t$ the time to expiration.

Proof. The proof follows from static no-arbitrage argument. Since the portfolio on the left-hand side generates the same payoff as the portfolio on the right-hand side at option expiry, their initial values must be identical due to the law of one price. □

[26] The (spot) moneyness can also be expressed as the ratio of the strike price K to the spot price S_t.

[27] Although it is not a theorem in a strict mathematical sense, put-call parity is often presented with the rigor and structure of a theorem to underscore its significance in financial mathematics.

3.1.2 The Black and Scholes (1973) Model

This subsection is dedicated to the seminal work of Black and Scholes (1973), who pioneered the first closed-form option pricing model. Despite its obsolescence in pure pricing applications, the model retains paramount importance not only for price communication, but also for deriving non-quoted, artificial option prices through volatility smile construction, as discussed Section 4.5.

In financial mathematics, the elegance of a simple closed-form pricing formula often necessitates strict and partially unrealistic assumptions, as it does in the Black and Scholes (1973) model. In particular, it is assumed that

1) the underlying is a non-dividend paying stock S, whose dynamics are determined by a geometric Brownian motion.
2) there are no transaction costs.
3) unlimited borrowing and lending is possible at the constant risk-free rate r.
4) there are no short-selling restrictions.

In more detail, the first assumption implies that under $\mathbb{Q}$ the evolution of S is specified as

$$\mathrm{d}S_t = rS_t\mathrm{d}t + \sigma S_t \mathrm{d}W_t, \tag{3.6}$$

where σ denotes the constant volatility and W is a standard Brownian motion. Applying Itô's formula for Itô processes to $f(t,x) = \ln(x)$ with partial derivatives[28]

$$\frac{\partial f}{\partial t}(t,S_t) = 0 \qquad \frac{\partial f}{\partial x}(t,S_t) = \frac{1}{S_t} \qquad \frac{\partial^2 f}{\partial x^2}(t,S_t) = -\frac{1}{S_t^2} \tag{3.7}$$

gives

$$\begin{aligned} \ln(S_T) &= \ln(S_0) + \int_0^T \left(r - \frac{1}{2}\sigma^2\right)\mathrm{d}t + \int_0^T \sigma \mathrm{d}W_t \\ &= \ln(S_0) + \left(r - \frac{1}{2}\sigma^2\right)T + \sigma W_T, \end{aligned} \tag{3.8}$$

[28]Readers unfamiliar with Itô's formula for Itô processes are referred to Theorem 47 in Appendix A.2.

where $\int_0^T \sigma \mathrm{d}W_t = \sigma W_T$ follows from construction of the Itô integral.[29] Taking the exponential of (3.8) yields

$$S_T = S_0 \exp\left\{\left(r - \frac{1}{2}\sigma^2\right)T + \sigma W_T\right\} \tag{3.9}$$

such that the discounted stock price process is a martingale according to Theorem 11. Equation (3.9) implies that S_T follows a log-normal distribution under the risk-neutral measure $\mathbb{Q}$, with a mean of $\ln S_0 + \left(r - \frac{1}{2}\sigma^2\right)T$ and a variance of $\sigma^2 T$. Equivalently, in terms of the log-return, $\ln(S_T/S_0)$ is normally distributed with mean $\left(r - \frac{1}{2}\sigma^2\right)T$ and variance $\sigma^2 T$. Clearly, the distributional assumptions of the Black and Scholes (1973) model deviate from the stylized facts of financial data, which will be discussed further at the end of this subsection. Nonetheless, their famous option pricing formula is presented first in the following theorem:[30]

Theorem 39 (Black-Scholes Formula)**.** *In the Black and Scholes (1973) model, the time-t no-arbitrage price of a European-style call option C_{BS} with underlying S, volatility σ, strike K, option expiry T, and risk-free interest rate r is given by*

$$C_{BS}(t, S; \sigma, r, K, T) = S_t \Phi(d_1) - e^{-r(T-t)} K \Phi(d_2), \tag{3.10}$$

where $\Phi(.)$ denotes the distribution function of the standard normal distribution and

$$d_1 = \frac{\ln(S_t/K) + (r + \frac{1}{2}\sigma^2)(T-t)}{\sigma\sqrt{T-t}} \quad \text{and} \quad d_2 = d_1 - \sigma\sqrt{T-t}. \tag{3.11}$$

Proof. Herein, we present a probabilistic proof, analogous to the one presented by Frey (2017).[31] Without loss of generality, assume $t = 0$ such that $\tau = T$. Then, according to

[29] For more details, readers are directed to Appendix A.1.

[30] Similarly to Theorem 38, the Black-Scholes formula is no theorem in a strict mathematical sense. Due to its importance in financial mathematics, though, it is presented as one.

[31] The proof presented in Frey (2017) differs slightly as it employs the Girsanov theorem, which is not covered in this thesis.

(3.3), the call option value is given by[32]

$$C(0,T;K) = e^{-rT}\mathbb{E}^{\mathbb{Q}}\left((S_T - K)^+\right), \tag{3.12}$$

where S_T is specified by Equation (3.9), i.e.

$$S_T = S_0 \exp\left\{\left(r - \frac{1}{2}\sigma^2\right)T + \sigma W_T\right\} \equiv \exp\{X\} \tag{3.13}$$

with $X \sim \mathcal{N}\left(\ln S_0 + \left(r - \frac{1}{2}\sigma^2\right)T, \sigma^2 T\right)$. Then, to ease notation, define

$$\alpha \equiv \frac{e^{-rT}}{\sqrt{2\pi\sigma^2 T}} \qquad \mu \equiv \ln S_0 + \left(r - \frac{1}{2}\sigma^2\right)T \qquad \tilde{\sigma} \equiv \sigma\sqrt{T} \tag{3.14}$$

such that

$$\begin{aligned}
C(0,T;K) &= e^{-rT}\mathbb{E}^{\mathbb{Q}}\left((e^X - K)^+\right) \\
&= \alpha \int_{-\infty}^{\infty} (e^x - K) \exp\left\{-\frac{(x-\mu)^2}{2\tilde{\sigma}^2}\right\} \mathbb{1}_{\{e^x > K\}} \mathrm{d}x \\
&= \alpha \int_{\ln K}^{\infty} e^x \exp\left\{-\frac{(x-\mu)^2}{2\tilde{\sigma}^2}\right\} \mathrm{d}x - \alpha K \int_{\ln K}^{\infty} \exp\left\{-\frac{(x-\mu)^2}{2\tilde{\sigma}^2}\right\} \mathrm{d}x \\
&= \alpha \underbrace{\int_{\ln K}^{\infty} \exp\left\{x - \frac{(x-\mu)^2}{2\tilde{\sigma}^2}\right\} \mathrm{d}x}_{\equiv I_1} - \alpha K \underbrace{\int_{\ln K}^{\infty} \exp\left\{-\frac{(x-\mu)^2}{2\tilde{\sigma}^2}\right\} \mathrm{d}x}_{\equiv I_2}.
\end{aligned} \tag{3.15}$$

To compute αI_1, we rewrite the integrand as a normal density with new mean including a deterministic correction term. The integrand is of the form $\exp\{\lambda(x)\}$ with

$$\begin{aligned}
\lambda(x) &= x - \frac{(x-\mu)^2}{2\tilde{\sigma}^2} \\
&= -\frac{-2\tilde{\sigma}^2 x + x^2 - 2\mu x + \mu^2}{2\tilde{\sigma}^2} \\
&= -\frac{\left(x - (\mu + \tilde{\sigma}^2)\right)^2 + (\mu^2 - (\mu + \tilde{\sigma}^2)^2)}{2\tilde{\sigma}^2} \\
&= -\frac{\left(x - (\ln S_0 + (r + \frac{1}{2}\sigma^2)T)\right)^2}{2\sigma^2 T} + (\ln S_0 + rT),
\end{aligned} \tag{3.16}$$

[32] Since $\mathcal{F}_0$ is trivial, we omit the conditioning for simplicity.

where in the last step we used $\mu + \tilde{\sigma}^2 = \ln S_0 + (r + \frac{1}{2}\sigma^2)T$ and $-\frac{\mu^2 - (\mu+\tilde{\sigma}^2)^2}{2\tilde{\sigma}^2} = \mu + \frac{1}{2}\tilde{\sigma}^2 = \ln S_0 + rT$. Since $\alpha \exp(\ln S_0 + rT) = \frac{1}{\sqrt{2\pi\sigma^2 T}} S_0$, we obtain

$$\alpha I_1 = S_0 \int_{\ln K}^{\infty} \frac{1}{\sqrt{2\pi\sigma^2 T}} \exp\left\{ -\frac{\left(x - \left(\ln S_0 + \left(r + \frac{1}{2}\sigma^2\right) T\right)\right)^2}{2\sigma^2 T} \right\} \mathrm{d}x. \tag{3.17}$$

Consider $\tilde{X} \sim \mathcal{N}\left(\ln S_0 + \left(r + \frac{1}{2}\sigma^2\right) T, \sigma^2 T\right)$ such that $\frac{\tilde{X} - \ln S_0 - \left(r + \frac{1}{2}\sigma^2\right)T}{\sigma\sqrt{T}} \sim \mathcal{N}(0,1)$. Then, we obtain

$$\begin{aligned}
\alpha I_1 &= S_0 \mathbb{Q}(\tilde{X} > \ln K) \\
&= S_0 \mathbb{Q}\left(\frac{\tilde{X} - \ln S_0 - \left(r + \frac{1}{2}\sigma^2\right) T}{\sigma\sqrt{T}} > -d_1 \right) \\
&= S_0 (1 - \Phi(-d_1)) \\
&= S_0 \Phi(d_1).
\end{aligned} \tag{3.18}$$

Similarly, it follows that $\alpha K I_2 = e^{-rT} K \Phi(d_2)$, where the quadratic substitution (Equation (3.16)) is not required. □

The corresponding formula for a European-style put option follows directly from put-call parity. Rearranging Equation (3.5) of Theorem 38 gives the put option pricing formula

$$\begin{aligned}
P_{BS}(t, S; \sigma, r, K, T) &= C_{BS}(t, S; \sigma, r, K, T) - S_t + e^{-r(T-t)} K \\
&= S_t \Phi(d_1) - e^{-r(T-t)} K \Phi(d_2) - S_t + e^{-r(T-t)} K \\
&= e^{-r(T-t)} K (1 - \Phi(d_2)) - S_t (1 - \Phi(d_1)) \\
&= e^{-r(T-t)} K \Phi(-d_2) - S_t \Phi(-d_1),
\end{aligned} \tag{3.19}$$

where the symmetry of the standard normal distribution was used in the last step. As previously mentioned, the Black and Scholes (1973) is widely used for price communication is financial markets. For equity options, prices of European-style options are commonly quoted in terms of the so-called *implied volatility* for a given strike price, which is defined as follows:

Definition 40 (Implied Volatility)**.** *Assume that a call option C^* with underlying S, strike price K, and option expiry T is traded at the market. The implied volatility, denoted by $\hat{\sigma}_{imp}$, is the volatility parameter in the Black-Scholes formula that, when used as a plug-in estimate, recovers the quoted option price, i.e.*

$$C_{BS}(t, S; \hat{\sigma}_{imp}, r, K, T) = C^*(t, \tau; K), \tag{3.20}$$

where $\tau = T - t$ denotes the time to expiration. The equivalent expression holds true for European put options as well.

It should be noted that $\frac{\partial C_{BS}}{\partial \sigma}$ $\left(\frac{\partial P_{BS}}{\partial \sigma}\right)$ – commonly referred to as the *Vega* of an option – is strictly positive, which implies that C_{BS} (P_{BS}) is strictly increasing in σ. Therefore, a unique solution to (3.20) exists, which is found by applying standard numerical procedures.

Again, we wish to emphasize that the model presented by Black and Scholes (1973) serves primarily as a tool for price communication rather than as a definitive pricing model. While this model assumes a constant volatility parameter across both strike prices and maturities, observed implied volatilities at various strike levels typically exhibit a characteristic pattern known as the *implied volatility smile*, which is illustrated in the figure below:[33]

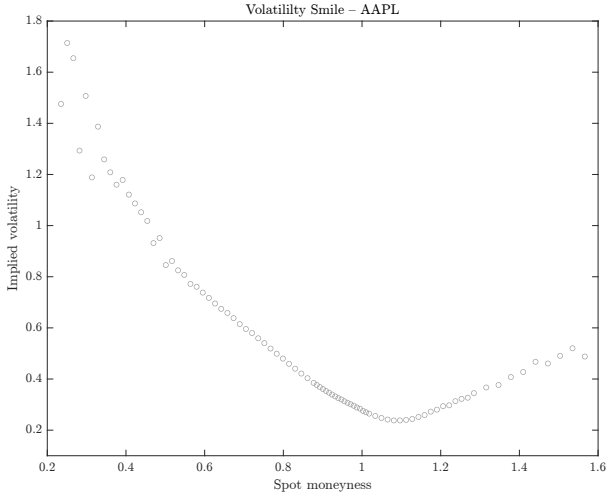

Figure 3.2: Volatility Smile – AAPL – This figure plots Black and Scholes (1973) implied volatilities of option contracts written on Apple (AAPL) stocks with 30 days to expiration, observed on May 20, 2020. Options data is obtained from OptionMetrics.

[33]Extending this concept across different maturities leads to the development of the *volatility surface*.

The empirical evidence of the existence of the volatility smile signifies a violation of the Black and Scholes (1973) model assumptions. In particular, the assumption of normally distributed log-returns is contrary to empirical facts of financial data, which include, but are non-exhaustive, the following:[34]

- Gain/loss asymmetry: Stock price declines are typically of larger amplitude than inclines, which leads to left-skewed log-returns.
- Volatility clustering: Periods of high volatility tend to cluster together in turbulent market phases, while periods of low volatility cluster together in tranquil market phases. This pattern is also evident in the autocorrelation of absolute returns, which exhibits a slow decay over time, contrasting with the faster decay observed in returns themselves.
- Heavy tails: The time series of log-returns exhibits heavy tails, a characteristic that persists to a considerable extend after adjusting for volatility clustering.

In response to the insufficiency of the Black and Scholes (1973) model, more sophisticated models incorporating stochastic volatility and/or jumps were developed, as discussed in the following subsection.

3.1.3 More Elaborate Models

Shortly after Black and Scholes (1973), Merton (1976) augmented the geometric Brownian motion process by incorporating an additional log-normally distributed jump component. It then took almost 20 years until Heston (1993) provided an option pricing model that accounts for the second source of risk, namely stochastic volatility. Specifically, he modeled the volatility component with a square-root process, also known as the CIR process.[35] Four years later, Bates (1996) combined both risk-factors in his jump-diffusion model by extending the Heston (1993) model with a log-normally distributed jump component. Bakshi et al. (1997) generalized the Bates (1996) model by relaxing the assumptions regarding the jump size distribution. At the turn of the millennium, Bates (2000) proposed a two-factor

[34] For further details, readers are referred to Pagan (1996), Campbell et al. (1997), and Cont (2001).

[35] The acronym CIR refers to the authors of Cox et al. (1985), who established this type of process. Readers unfamiliar with this process are recommended to consult this source.

jump diffusion model, incorporating a second square-root process to enhance flexibility in modeling stochastic volatility. Almost simultaneously, Duffie et al. (2000) presented their affine jump-diffusion model with stochastic volatility and contemporaneous jumps (SVCJ). This model allows for jumps not only is the stock's return process, but also in the volatility dynamics, hereby facilitating interaction between the jump sizes. This enormous degree of flexibility is the reason why it still serves as a benchmark model for various studies, e.g. Aschakulporn and Zhang (2022b).

Due to their relevance for subsequent sections of this thesis, we confine ourselves to present the jump diffusion model of Merton (1976) and the SVCJ model of Duffie et al. (2000). Besides the models' dynamics, we also provide their implementation based on Fourier transform techniques. Details to option pricing via Fourier transform can be found in Appendix B.

Jump-Diffusion Model of Merton (1976)

In the jump diffusion model of Merton (1976) the stock price dynamics under $\mathbb{Q}$ are[36]

$$\mathrm{d}S_t = (r - \lambda\mu_X)S_t\mathrm{d}t + \sigma S_t \mathrm{d}W_t + S_t\left(e^{X_t} - 1\right)\mathrm{d}N_t, \tag{3.21}$$

where r denotes the constant risk-free rate, σ denotes the volatility, and W_t is a standard Brownian motion. N_t is a Poisson counter with intensity λ. The jump size X at time t follows a normal distribution

$$X_t \sim \mathcal{N}\Big(\underbrace{\ln(1+\mu_X) - \frac{1}{2}\sigma_X^2}_{\equiv\alpha}, \sigma_X^2\Big) \tag{3.22}$$

such that $\mathbb{E}^{\mathbb{Q}}\left[e^{X_t} - 1\right] = e^{\alpha + \frac{1}{2}\sigma_X^2} - 1 = \mu_X$ is the expected (relative) jump size and σ_X the (relative) jump size volatility.

[36] As it is common in finance, stock price dynamics are given in differential form. The last term with respect to the Poisson counter is equivalent to $\int_0^T \int_{\mathbb{R}_0} (e^x - 1) S_t \mathcal{J}_X(\mathrm{d}x, \mathrm{d}t)$ in integral form, as utilized in the previous chapter.

First introduced by Lewis (2002), the characteristic function of the logarithmic stock price, according to Branger (2004), is given by[37]

$$\varphi(u) = e^{\alpha(u,\tau)+\mathrm{i}u\ln S_t}, \tag{3.23}$$

where $\tau = T - t$ and

$$\alpha(u,\tau) = r\mathrm{i}u\tau + 0.5\mathrm{i}u(\mathrm{i}u-1)\sigma^2\tau - \left(\mathbb{E}^{\mathbb{Q}}\left(e^{X_t}-1\right)\mathrm{i}u - \mathbb{E}^{\mathbb{Q}}\left(e^{\mathrm{i}uX_t}-1\right)\right)\lambda\tau \tag{3.24}$$

with

$$\mathbb{E}^{\mathbb{Q}}\left(e^{X_t}-1\right) = \mu_X \quad \text{and} \quad \mathbb{E}^{\mathbb{Q}}\left(e^{\mathrm{i}uX_t}-1\right) = (1+\mu_X)^{\mathrm{i}u}\exp\left\{-\frac{1}{2}\sigma_X^2\left(\mathrm{i}u+u^2\right)\right\} - 1. \tag{3.25}$$

Using the Black-Scholes style pricing formula, the call option price follows from[38]

$$C(0,T;K) = S_0\Pi_1 - e^{-rT}K\Pi_2, \tag{3.26}$$

where[39]

$$\begin{aligned}\Pi_j &= \frac{1}{2} + \frac{1}{\pi}\int_{-\infty}^{\infty}\Re\left(\frac{e^{-\mathrm{i}u\ln K}\varphi_j(u)}{\mathrm{i}u}\right)\mathrm{d}u,\\ \varphi_j(u) &= \begin{cases}\dfrac{\varphi(u-\mathrm{i})}{\varphi(-\mathrm{i})}, & \text{if } j=1,\\ \varphi(u), & \text{if } j=2.\end{cases}\end{aligned} \tag{3.27}$$

The corresponding put option price formula follows from put-call parity, as demonstrated in Appendix B.2.

[37] It is important to note that in Branger (2004), $\varphi(u)$ denotes the state-price density of $\ln S_T$, defined as $\varphi(u) = \mathbb{E}^{\mathbb{Q}}\left(e^{-rT}e^{\mathrm{i}u\ln S_T}\right)$. Accordingly, to utilize the framework presented in Appendix B, $\varphi(u)$ is adjusted appropriately.

[38] For readers unfamiliar with this pricing formula, we refer to Appendix B.2.

[39] The adjustment of $\varphi(u)$ leads to slightly different conditional probabilities Π_j compared to those of Branger (2004). However, the overall pricing formulas remain equivalent.

SVCJ Model of Duffie et al. (2000)

In the SVCJ model of Duffie et al. (2000), the dynamics of the stock price under $\mathbb{Q}$ are specified by

$$\begin{aligned} \mathrm{d}S_t &= (r - \lambda\,\mu_X)S_t\mathrm{d}t + \sqrt{V_t}S_t\mathrm{d}W_t^S + (e^{X_t} - 1)S_t\mathrm{d}N_t, \\ \mathrm{d}V_t &= \kappa(\theta - V_t)\mathrm{d}t + \sigma\sqrt{V_t}\,\mathrm{d}W_t^V + y\mathrm{d}N_t - \lambda\mu_y\mathrm{d}t, \end{aligned} \tag{3.28}$$

where r denotes the constant risk-free interest rate. V_t denotes the stochastic variance driven by a square-root process with speed κ, long-term mean θ, and diffusive volatility σ. The Brownian motion of the stock price process W_t^S and of the variance W_t^V have correlation ρ. N_t is a Poisson counter with intensity λ. Given the occurrence of a contemporaneous jump, the variance rate jump size y is exponentially distributed with mean μ_y, while the price jump size X is normally distributed with mean $\mu_X + \rho_J y$ and variance σ_X, where ρ_J denotes the jump sizes correlation.

According to Aschakulporn and Zhang (2022b), the characteristic function of log-returns is given by

$$\varphi(u) = e^{\alpha(u,\tau)+\beta(u,\tau)V_t}, \tag{3.29}$$

where

$$\begin{aligned} \alpha(u,\tau) = {} & r\mathrm{i}u\tau + \frac{\kappa\theta - \lambda\mu_y}{\sigma^2}\left((\kappa - \rho\sigma\mathrm{i}u + d)\tau - 2\ln\left(\frac{1 - ge^{d\tau}}{1-g}\right)\right) \\ & + \lambda\frac{\exp\left\{\mathrm{i}u\mu_X + \frac{1}{2}(\mathrm{i}u)^2\sigma_X^2\right\}}{1 - \mathrm{i}u\rho_J\mu_y} \times \left(\frac{\tau}{1-a} - \frac{a(1-g)}{d(1-a)(a-g)}\ln\left(1 + \frac{(g-a)(1-e^{d\tau})}{1-g}\right)\right) \\ & - \lambda\tau\left(1 + \mathrm{i}u\left(\frac{e^{\mu_X + \frac{1}{2}\sigma_X}}{1 - \rho_J\mu_y} - 1\right)\right), \\ \beta(u,\tau) = {} & \frac{\kappa - \rho\sigma\mathrm{i}u + d}{\sigma^2}\left(\frac{1 - e^{d\tau}}{1 - ge^{d\tau}}\right), \end{aligned} \tag{3.30}$$

and

$$d = \sqrt{(\rho\sigma \mathrm{i}u - \kappa)^2 + \sigma^2 \mathrm{i}u(1 - \mathrm{i}u)}, \quad g = \frac{\kappa - \rho\sigma \mathrm{i}u + d}{\kappa - \rho\sigma \mathrm{i}u - d}, \quad a = \frac{\mu_y}{1 - \mathrm{i}u\rho_J\mu_y} \frac{\kappa - \rho\sigma \mathrm{i}u + d}{\sigma^2}. \tag{3.31}$$

Using the Black-Scholes style pricing formula, the call option price follows from[40]

$$C(0, T; K) = S_0\Pi_1 - e^{-rT}K\Pi_2, \tag{3.32}$$

where

$$\begin{aligned} \Pi_j &= \frac{1}{2} + \frac{1}{\pi}\int_{-\infty}^{\infty} \Re\left(\frac{e^{-\mathrm{i}u\ln(K/S_0)}\varphi_j(u)}{\mathrm{i}u}\right) \mathrm{d}u, \\ \varphi_j(u) &= \begin{cases} \dfrac{\varphi(u - \mathrm{i})}{\varphi(-\mathrm{i})}, & \text{if } j = 1, \\ \varphi(u), & \text{if } j = 2. \end{cases} \end{aligned} \tag{3.33}$$

The corresponding put option price formula follows from put-call parity, as demonstrated in Appendix B.2.

3.2 Extraction of the RND from Option Prices

In the preceding section, mathematical models for option pricing were examined, wherein assumptions about the RND were predetermined. In the present context, we invert this approach by deducing the RND from traded option prices. Therefore, we first expose the relation between option prices and the RND, as shown by Breeden and Litzenberger (1978), before addressing issues in the context of estimation:

By recalling Equation (3.3), the value of a call option C at time t follows from

$$C(t, \tau; K) = e^{-r\tau}\int_K^{\infty} (S_T - K)\, q\,(S_T)\, \mathrm{d}S_T. \tag{3.34}$$

[40] For readers unfamiliar with this pricing formula, we refer to Appendix B.2.

Taking the first derivative of $C(t,\tau;K)$ with respect to K yields

$$\begin{aligned}\frac{\partial C(t,\tau;K)}{\partial K} &= \frac{\partial}{\partial K}\left(e^{-r(T-t)}\int_K^\infty (S_T-K)\,q\,(S_T)\,\mathrm{d}S_T\right)\\ &= e^{-r\tau}\left(-(K-K)\,f(K)+\int_K^\infty -q\,(S_T)\,\mathrm{d}S_T\right)\\ &= -e^{-r\tau}\int_K^\infty q(S_T)\mathrm{d}S_T\\ &= -e^{-r\tau}\,(1-Q(K))\,,\end{aligned} \tag{3.35}$$

where $Q(.)$ denotes the (time-t conditional) risk-neutral cumulative distribution function (CDF) evaluated at strike K. Rearranging Equation (3.35) to $Q(K)$ gives

$$Q(K) = e^{r\tau}\frac{\partial C(t,\tau;K)}{\partial K} + 1. \tag{3.36}$$

The risk-neutral probability density function (PDF) evaluated at strike K follows from the second derivative of $C(t,\tau;K)$ with respect to K

$$q(K) = e^{r\tau}\frac{\partial^2 C(t,\tau;K)}{\partial K^2}. \tag{3.37}$$

However, since the exact functional relation is unknown, CDF and PDF values in Equations (3.36) and (3.37) must be approximated. One possible approach is to use finite differences, as pointed out by Birru and Figlewski (2012):

Consider N option contracts with evenly spaced strike prices $K_1, K_2, \ldots, K_N$ in ascending order and let $\Delta K = K_{n+1} - K_n$. Then, for strike price K_n we get

$$\hat{Q}(K_n) = e^{r\tau}\frac{C(t,\tau;K_{n+1}) - C(t,\tau,K_{n-1})}{2\Delta K} + 1 \tag{3.38}$$

and

$$\hat{q}(K_n) = e^{r\tau}\frac{C(t,\tau;K_{n+1}) - 2C(t,\tau;K_n) + C(t,\tau;K_{n-1})}{(\Delta K)^2}, \tag{3.39}$$

where $\hat{Q}(.)$ and $\hat{q}(.)$ denote the approximated risk-neutral CDF and PDF, respectively.

For put options, which are priced by Equation (3.4) as follows

$$P(t,\tau;K) = e^{-r\tau}\int_0^K (K - S_T)\, q\,(S_T)\,\mathrm{d}S_T, \tag{3.40}$$

the equivalent expressions for Equations (3.36) and (3.37) are

$$Q(K) = e^{r\tau}\frac{\partial P(t,\tau;K)}{\partial K}, \tag{3.41}$$

$$q(K) = e^{r\tau}\frac{\partial^2 P(t,\tau;K)}{\partial K^2}. \tag{3.42}$$

Similarly, (3.41) and (3.42) can be approximated as follows

$$\hat{Q}(K_n) = e^{r\tau}\frac{P(t,\tau;K_{n+1}) - P(t,\tau;K_{n-1})}{2\Delta K}, \tag{3.43}$$

$$\hat{q}(K_n) = e^{r\tau}\frac{P(t,\tau;K_{n+1}) - 2P(t,\tau;K_n) + P(t,\tau;K_{n-1})}{(\Delta K)^2}. \tag{3.44}$$

Equations (3.38) and (3.39), or rather (3.43) and (3.44), imply that options must be available for a dense grid of evenly spaced strikes covering a sufficiently wide moneyness range in order to approximate the entire RND by finite differences. Since this prerequisite is typically not fulfilled in the marketplace, semi-parametric techniques are usually employed for RND modeling.[41] The central portion of the RND is approximated by finite differences, utilizing non-parametric interpolation and smoothing techniques to generate the required strike price grid. The tails of the RND are modeled parametrically, with appropriate distributions parameterized such that the overall RND constitutes a composite distribution. Given that RND tail modeling involves extrapolating option prices according to (3.3) and (3.4), it can also be interpreted as the extrapolation of the volatility smile. Consequently, as interpolation and smoothing are typically performed in the implied volatility domain, estimating the RND from option prices necessitates the construction of the entire volatility smile. Since option-implied risk measures require the same task for estimation, as discussed in Section

[41] There are also pure parametric approaches for RND modeling, such as the mixture of lognormal distributions (Bahra (1997)). However, due to their limited flexibility, they are considered obsolete (Birru and Figlewski (2012)).

4.5, volatility smile constructions is regarded as the fundamental basis for both of these objectives. Therefore, owing to its paramount significance within the scope of this thesis, an entire chapter is dedicated to our arbitrage-free RND-based smile construction approach, which guarantees robust risk measure estimation despite the presence of microstructure noise.

Chapter 4

Option-Implied Risk Measures

This chapter introduces the option-implied risk measures integral to this thesis, which are the BKM risk-neutral moments of the holding period log-return, the CBOE Volatility Index, commonly referred to as the $\mathbb{VIX}$, and the rare disaster concern index of Gao et al. (2018), known as the $\mathbb{RIX}$. The term *option-implied* indicates that these risk measures are derived exclusively from traded option prices, making them inherently forward-looking by construction. To estimate these measures, it is necessary to approximate their associated payoff structures, which is typically achieved by constructing replication portfolios consisting of OTM put and call options. The underlying cooking recipe for setting up these portfolios – known as generic spanning – is based on the fundamental theorem of calculus in conjunction with risk-neutral option pricing. As it requires a continuum of OTM option prices, which is typically not fulfilled in the market, volatility smile construction is required to approximate the missing prices.

To provide a thorough understanding of the risk-measures discussed of this thesis, the chapter is structured as follows: Section 4.1 presents a step-by-step derivation of the generic spanning formula, which forms the foundation for the replication portfolios addressed in subsequent sections. Thereafter, the BKM risk-neutral moments of the holding period log-return are examined in Section 4.2, followed up by the most prominent option-implied risk measure, the $\mathbb{VIX}$, in Section 4.3. Finally, the most complex yet relevant risk measure of this thesis in presented in Section 4.4, namely jump and tail risk measure $\mathbb{RIX}$. Since the $\mathbb{RIX}$ is

grounded in the jump and tail index ($\mathbb{JTIX}$) of Kapadia and Du (2012), the $\mathbb{JTIX}$ will be elucidated first, before discussing the $\mathbb{RIX}$ and its associated replication portfolio. The chapter concludes with the estimation of the respective risk measures via volatility smile construction in Section 4.5. This section also outlines the limitations of prevalent smile construction techniques, which serve as a motivation for our arbitrage-free RND-based smile construction approach, covered in the subsequent chapter.

4.1 Generic Spanning

The term *generic spanning* refers to linear algebra. In a financial context, this means that the space of a wide range of complex payoffs is spanned by standard (generic) derivatives, specifically European-style OTM option contracts. This concept serves as the foundational framework for constructing replication portfolios associated with the risk measures discussed subsequently and will be introduced in the following:

Consistent with Bakshi et al. (2003), let S be an abbreviation for S_T, then for any twice continuously differentiable payoff function $H(S)$, i.e. $H(S) \in \mathcal{C}^2$, which is integrable with respect to risk-neutral measure $\mathbb{Q}$, i.e. $\int_0^\infty |H(S)|\, q(S)\mathrm{d}S < \infty$, it holds

$$\begin{aligned}
H(S) - H(\bar{S}) &= \int_{\bar{S}}^{S} H'(x)\mathrm{d}x \\
&= \int_{\bar{S}}^{S} (H'(x) - H'(\bar{S}) + H'(\bar{S}))\mathrm{d}x \\
&= \int_{\bar{S}}^{S} H'(\bar{S})\mathrm{d}x + \int_{\bar{S}}^{S} (H'(x) - H'(\bar{S}))\mathrm{d}x \\
&= (S - \bar{S})H'(\bar{S}) + \int_{\bar{S}}^{S}\int_{\bar{S}}^{x} H''(K)\mathrm{d}K\,\mathrm{d}x \\
&= (S - \bar{S})H'(\bar{S}) + \int_{\bar{S}}^{S}\int_{K}^{S} H''(K)\mathrm{d}x\,\mathrm{d}K \\
&= (S - \bar{S})H'(\bar{S}) + \int_{\bar{S}}^{S} (S - K)H''(K)\mathrm{d}K, \qquad (4.1)
\end{aligned}$$

where $H'(\bar{S})$ ($H''(K)$) denotes the first (second) derivative of H with respect to S evaluated at some fixed $\bar{S}$ (strike price K). Applying general calculus rules, this can be rewritten as follows

$$
\begin{aligned}
&H(S)\\
&= H(\bar{S}) + (S-\bar{S})H'(\bar{S}) + \int_{\bar{S}}^{S}(S-K)H''(K)\mathrm{d}K\\
&= H(\bar{S}) + (S-\bar{S})H'(\bar{S}) + \int_{\bar{S}}^{S}(\mathbb{1}_{\bar{S}\leq S}+\mathbb{1}_{\bar{S}>S})(S-K)H''(K)\mathrm{d}K\\
&= H(\bar{S}) + (S-\bar{S})H'(\bar{S}) + \int_{\bar{S}}^{S}\mathbb{1}_{\bar{S}\leq S}(S-K)H''(K)\mathrm{d}K + \int_{\bar{S}}^{S}\mathbb{1}_{\bar{S}>S}(S-K)H''(K)\mathrm{d}K\\
&= H(\bar{S}) + (S-\bar{S})H'(\bar{S}) + \int_{\bar{S}}^{S}\mathbb{1}_{\bar{S}\leq S}(S-K)H''(K)\mathrm{d}K + \int_{S}^{\bar{S}}\mathbb{1}_{\bar{S}>S}(K-S)H''(K)\mathrm{d}K\\
&= H(\bar{S}) + (S-\bar{S})H'(\bar{S}) + \int_{\bar{S}}^{S}\mathbb{1}_{\bar{S}\leq S}(S-K)^{+}H''(K)\mathrm{d}K + \int_{S}^{\bar{S}}\mathbb{1}_{\bar{S}>S}(K-S)^{+}H''(K)\mathrm{d}K\\
&= H(\bar{S}) + (S-\bar{S})H'(\bar{S}) + \int_{\bar{S}}^{\infty}\mathbb{1}_{\bar{S}\leq S}(S-K)^{+}H''(K)\mathrm{d}K + \int_{0}^{\bar{S}}\mathbb{1}_{\bar{S}>S}(K-S)^{+}H''(K)\mathrm{d}K\\
&= H(\bar{S}) + (S-\bar{S})H'(\bar{S}) + \int_{\bar{S}}^{\infty}(1-\mathbb{1}_{\bar{S}>S})(S-K)^{+}H''(K)\mathrm{d}K\\
&\qquad\qquad + \int_{0}^{\bar{S}}(1-\mathbb{1}_{\bar{S}\leq S})(K-S)^{+}H''(K)\mathrm{d}K\\
&= H(\bar{S}) + (S-\bar{S})H'(\bar{S}) + \int_{\bar{S}}^{\infty}(S-K)^{+}H''(K)\mathrm{d}K + \int_{0}^{\bar{S}}(K-S)^{+}H''(K)\mathrm{d}K, \qquad (4.2)
\end{aligned}
$$

where $\mathbb{1}$ is the indicator function. Taking the time-t conditional expectation under $\mathbb{Q}$ yields

$$
\begin{aligned}
\mathbb{E}^{\mathbb{Q}}\left(e^{-r\tau}H(S)\mid\mathcal{F}_t\right) &= \int_0^{\infty}e^{-r\tau}(H(\bar{S})-\bar{S}H'(\bar{S}))q(S)\mathrm{d}S + \int_0^{\infty}e^{-r\tau}H'(\bar{S})Sq(S)\mathrm{d}S\\
&\quad + \int_0^{\infty}e^{-r\tau}\left(\int_{\bar{S}}^{\infty}(S-K)^{+}H''(K)\mathrm{d}K\right)q(S)\mathrm{d}S\\
&\quad + \int_0^{\infty}e^{-r\tau}\left(\int_0^{\bar{S}}(K-S)^{+}H''(K)\mathrm{d}K\right)q(S)\mathrm{d}S\\
&= e^{-r\tau}(H(\bar{S})-\bar{S}H'(\bar{S})) + H'(\bar{S})\,S_t\\
&\quad + \int_{\bar{S}}^{\infty}H''(K)\left(e^{-r\tau}\int_0^{\infty}(S-K)^{+}q(S)\mathrm{d}S\right)\mathrm{d}K\\
&\quad + \int_0^{\bar{S}}H''(K)\left(e^{-r\tau}\int_0^{\infty}(K-S)^{+}q(S)\mathrm{d}S\right)\mathrm{d}K\\
&= e^{-r\tau}(H(\bar{S})-\bar{S}H'(\bar{S})) + H'(\bar{S})\,S_t\\
&\quad + \int_{\bar{S}}^{\infty}H''(K)\,C(t,\tau;K)\mathrm{d}K + \int_0^{\bar{S}}H''(K)\,P(t,\tau;K)\mathrm{d}K, \qquad (4.3)
\end{aligned}
$$

where $\tau = T-t$ and r denotes the risk-free rate, which is assumed to be constant.[42]

[42] This is a special case of Theorem 1 of Bakshi and Madan (2000). See also Carr and Madan (2001).

Equation (4.3) represents the generic spanning formula. As pointed out by Bakshi et al. (2003), this formula implies that the payoff of any function $H(S)$ can be replicated at time t by holding $H(\bar{S}) + \bar{S}H'(\bar{S})$ long positions in a zero bond maturing at T, $H(\bar{S})$ long positions in the stock S_t, and a linear combination of $H''(K)$ long positions of OTM call and put options with underlying the S, strike K and expiration T. Thus, for any option-implied risk measure with an associated payoff function of the form $H(S)$, this formula can be employed for replication, as it will be applied to all the measures covered in this thesis, beginning with the BKM risk-neutral moments in the following section.

4.2 Risk-Neutral Moments of Bakshi, Kapadia, and Madan (2003)

In 2003, Bakshi et al. (2003) presented a theorem detailing how to extract higher-order risk-neutral moments of the holding period log-return using OTM option contracts, without relying on any model assumptions. Despite being published over 20 years ago, their work remains of paramount importance to both researchers and practitioners due to its versatile application possibilities. This significance is evidenced not only by recent publications such as Ammann and Feser (2019), Aschakulporn and Zhang (2022b), and Aschakulporn and Zhang (2022a), but also by the establishment of the CBOE Skewness (SKEW) Index, which is based on the BKM risk-neutral skewness estimated from S&P 500 options. Therefore, this entire section is dedicated to their renowned theorem on risk-neutral return moments, which, after introducing some necessary definitions, is presented as follows:

Let $R(t, \tau)$ denote the τ-period log-return defined as the log price relative

$$R(t, \tau) \equiv \ln(S_T) - \ln(S_t)\,. \tag{4.4}$$

Further, let the respective return powers represent the payoff of the volatililty, the cubic,

and the quartic contract

$$H(S) = \begin{cases} R(t,\tau)^2 & \text{volatility contract,} \\ R(t,\tau)^3 & \text{cubic contract,} \\ R(t,\tau)^4 & \text{quartic contract,} \end{cases} \tag{4.5}$$

where S denotes the time-T stock price S_T. Then, the contracts' present values under the measure $\mathbb{Q}$ are defined as follows:[43]

$$\begin{aligned} &\mathcal{V}(t,\tau) \equiv \mathbb{E}_t^{\mathbb{Q}}\left(e^{-r\tau}R(t,\tau)^2\right), \quad \mathcal{W}(t,\tau) \equiv \mathbb{E}_t^{\mathbb{Q}}\left(e^{-r\tau}R(t,\tau)^3\right), \text{ and} \\ &\mathcal{X}(t,\tau) \equiv \mathbb{E}_t^{\mathbb{Q}}\left(e^{-r\tau}R(t,\tau)^4\right). \end{aligned} \tag{4.6}$$

As a consequence of the generic spanning formula (4.3), we can state the following theorem, as stated by Bakshi et al. (2003):

Theorem 41 (BKM Moments)**.** *Under all martingale pricing measures, the contract prices of the risk-neutral moments can be extracted from market prices of European OTM call and put options:*

1. The τ-period risk-neutral return variance, $Var^{\mathbb{Q}}(t,\tau)$, is given by

$$\begin{aligned} Var^{\mathbb{Q}}(t,\tau) &\equiv \mathbb{E}_t^{\mathbb{Q}}\left(\Big(R(t,\tau) - \mathbb{E}_t^{\mathbb{Q}}\Big(R(t,\tau)\Big)\Big)^2\right) \\ &= e^{r\tau}\mathcal{V}(t,\tau) - \mathcal{M}(t,\tau)^2. \end{aligned} \tag{4.7}$$

2. The τ-period risk-neutral return skewness, $Skew^{\mathbb{Q}}(t,\tau)$, is given by

$$\begin{aligned} Skew^{\mathbb{Q}}(t,\tau) &\equiv \frac{\mathbb{E}_t^{\mathbb{Q}}\left(\Big(R(t,\tau) - \mathbb{E}_t^{\mathbb{Q}}\Big(R(t,\tau)\Big)\Big)^3\right)}{\left(\mathbb{E}_t^{\mathbb{Q}}\left(\Big(R(t,\tau) - \mathbb{E}_t^{\mathbb{Q}}\Big(R(t,\tau)\Big)\Big)^2\right)\right)^{3/2}} \\ &= \frac{e^{r\tau}\mathcal{W}(t,\tau) - 3\mathcal{M}(t,\tau)e^{r\tau}\mathcal{V}(t,\tau) + 2\mathcal{M}(t,\tau)^3}{\left(e^{r\tau}\mathcal{V}(t,\tau) - \mathcal{M}(t,\tau)^2\right)^{3/2}}. \end{aligned} \tag{4.8}$$

[43] To simplify notation, we utilize $\mathbb{E}_t^{\mathbb{Q}}(.)$ in place of $\mathbb{E}^{\mathbb{Q}}(\,.\mid \mathcal{F}_t)$.

3. The τ-period risk-neutral return kurtosis, $Kurt^{\mathbb{Q}}(t,\tau)$, is given by

$$\begin{aligned} Kurt^{\mathbb{Q}}(t,\tau) &\equiv \frac{\mathbb{E}_t^{\mathbb{Q}}\left(\left(R(t,\tau)-\mathbb{E}_t^{\mathbb{Q}}\big(R(t,\tau)\big)\right)^4\right)}{\left(\mathbb{E}_t^{\mathbb{Q}}\big(R(t,\tau)-\mathbb{E}_t^{\mathbb{Q}}(R(t,\tau))\big)^2\right)^2} \\ &= \frac{e^{r\tau}\mathcal{X}(t,\tau)-4\mathcal{M}(t,\tau)e^{r\tau}\mathcal{W}(t,\tau)+6e^{r\tau}\mathcal{M}(t,\tau)^2\mathcal{V}(t,\tau)-3\mathcal{M}(t,\tau)^4}{\left(e^{r\tau}\mathcal{V}(t,\tau)-\mathcal{M}(t,\tau)^2\right)^2}, \end{aligned} \tag{4.9}$$

where $\mathcal{M}(t,\tau)$ is defined as

$$\mathcal{M}(t,\tau) \equiv e^{r\tau}-1-\frac{e^{r\tau}}{2}\mathcal{V}(t,\tau)-\frac{e^{r\tau}}{6}\mathcal{W}(t,\tau)-\frac{e^{r\tau}}{24}\mathcal{X}(t,\tau). \tag{4.10}$$

The price of the volatility contract is given by

$$\mathcal{V}(t,\tau)=\int_{S_t}^{\infty}\frac{2\left(1-\ln\left(K/S_t\right)\right)}{K^2}C(t,\tau;K)\mathrm{d}K+\int_0^{S_t}\frac{2\left(1+\ln\left(S_t/K\right)\right)}{K^2}P(t,\tau;K)\mathrm{d}K, \tag{4.11}$$

the price of the cubic contract is given by

$$\begin{aligned} \mathcal{W}(t,\tau)=\int_{S_t}^{\infty}\frac{6\ln(K/S_t)-3\left(\ln\left(K/S_t\right)\right)^2}{K^2}C(t,\tau;K)\mathrm{d}K \\ -\int_0^{S_t}\frac{6\ln\left(S_t/K\right)+3\left(\ln\left(S_t/K\right)\right)^2}{K^2}P(t,\tau;K)\mathrm{d}K, \end{aligned} \tag{4.12}$$

and the price of the quartic contract is given by

$$\begin{aligned} \mathcal{X}(t,\tau)=\int_{S_t}^{\infty}\frac{12\left(\ln\left(K/S_t\right)\right)^2-4\left(\ln\left(K/S_t\right)\right)^3}{K^2}C(t,\tau;K)\mathrm{d}K \\ +\int_0^{S_t}\frac{12\left(\ln\left(S_t/K\right)\right)^2+4\left(\ln\left(S_t/K\right)\right)^3}{K^2}P(t,\tau;K)\mathrm{d}K. \end{aligned} \tag{4.13}$$

Proof. Recall (4.3) with $H(S)$ specified by (4.5) and set $\bar{S} = S_t$. By arguments of standard differentiation, all terms in (4.3) cancel out for the respective contracts, except for the integrating terms, where we use

$$H''(K) = \begin{cases} \frac{2(1-\ln(K/S_t))}{K^2} & \text{volatility contract} \\ \frac{6\ln(K/S_t)-3(\ln(K/S_t))^2}{K^2} & \text{cubic contract} \\ \frac{12(\ln(K/S_t))^2-4(\ln(K/S_t))^3}{K^2} & \text{quartic contract} \end{cases} \tag{4.14}$$

to obtain Equations (4.11) - (4.13). Then, to determine (4.10), use the martingale property

$$\begin{aligned} e^{r\tau} &= \mathbb{E}_t^{\mathbb{Q}}\left(S_T/S_t\right) = \mathbb{E}_t^{\mathbb{Q}}\Big(\exp\left\{R(t,\tau)\right\}\Big) \\ &= 1 + \mathbb{E}_t^{\mathbb{Q}}\left(R(t,\tau)\right) + \frac{1}{2}\mathbb{E}_t^{\mathbb{Q}}\left(R(t,\tau)^2\right) + \frac{1}{6}\mathbb{E}_t^{\mathbb{Q}}\left(R(t,\tau)^3\right) + \frac{1}{24}\mathbb{E}_t^{\mathbb{Q}}\left(R(t,\tau)^4\right), \end{aligned} \tag{4.15}$$

where the second line results from a Taylor Series expansion of degree four, i.e.

$$\exp\{x\} = 1 + x + \frac{x^2}{2} + \frac{x^3}{6} + \frac{x^4}{24} + \mathcal{O}(x^5). \tag{4.16}$$

Further, define $\mathcal{M}(t,\tau) \equiv \mathbb{E}_t^{\mathbb{Q}}\left(R(t,\tau)\right)$ and rearrange (4.15) such that

$$\begin{aligned} \mathcal{M}(t,\tau) &= e^{r\tau} - 1 - \frac{1}{2}\mathbb{E}_t^{\mathbb{Q}}\left(R(t,\tau)^2\right) - \frac{1}{6}\mathbb{E}_t^{\mathbb{Q}}\left(R(t,\tau)^3\right) - \frac{1}{24}\mathbb{E}_t^{\mathbb{Q}}\left(R(t,\tau)^4\right) \\ &= e^{r\tau} - 1 - \frac{e^{r\tau}}{2}\mathcal{V}(t,\tau) - \frac{e^{r\tau}}{6}\mathcal{W}(t,\tau) - \frac{e^{r\tau}}{24}\mathcal{X}(t,\tau). \end{aligned} \tag{4.17}$$

Finally, (4.7) - (4.9) follow from the standard definitions, i.e. for the second moment

$$\begin{aligned} \mathrm{Var}^{\mathbb{Q}}(t,\tau) &\equiv \mathbb{E}_t^{\mathbb{Q}}\left(\Big(R(t,\tau) - \mathbb{E}_t^{\mathbb{Q}}\Big(R(t,\tau)\Big)\Big)^2\right) \\ &= \mathbb{E}_t^{\mathbb{Q}}\Big(R(t,\tau)^2\Big) - \mathbb{E}_t^{\mathbb{Q}}\Big(R(t,\tau)\Big)^2 \\ &= e^{r\tau}\mathcal{V}(t,\tau) - \mathcal{M}(t,\tau)^2. \end{aligned} \tag{4.18}$$

The same applies to $\mathrm{Skew}^{\mathbb{Q}}(t,\tau)$ and $\mathrm{Kurt}^{\mathbb{Q}}(t,\tau)$. □

Before moving on to the CBOE $\mathbb{VIX}$, we would like to highlight an additional feature of the second risk-neutral moment. Specifically, under certain assumptions regarding the underlying stock price dynamics, $\text{Var}^{\mathbb{Q}}(t,\tau)$ serves as an unbiased estimator of the expected quadratic variation of $\ln S$, as detailed in Section 4.4. This fact is utilized in the construction on the jump and tail risk measure $\mathbb{RIX}$, which acts as a forward-looking measure for disaster risk. Therefore, with the additional consideration of the CBOE SKEW Index, the BKM risk-neutral moments are not only significant as option-implied risk measures in their own right, but also crucial as components for deriving other risk measures, thereby underscoring their importance.

4.3 CBOE Volatility Index

In 1993, the CBOE introduced the CBOE Volatility Index, commonly known as $\mathbb{VIX}$. This index was developed to serve as a measure of expected 30-day volatility and soon became the benchmark for U.S. stock market volatility (CBOE (2019)). In its first version, the $\mathbb{VIX}$ construction was based on ATM S&P 100 Index options to compute an average Black and Scholes (1973) implied volatility. This implied volatility measure was frequently seen by the market as both a predictor for future realized volatility and a gauge for market stress, as argued by Whaley (2000). Ten years later, and in light of the shortcomings of the Black and Scholes (1973) model, the CBOE updated the $\mathbb{VIX}$ computation in collaboration with Goldman Sachs, in particular with Demeterfi et al. (1999b). The new version is based on the S&P 500 Index and uses a wide range of OTM put and call option prices instead of ATM implied volatilities. By using a specific weighting scheme, these options are combined into a portfolio to reflect volatility risk in such a way that the new $\mathbb{VIX}$ represents an unbiased estimate of future realized volatility, given the absence of event risk.[44] According to the White Paper published by the CBOE (2019), the updated $\mathbb{VIX}$ formula reads

$$\mathbb{VIX} = 100 \cdot \sqrt{\frac{2}{T}\sum_i \frac{\Delta K_i}{K_i^2} e^{rT} Q(K_i) - \frac{1}{T}\left(\frac{F_0}{K_0} - 1\right)^2}, \tag{4.19}$$

[44] Further information about the outdated index version and a comparison to the new $\mathbb{VIX}$, including the case of jump risk, can be found in Carr and Wu (2006).

where T is the time to expiration, K_i the strike price of the i'th OTM option contract, $\Delta K_i = \frac{K_{i+1}-K_{i-1}}{2}$, r the risk-free rate, $Q(K_i)$ the midpoint of the bid-ask spread for each OTM option with strike K_i, F_0 the current S&P 500 forward index level derived from index options, and K_0 the largest strike below F_0.[45] To gain comprehension of (4.19), the underlying mathematics are gradually revealed in the following:

For some $T > 0$, assume the forward price follows an Itô process with zero drift and diffusion component equal to $F_t\sigma_t$, i.e.

$$F_T = F_0 + \int_0^T F_t\sigma_t \mathrm{d}W_t. \tag{4.20}$$

Applying Itô's formula for Itô processes to $f(t,x) = \ln(x)$ with partial derivatives[46]

$$\frac{\partial f}{\partial t}(t,F_t) = 0 \qquad \frac{\partial f}{\partial x}(t,F_t) = \frac{1}{F_t} \qquad \frac{\partial^2 f}{\partial x^2}(t,F_t) = -\frac{1}{F_t^2} \tag{4.21}$$

gives

$$\ln(F_T) = \ln(F_0) - \frac{1}{2}\int_0^T \sigma_t^2 \mathrm{d}t + \int_0^T \sigma_t \mathrm{d}W_t. \tag{4.22}$$

According to Proposition 28, the quadratic variation of $\ln F$ accumulated up to time T is given by

$$[\ln F, \ln F]_T = \int_0^T \sigma_t^2 \mathrm{d}t, \tag{4.23}$$

where the right-hand side is referred to as integrated variance. By substitution and some rearrangement, Equation (4.22) can be rewritten as

$$[\ln F, \ln F]_T = 2\left(\int_0^T \sigma_t \mathrm{d}W_t - \ln\left(\frac{F_T}{F_0}\right)\right). \tag{4.24}$$

[45] Please note that here the case $t = 0$ is considered which can be generalized to arbitrary times t. For general t, it is understood that T is the option expiration date and $\tau = T - t$ is the time to expiry. The following derivations and formulae must be adjusted accordingly.

[46] Readers unfamiliar with Itô's formula for Itô processes are referred to Theorem 47 in Appendix A.2.

Taking the expectation under $\mathbb{Q}$ yields

$$\mathbb{E}^{\mathbb{Q}}[\ln F, \ln F]_T = -2\mathbb{E}^{\mathbb{Q}}\left(\ln\left(\frac{F_T}{F_0}\right)\right), \tag{4.25}$$

where $\mathbb{E}^{\mathbb{Q}}\int_0^T \sigma_t \mathrm{d}W_t = 0$ was utilized. To evaluate the right-hand side, recall the generic spanning formula (4.3) with $H(.) = e^{rT}\ln(.)$, $S = F_T$, and $\bar{S} = F_0$ such that

$$\begin{aligned}\mathbb{E}^{\mathbb{Q}}\Big(\ln(F_T)\Big) &= e^{-rT}\left(e^{rT}\ln(F_0) - e^{rT}F_0\frac{1}{F_0}\right) + \frac{e^{rT}}{F_0}S_0 - e^{rT}\int_{F_0}^{\infty}\frac{1}{K^2}\,C(0,T;K)\mathrm{d}K \\ &\quad - e^{rT}\int_0^{F_0}\frac{1}{K^2}\,P(0,T;K)\mathrm{d}K \\ &= \ln(F_0) - e^{rT}\left(\int_{F_0}^{\infty}\frac{1}{K^2}\,C(0,T;K)\mathrm{d}K + \int_0^{F_0}\frac{1}{K^2}\,P(0,T;K)\mathrm{d}K\right),\end{aligned} \tag{4.26}$$

where $F_0 = e^{rT}S_0$ was used such that the second and third term cancel out. This can be rearranged as follows

$$\mathbb{E}^{\mathbb{Q}}\left(\ln\left(\frac{F_T}{F_0}\right)\right) = -e^{rT}\left(\int_{F_0}^{\infty}\frac{1}{K^2}\,C(0,T;K)\mathrm{d}K + \int_0^{F_0}\frac{1}{K^2}\,P(0,T;K)\mathrm{d}K\right). \tag{4.27}$$

Hence, (4.25) can be rewritten as

$$\mathbb{E}^{\mathbb{Q}}[\ln F, \ln F]_T = 2e^{rT}\left(\int_{F_0}^{\infty}\frac{1}{K^2}\,C(0,T;K)\mathrm{d}K + \int_0^{F_0}\frac{1}{K^2}\,P(0,T;K)\mathrm{d}K\right), \tag{4.28}$$

which, after annualizing and taking the square root, yields the mathematically rigorous formula for the $\mathbb{VIX}$. Additionally, since $\mathbb{E}^{\mathbb{Q}}[\ln F, \ln F]_T = \mathbb{E}^{\mathbb{Q}}\int_0^T \sigma_t^2 \mathrm{d}t$ by (4.23), the replicating portfolio in (4.28) represents not only an estimate of quadratic variation, but also an estimate of the integrated variance. Then, by including the first strike price below F_0 denoted K_0, (4.28) can be reformulated as follows

$$\begin{aligned}\mathbb{E}^{\mathbb{Q}}[\ln F, \ln F]_T &= 2e^{rT}\left(\int_{K_0}^{\infty}\frac{1}{K^2}\,C(0,T;K)\mathrm{d}K + \int_0^{K_0}\frac{1}{K^2}\,P(0,T;K)\mathrm{d}K\right) \\ &\quad + 2e^{rT}\int_{K_0}^{F_0}\frac{1}{K^2}\left(P(0,T;K) - C(0,T;K)\right)\mathrm{d}K.\end{aligned} \tag{4.29}$$

For the latter integral, note that put-call parity implies

$$P(0,T;K) - C(0,T;K) = -e^{-rT}(F_0 - K), \tag{4.30}$$

where again $F_0 = e^{rT}S_0$ was utilized. By substitution, the last term of (4.29) becomes

$$-2\int_{K_0}^{F_0} \frac{F_0 - K}{K^2}\mathrm{d}K = -2\left(\left(\frac{F_0}{K_0} - 1\right) - \ln\left(\frac{F_0}{K_0}\right)\right). \tag{4.31}$$

Since $\ln(1+x) = x - \frac{1}{2}x^2 + \mathcal{O}(x^3)$ by arguments of Taylor series expansion, $\ln(F_0/K_0)$ can be approximated by

$$\ln\left(\frac{F_0}{K_0}\right) = \ln\left(1 + \frac{F_0 - K_0}{K_0}\right) \approx \frac{F_0 - K_0}{K_0} - \frac{1}{2}\left(\frac{F_0 - K_0}{K_0}\right)^2 \tag{4.32}$$

such that the last term of (4.29) is approximately equal to

$$-2\left(\left(\frac{F_0}{K_0} - 1\right) - \ln\left(\frac{F_0}{K_0}\right)\right) \approx -\left(\frac{F_0 - K_0}{K_0}\right)^2. \tag{4.33}$$

Additionally, let $Q(K)$ denote $C(0,T;K)$ or $P(0,T;K)$ depending on K, (4.29) becomes

$$\mathbb{E}^{\mathbb{Q}}[\ln F, \ln F]_T \approx 2e^{rT}\int_0^{\infty} \frac{1}{K^2}\,Q(K)\mathrm{d}K - \left(\frac{F_0 - K_0}{K_0}\right)^2. \tag{4.34}$$

Multiplying both sides by $\frac{1}{T}$ for annualization and discretizing the integral gives

$$\frac{1}{T}\mathbb{E}^{\mathbb{Q}}[\ln F, \ln F]_T \approx \frac{2}{T}\sum_i \frac{\Delta K_i}{K_i^2}e^{rT}Q(K_i) - \frac{1}{T}\left(\frac{F}{K_0} - 1\right)^2, \tag{4.35}$$

which is the radicand in the $\mathbb{VIX}$ formula (4.19). So, it can be deduced that

$$\mathbb{VIX} \approx 100 \cdot \sqrt{\frac{1}{T}\mathbb{E}^{\mathbb{Q}}[\ln F, \ln F]_T}\,. \tag{4.36}$$

Thus, technically speaking, the $\mathbb{VIX}$ measures the square root of the annualized expected quadratic variation of the forward's log-price process. Or less formal, as quadratic variation is the continuous counterpart of realized variance, the $\mathbb{VIX}$ indeed estimates realized volatility.

Before progressing to the final risk measure covered in this thesis, the $\mathbb{RIX}$, we would like to emphasize an additional feature of the $\mathbb{VIX}$: under the assumption of (4.20), which assumes that the forward price follows a purely diffusive process, the $\mathbb{VIX}$ – or more precisely, the $\mathbb{VIX}$-type integrated variance estimate in (4.28) – captures stochastic volatility. However, it provides an exact estimate of quadratic variation only in the absence of discontinuities, as noted by Carr and Madan (1998), Demeterfi et al. (1999a), Britten-Jones and Neuberger (2000), and Carr and Wu (2006). The $\mathbb{RIX}$, which will be discussed in the following section, utilizes this limitation of the $\mathbb{VIX}$-type estimator of quadratic variation in conjunction with the BKM variance to isolate the impact of jump risk on expected quadratic variation.

4.4 Rare Disaster Concern Index

The last option-implied risk measure discussed in this chapter is the so-called $\mathbb{RIX}$, which was proposed by Gao et al. (2018) and essentially covers downside event risk. In its methodology, the $\mathbb{RIX}$ is based on the $\mathbb{JTIX}$ of Kapadia and Du (2012). Intuitively speaking, this index represents the difference between the quadratic variation of the stock price return process with and without event risk and thus isolates the impact of jumps. In order to achieve a more thorough understanding of the $\mathbb{JTIX}$, we follow Kapadia and Du (2012) and use the jump diffusion model of Merton (1976), introduced in Subsection 3.1.3, for an analytical illustration first. Subsequently, the $\mathbb{RIX}$ is discussed in more detail, where we also present the replication portfolios required for estimation.

4.4.1 $\mathbb{JTIX}$ of Kapadia and Du (2012)

We now derive the $\mathbb{JTIX}$-construction step-by-step using the jump diffusion model of Merton (1976). In a first step, we will show that for this model the following identity is true[47]

$$\mathbb{E}^{\mathbb{Q}}[\ln S, \ln S]_T = \mathrm{Var}^{\mathbb{Q}}\left(\ln\left(S_T/S_0\right)\right), \tag{4.37}$$

[47] In Section 4.2, we adhered to the notation of Bakshi et al. (2003) and denoted the risk-neutral variance by $\mathrm{Var}^{\mathbb{Q}}(t,\tau)$. To enhance clarity in the current section, we have updated the notation to $\mathrm{Var}^{\mathbb{Q}}\left(\ln\left(S_T/S_0\right)\right)$.

i.e. the BKM variance of the holding period log-return is an unbiased estimate of the quadratic variation of $\ln S$. In a second step, we recall the results Carr and Madan (1998), Demeterfi et al. (1999a), and Britten-Jones and Neuberger (2000), who demonstrated that for a pure continuous process S^c it holds

$$\mathbb{E}^{\mathbb{Q}}[\ln S, \ln S]_T^c = 2\mathbb{E}^{\mathbb{Q}}\left(\int_0^T \frac{1}{S_t^c}\mathrm{d}S_t^c - \ln(S_T^c/S_0^c)\right), \tag{4.38}$$

where the term on the right-hand side is the $\mathbb{VIX}$-type integrated variance. Note that the integrated variance is frequently used as a general measure of expected quadratic variation despite assuming continuity. Thus, for discontinuous stock price processes it is biased, as pointed out by Bollerslev et al. (2011), Jiang and Tian (2005), and Carr and Wu (2009). In the last step, we follow Kapadia and Du (2012) and define the difference between the two expressions of quadratic variation, both expressed on an annualized basis, as the $\mathbb{JTIX}$

$$\begin{aligned}\mathbb{JTIX} &\equiv \frac{1}{T}\left(\mathbb{E}^{\mathbb{Q}}[\ln S, \ln S]_T - \mathbb{E}^{\mathbb{Q}}[\ln S, \ln S]_T^c\right) \\ &= \frac{1}{T}\left(\mathrm{Var}^{\mathbb{Q}}\left(\ln\left(S_T/S_0\right)\right) - 2\mathbb{E}^{\mathbb{Q}}\left(\int_0^T \frac{1}{S_t}\mathrm{d}S_t - \ln(S_T/S_0)\right)\right),\end{aligned} \tag{4.39}$$

where the superscript c is omitted in the last term to highlight that in the presence of discontinuities the biased estimate is plugged in.[48] Applied to the Merton (1976) jump-diffusion model, this leads to

$$\mathbb{JTIX} = \frac{2}{T}\mathbb{E}^{\mathbb{Q}}\int_0^T \int_{\mathbb{R}_0}\left(1 + x + \frac{x^2}{2} - e^x\right)\mathcal{J}_X(\mathrm{d}x, \mathrm{d}t). \tag{4.40}$$

To begin with the step-by-step derivation, we first recall the stock price dynamics assumed by Merton (1976). According to Equation (3.21), now presented in integral form, the evolution of the stock price under the risk-neutral measure $\mathbb{Q}$ is specified as follows

$$S_T = S_0 + \int_0^T (r - \lambda\mu_X)S_t\mathrm{d}t + \int_0^T \sigma S_t \mathrm{d}W_t + \int_0^T \int_{\mathbb{R}_0} S_t\left(e^x - 1\right)\mathcal{J}_X(\mathrm{d}x, \mathrm{d}t), \tag{4.41}$$

[48] The precise definition of the $\mathbb{JTIX}$ is $\mathbb{JTIX} \equiv \frac{1}{T}\left(\mathrm{Var}^{\mathbb{Q}}\left(\ln\left(S_T/S_0\right)\right) - \mathbb{E}^{\mathbb{Q}}[\ln S, \ln S]_T^c\right)$. To highlight the underlying economic rationale, we use the modified definition which is equivalent under the Merton (1976) model due to Equation (4.37).

where again r denotes the constant risk-free rate, σ the volatility, and W_t a standard Brownian motion. The jump measure of the compound Poisson process with intensity λ is represented by $\mathcal{J}_X(\mathrm{d}x, \mathrm{d}t)$, where $\mathbb{R}_0$ represents the real line excluding zero. As previously noted, the jump size X at time t follows a normal distribution

$$X_t \sim \mathcal{N}\Big(\underbrace{\ln(1+\mu_X) - \frac{1}{2}\sigma_X^2}_{\equiv\alpha}, \sigma_X^2 \Big), \tag{4.42}$$

such that $\mathbb{E}^{\mathbb{Q}}\left[e^{X_t} - 1\right] = e^{\alpha + \frac{1}{2}\sigma_X^2} - 1 = \mu_X$ is the expected (relative) jump size and σ_X the (relative) jump size volatility. The compensator of $\mathcal{J}_X$ is given by $\lambda \frac{1}{\sqrt{2\pi}\sigma_X} e^{-\frac{1}{2}(x-\alpha)^2/\sigma_X^2}$. In order to establish the identity (4.37), Itô's formula for jump-diffusion processes is applied first to $f(t,x) = \ln(x)$.[49] Considering the following partial derivatives

$$\frac{\partial f}{\partial t}(t, S_t) = 0 \qquad \frac{\partial f}{\partial x}(t, S_t) = \frac{1}{S_t} \qquad \frac{\partial^2 f}{\partial x^2}(t, S_t) = -\frac{1}{S_t^2}, \tag{4.43}$$

this gives

$$\begin{aligned}
\ln(S_T) &= \ln(S_0) + \int_0^T \left(\frac{1}{S_t}(r - \lambda\mu_X)S_t + \frac{1}{2}\left(-\frac{1}{S_t^2}\right)\sigma^2 S_t^2 \right) \mathrm{d}t + \int_0^T \frac{1}{S_t}\sigma S_t \mathrm{d}W_t \\
&\quad + \sum_{t\in[0,T]}^{\Delta S_t \neq 0} \left(\ln\left(S_t e^{X_t}\right) - \ln(S_t) \right) \\
&= \ln(S_0) + \int_0^T \left(r - \lambda\mu_X - \frac{1}{2}\sigma^2 \right) \mathrm{d}t + \int_0^T \sigma \mathrm{d}W_t + \sum_{t\in[0,T]}^{\Delta S_t \neq 0} X_t \\
&= \ln(S_0) + \int_0^T \left(r - \lambda\mu_X - \frac{1}{2}\sigma^2 \right) \mathrm{d}t + \int_0^T \sigma \mathrm{d}W_t + \int_0^T \int_{\mathbb{R}_0} x \mathcal{J}_X(\mathrm{d}x, \mathrm{d}t).
\end{aligned} \tag{4.44}$$

Then, Itô's formula for jump-diffusion processes is applied a second time, but now to $f(t,x) = \ln^2(x/S_0)$.[50] Considering the following partial derivatives

$$\frac{\partial f}{\partial t}(t, S_t) = 0 \qquad \frac{\partial f}{\partial x}(t, S_t) = 2\frac{\ln(S_t/S_0)}{S_t} \qquad \frac{\partial^2 f}{\partial x^2}(t, S_t) = \frac{2(1 - \ln(S_t/S_0))}{S_t^2}, \tag{4.45}$$

[49] Readers unfamiliar with Itô's formula for jump-diffusion processes are referred to Theorem 48 in Appendix A.2.

[50] Cf. previous footnote.

this gives

$$\begin{aligned}
\ln^2(S_T/S_0) &= \ln^2(S_0/S_0) + \int_0^T \left(2\frac{\ln(S_t/S_0)}{S_t}(r-\lambda\mu_X)S_t + \frac{1}{2}\frac{2(1-\ln(S_t/S_0))}{S_t^2}\sigma^2 S_t^2\right)\mathrm{d}t \\
&\quad + \int_0^T 2\frac{\ln(S_t/S_0)}{S_t}\sigma S_t \mathrm{d}W_t \quad + \sum_{t\in[0,T]}^{\Delta S_t\neq 0}\left(\ln^2\left(\frac{S_t e^{X_t}}{S_0}\right) - \ln^2\left(\frac{S_t}{S_0}\right)\right) \\
&= \int_0^T \left(2\ln(S_t/S_0)(r-\lambda\mu_X) + \frac{1}{2}(2-2\ln(S_t/S_0))\sigma^2\right)\mathrm{d}t \\
&\quad + \int_0^T 2\ln(S_t/S_0)\,\sigma\mathrm{d}W_t + \sum_{t\in[0,T]}^{\Delta S_t\neq 0} 2\left(\ln(S_t/S_0)X_t + X_t^2\right) \\
&= \int_0^T 2\ln(S_t/S_0)\left(r-\lambda\mu_X-\frac{1}{2}\sigma^2\right)\mathrm{d}t + \int_0^T 2\ln(S_t/S_0)\,\sigma\mathrm{d}W_t \\
&\quad + \int_0^T\int_{\mathbb{R}_0} 2\ln(S_t/S_0)\,x\,\mathcal{J}_X(\mathrm{d}x,\mathrm{d}t) + \int_0^T \sigma^2\mathrm{d}t + \int_0^T\int_{\mathbb{R}_0} x^2\mathcal{J}_X(\mathrm{d}x,\mathrm{d}t) \\
&= \int_0^T 2\ln(S_t/S_0)\mathrm{d}\ln S_t + [\ln S, \ln S]_T,
\end{aligned} \tag{4.46}$$

where we used the result $[\ln S, \ln S]_T = \int_0^T \sigma^2\mathrm{d}t + \int_0^T\int_{\mathbb{R}_0} x^2\mathcal{J}_X(\mathrm{d}x,\mathrm{d}t)$, as stated in Proposition 31. Taking the expectation under $\mathbb{Q}$ and rearranging yields

$$\mathbb{E}^{\mathbb{Q}}[\ln S, \ln S]_T = \mathbb{E}^{\mathbb{Q}}\left(\ln^2(S_T/S_0)\right) - \mathbb{E}^{\mathbb{Q}}\int_0^T 2\ln(S_t/S_0)\,\mathrm{d}\ln S_t. \tag{4.47}$$

To evaluate the latter integral, note that Equation (4.44) implies

$$\mathbb{E}^{\mathbb{Q}}\left(\ln(S_t/S_0)\right) = \left(r-\lambda\mu_X-\frac{1}{2}\sigma^2\right)t + \lambda\alpha t \tag{4.48}$$

such that

$$\begin{aligned}
\mathbb{E}^{\mathbb{Q}}\int_0^T 2\ln(S_t/S_0)\mathrm{d}\ln S_t &= 2\mathbb{E}^{\mathbb{Q}}\int_0^T \ln(S_t/S_0)\left(r-\lambda\mu_X-\frac{1}{2}\sigma^2\right)\mathrm{d}t + 2\mathbb{E}^{\mathbb{Q}}\int_0^T \ln(S_t/S_0)\,\sigma\mathrm{d}W_t \\
&\quad + 2\mathbb{E}^{\mathbb{Q}}\int_0^T\int_{\mathbb{R}_0}\ln(S_t/S_0)\,x\,\mathcal{J}_X(\mathrm{d}x,\mathrm{d}t) \\
&= 2\int_0^T \mathbb{E}^{\mathbb{Q}}\left(\ln(S_t/S_0)\right)\left(r-\lambda\mu_X-\frac{1}{2}\sigma^2\right)\mathrm{d}t \\
&\quad + 2\int_0^T\int_{\mathbb{R}_0}\mathbb{E}^{\mathbb{Q}}\left(\ln(S_t/S_0)\right)x\frac{\lambda}{\sqrt{2\pi}\sigma_X}e^{-\frac{(x-\alpha)^2}{2\sigma_X^2}}\mathrm{d}x\,\mathrm{d}t \\
&= \left(\left(r-\lambda\mu_X-\frac{1}{2}\sigma^2\right)+\lambda\alpha\right)^2 T^2 \\
&= \left(\mathbb{E}^{\mathbb{Q}}\left(\ln(S_T/S_0)\right)\right)^2,
\end{aligned} \tag{4.49}$$

where the expected value of the Itô integral is zero by construction.[51] Therefore, Equation (4.47) simplifies to

$$\begin{aligned}\mathbb{E}^{\mathbb{Q}}[\ln S, \ln S]_T &= \mathbb{E}^{\mathbb{Q}}\left(\ln^2(S_T/S_0)\right) - \mathbb{E}^{\mathbb{Q}}\left(\ln(S_T/S_0)\right)^2 \\ &= \mathrm{Var}^{\mathbb{Q}}\left(\ln\left(S_T/S_0\right)\right), \end{aligned} \tag{4.50}$$

which establishes the first step. For the second step, we first show that the identity (4.38) holds assuming a purely continuous stock price process S^c, which is defined under $\mathbb{Q}$ as[52]

$$S_T^c = S_0^c + \int_0^T r S_t^c \mathrm{d}t + \int_0^T \sigma_t S_t^c \mathrm{d}W_t. \tag{4.51}$$

Applying Itô's formula for Itô processes to $f(t,x) = \ln(x)$ with the following partial derivatives[53]

$$\frac{\partial f}{\partial t}\left(t, S_t^c\right) = 0 \qquad \frac{\partial f}{\partial x}\left(t, S_t^c\right) = \frac{1}{S_t^c} \qquad \frac{\partial^2 f}{\partial x^2}\left(t, S_t^c\right) = -\frac{1}{\left(S_t^c\right)^2} \tag{4.52}$$

provides

$$\ln\left(S_T^c\right) = \ln\left(S_0^c\right) + \int_0^T \left(r - \frac{1}{2}\sigma_t^2\right)\mathrm{d}t + \int_0^T \sigma_t \mathrm{d}W_t. \tag{4.53}$$

Then, according to Proposition 28, the quadratic variation of $\ln S^c$ is given by

$$[\ln S, \ln S]_T^c = \int_0^T \sigma_t^2 \mathrm{d}t. \tag{4.54}$$

Please note that Equation (4.51) implies

$$\int_0^T \frac{1}{S_t^c}\mathrm{d}S_t^c = \int_0^T r\mathrm{d}t + \int_0^T \sigma_t \mathrm{d}W_t, \tag{4.55}$$

[51] Readers unfamiliar to the Itô integral are referred to Appendix A.1.

[52] To be consistent with previous notation, we assume r to be constant. Results do not change for stochastic r_t, though.

[53] Readers unfamiliar with Itô's formula for Itô processes are referred to Theorem 47 in Appendix A.2.

and further Equation (4.53) implies

$$\ln(S_T^c/S_0^c) = \int_0^T \left(r - \frac{1}{2}\sigma_t^2\right) \mathrm{d}t + \int_0^T \sigma_t \mathrm{d}W_t \tag{4.56}$$

such that twice their difference gives

$$2\left(\int_0^T \frac{1}{S_t^c}\mathrm{d}S_t^c - \ln(S_T^c/S_0^c)\right) = \int_0^T \sigma_t^2 \mathrm{d}t. \tag{4.57}$$

Thus, the left-hand side is equivalent to the integrated variance, introduced in the previous section. Finally, by Equation (4.54), it holds

$$\mathbb{E}^{\mathbb{Q}}[\ln S, \ln S]_T^c = 2\mathbb{E}^{\mathbb{Q}}\left(\int_0^T \frac{1}{S_t^c}\mathrm{d}S_t^c - \ln(S_T^c/S_0^c)\right), \tag{4.58}$$

which completes the claim for the continuous stock price process S^c. In the presence of discontinuities, the $\mathbb{VIX}$-type integrated variance is biased, though. To see this, note that Equation (3.21) implies

$$\int_0^T \frac{1}{S_t}\mathrm{d}S_t = \int_0^T (r - \lambda\mu_X)\mathrm{d}t + \int_0^T \sigma \mathrm{d}W_t + \int_0^T \int_{\mathbb{R}_0} (e^x - 1)\, \mathcal{J}_X(\mathrm{d}x, \mathrm{d}t), \tag{4.59}$$

and Equation (4.44) implies

$$\ln(S_T/S_0) = \int_0^T \left(r - \lambda\mu_X - \frac{1}{2}\sigma^2\right) \mathrm{d}t + \int_0^T \sigma \mathrm{d}W_t + \int_0^T \int_{\mathbb{R}_0} x\, \mathcal{J}_X(\mathrm{d}x, \mathrm{d}t) \tag{4.60}$$

such that

$$2\mathbb{E}^{\mathbb{Q}}\left(\int_0^T \frac{1}{S_t}\mathrm{d}S_t - \ln(S_T/S_0)\right) = \mathbb{E}^{\mathbb{Q}}\int_0^T \sigma^2 \mathrm{d}t + 2\mathbb{E}^{\mathbb{Q}}\int_0^T \int_{\mathbb{R}_0} (e^x - 1 - x)\, \mathcal{J}_X(\mathrm{d}x, \mathrm{d}t), \tag{4.61}$$

where the double integral reflects the bias of the $\mathbb{VIX}$-type integrated variance. Now, we arrive at the last step of the $\mathbb{JTIX}$ construction. First, recall in Equation (4.46) we used

$$[\ln S, \ln S]_T = \int_0^T \sigma^2 \mathrm{d}t + \int_0^T \int_{\mathbb{R}_0} x^2 \mathcal{J}_X(\mathrm{d}x, \mathrm{d}t). \tag{4.62}$$

Second, we have already shown that $\text{Var}^{\mathbb{Q}}\left(\ln(S_T/S_0)\right)$ is an unbiased estimate of $\mathbb{E}^{\mathbb{Q}}[\ln S, \ln S]_T$. Hence, the $\mathbb{JTIX}$, which is defined as the difference between the unbiased estimate of $\mathbb{E}^{\mathbb{Q}}[\ln S, \ln S]_T$ and the biased estimate of $\mathbb{E}^{\mathbb{Q}}[\ln S, \ln S]_T^c$ – as specified in (4.61) – with both estimates expressed in annualized terms, is given by

$$\begin{aligned}
\mathbb{JTIX} &= \frac{1}{T}\left(\text{Var}^{\mathbb{Q}}\left(\ln(S_T/S_0)\right) - 2\mathbb{E}^{\mathbb{Q}}\left(\frac{1}{S_t}\mathrm{d}S_t - \ln(S_T/S_0)\right)\right) \\
&= \frac{1}{T}\left(\mathbb{E}^{\mathbb{Q}}[\ln S, \ln S]_T - 2\mathbb{E}^{\mathbb{Q}}\left(\frac{1}{S_t}\mathrm{d}S_t - \ln(S_T/S_0)\right)\right) \\
&= \frac{1}{T}\left(\mathbb{E}^{\mathbb{Q}}\left(\int_0^T \sigma^2 \mathrm{d}t + \int_0^T \int_{\mathbb{R}_0} x^2 \mathcal{J}_X(\mathrm{d}x, \mathrm{d}t)\right)\right. \\
&\quad \left. - \mathbb{E}^{\mathbb{Q}}\left(\int_0^T \sigma^2 \mathrm{d}t + 2\int_0^T \int_{\mathbb{R}_0} \left(e^x - 1 - x\right) \mathcal{J}_X(\mathrm{d}x, \mathrm{d}t)\right)\right) \\
&= \frac{2}{T}\mathbb{E}^{\mathbb{Q}} \int_0^T \int_{\mathbb{R}_0} \left(1 + x + \frac{x^2}{2} - e^x\right) \mathcal{J}_X(\mathrm{d}x, \mathrm{d}t) \\
&= -\frac{2}{T}\mathbb{E}^{\mathbb{Q}} \int_0^T \int_{\mathbb{R}_0} \left(\frac{x^3}{6} + \frac{x^4}{24} + \mathcal{O}(x^5)\right) \mathcal{J}_X(\mathrm{d}x, \mathrm{d}t). \qquad (4.63)
\end{aligned}$$

Hence, the difference between the BKM variance and the $\mathbb{VIX}$-type integrated variance is solely driven by discontinuities in the stock price process. Therefore, the $\mathbb{JTIX}$ can indeed be considered a jump and tail risk measure, as it quantifies the impact of event risk – in particular, its associated skewness and kurtosis – on the expected quadratic variation.

Note that the previous derivation is based on the Merton (1976) jump diffusion model, in which volatility is assumed to be constant. For stochastic volatility leading to non-stationary processes, though, the BKM variance does not exactly coincide with the expected quadratic variation of $\ln S$, i.e. Equation (4.50) does not hold precisely in such cases.[54] However, since the $\mathbb{JTIX}$ is designed for a 30 day time horizon only, the measurement error in the BKM variance arising from stochastic volatility is negligible, as argued by Kapadia and Du (2012). In particular, they conduct a numerical analysis which shows that the jump component of the stock price process is the main driver of the $\mathbb{JTIX}$, as it dominates the diffusive component for short periods of time.

[54] Kapadia and Du (2012) demonstrate that the two measures are equivalent for the entire class of Lévy processes, specified in Definition 6.

4.4.2 $\mathbb{RIX}$ of Gao, Gao, and Song (2018)

Following the discussion of its building block, we now turn to the $\mathbb{RIX}$ of Gao et al. (2018). Analogous to the $\mathbb{JTIX}$, this index captures the difference between the two previously mentioned measures of quadratic variation: the BKM holding period return variance and the $\mathbb{VIX}$-type integrated variance. In contrast to Kapadia and Du (2012), Gao et al. (2018) resort to the non-centered second moment $\mathbb{V}$ of the holding period log-return, though. According to Theorem 41, the annualized version is defined by the following replication portfolio[55]

$$\mathbb{V} \equiv 2\frac{e^{rT}}{T}\left(\int_{S_0}^{\infty}\frac{1-\ln\left(K/S_0\right)}{K^2}C\left(0,T;K\right)\mathrm{d}K + \int_{0}^{S_0}\frac{1+\ln\left(S_0/K\right)}{K^2}P\left(0,T;K\right)\mathrm{d}K\right). \quad (4.64)$$

Further, Gao et al. (2018) define the annualized $\mathbb{VIX}$-type integrated variance $\mathbb{IV}$ as follows

$$\mathbb{IV} \equiv 2\frac{e^{rT}}{T}\left(\int_{S_0}^{\infty}\frac{1}{K^2}C\left(0,T;K\right)\mathrm{d}K + \int_{0}^{S_0}\frac{1}{K^2}P\left(0,T;K\right)\mathrm{d}K\right), \quad (4.65)$$

which is essentially equivalent to the replication portfolio of the (squared) $\mathbb{VIX}$ derived in Section 4.3.[56] As investors are typically more concerned about extreme negative price deviations, they create downside versions of $\mathbb{V}$ and $\mathbb{IV}$ by constructing replication portfolios from European-style OTM put options only.

$$\begin{aligned}\mathbb{V}^{-} &\equiv 2\frac{e^{rT}}{T}\int_{0}^{S_0}\frac{1+\ln\left(S_0/K\right)}{K^2}P\left(0,T;K\right)\mathrm{d}K,\\ \mathbb{IV}^{-} &\equiv 2\frac{e^{rT}}{T}\int_{0}^{S_0}\frac{1}{K^2}P\left(0,T;K\right)\mathrm{d}K.\end{aligned} \quad (4.66)$$

In analogy to the $\mathbb{JTIX}$, the difference between $\mathbb{V}^{-}$ and $\mathbb{IV}^{-}$ captures the risk of downside rare events. Gao et al. (2018) label this difference the rare disaster concern index

$$\mathbb{RIX} \equiv \mathbb{V}^{-} - \mathbb{IV}^{-} = 2\frac{e^{rT}}{T}\int_{0}^{S_0}\frac{\ln\left(S_0/K\right)}{K^2}P\left(0,T;K\right)\mathrm{d}K, \quad (4.67)$$

[55] In notation of Theorem 41, $\mathbb{V} \equiv \frac{1}{T}e^{rT}\mathcal{V}(0,T)$.

[56] Technically, there is a minor difference between $\mathbb{IV}$ and the replication portfolio of the (squared) $\mathbb{VIX}$. The (squared) $\mathbb{VIX}$ measures the expected quadratic variation of $\ln F$ instead of $\ln S$ such that the corresponding integral limit is F_0 rather than S_0. From a mathematical perspective, applying the generic spanning formula analogously to $\ln S$ would require an additional correction term in (4.65). Gao et al. (2018) drop this correction term, similarly to how they drop $\mathcal{M}(0,T)^2$ by using the non-centered second moment $\mathbb{V}$ instead of $\mathrm{Var}^{\mathbb{Q}}\left(\ln(S_T/S_0)\right)$, since the difference between the two dropped terms is negligibly small.

which serves as a forward-looking measure for variations in disaster concerns. Thus, it can be seen as the current price of insurance against extreme future downside movements.

4.5 Estimation via Volatility Smile Construction

Similar to the RND extraction from option prices, as discussed in Section 3.2, estimating option-implied risk measures via replication portfolios boils down to providing a continuum of OTM put and call option prices, a condition that is initially not met in the marketplace. Consequently, it becomes necessary to interpolate and smooth between the available, unevenly sampled strike prices, as well as to extrapolate beyond their range. Corresponding approaches operate typically in the implied volatility space rather than in the option price domain. The advantage of switching to implied volatilites is the substantially reduced degree of non-linearity (Rosenberg (2000)) and the numerical stability (Bliss and Panigirtzoglou (2002)) in comparsion to initial option prices. According to Shimko (1993), who introduced the concept of volatility smile construction, they also tend to be smoother than their price counterparts. In his methodology, he employed a quadratic polynomial to interpolate observable implied volatilities and utilized the implied volatility of the most distant OTM option for flat extrapolation, known as the endpoint volatility. Malz (1997) deployed a quadratic spline for the entire smile construction in the context of currency options. He separately fitted two quadratic polynomials to the three data points available in foreign exchange (FX) quotation and then combined them under specific continuity and differentiability conditions. Consistent with FX market conventions, he conducted his procedure in the delta domain rather than the strike price domain, which alters the scaling and thereby places greater emphasis on the ATM region.[57] Although operating within the FX markets, Campa et al. (1998) adhered to the strike price domain and adopted the approach of Shimko (1993), enhancing the interpolation by employing a cubic spline instead of a quadratic polynomial. Then, shortly after the turn of the millennium, Bliss and Panigirtzoglou (2002) introduced the first smile construction technique which includes additional smoothing for

[57] Within the context of FX options, Muck (2022) has recently developed a sophisticated smile construction technique, not based on splines, that ensures no-arbitrage. As this technique is specifically tailored for FX options, it is not covered in this thesis.

distorted data. In particular, they resorted to a cubic smoothing spline to interpolate and smooth implied volatilities in the delta domain. In their revised version (Bliss and Panigirtzoglou (2004)), they also addressed the issue of smile extrapolation. Due to numerical stability, they again extended the smile horizontally, i.e. they utilized endpoint volatility. Over the years, the cubic smoothing spline has established itself as the standard technique for interpolation and smoothing in the context of equity options, predominantly applied in the strike domain, as pointed out by Figlewski (2018) and Ammann and Feser (2019).[58] In the field of smile extrapolation, the other standard technique employed alongside endpoint volatility is linear regression, i.e. the linear extension of the volatiltiy smile, as described in Ulrich and Walther (2020). Both of these approaches are relatively straightforward. However, several studies have confirmed that they can induce significant errors when estimating option-implied risk measures (Ammann and Feser (2019); Aschakulporn and Zhang (2022b)). In the case of endpoint volatility, horizontal extrapolation involves assuming log-normally distributed RND tails, which evidently contradicts empirical observations. Therefore, the steeper the "true" volatiltiy smile, the heavier the tails and thus the larger the induced bias. Linear regression mitigates this issue by estimating the slope of the volatility smile at its outer strikes and extending it linearly beyond these points (Jiang and Tian (2007)). Approximation errors may arise from the curvature of the smile or from imprecise estimates of the slope coefficients. The latter presents a significant issue in the presence of microstructure noise. Not only do the resulting risk measure estimates exhibit high sensitivity to distorted data when employing this method, but extended implied volatilities can also become negative, as highlighted by Ammann and Feser (2019) and Aschakulporn and Zhang (2022b). Consequently, despite underestimating the tails of the RND, contemporary studies, such as those by Gao et al. (2018) and Gao et al. (2019), employ endpoint volatility for estimating tail risk measures like the $\mathbb{RIX}$, due to its robustness. This apparent contradiction prompted us to develop a new smile construction approach, which entails a robust and RND-consistent extrapolation technique and is presented in the following chapter.

[58] Although this method is also employed in the delta domain by some practitioners, Fengler (2009) applied the cubic smoothing spline within the option price domain, incorporating additional convexity constraints derived from no-arbitrage conditions associated with option prices.

Chapter 5

Volatility Smile Construction

This chapter focuses on the core contribution of this thesis: the arbitrage-free RND-based smile construction approach, which, unlike standard techniques, extrapolates implied volatilities in an arbitrage-free manner through RND tail modeling. Our tail modeling approach, similar yet distinct from that of Birru and Figlewski (2012), is highly flexible, encompassing a variety of distributions to model different tail shapes. To ensure robust extrapolation in the presence of microstructure noise, we employ a convexity-preserving cubic smoothing spline for interpolation and smoothing. As detailed in the subsequent chapter, these features make our smile construction approach superior to traditional techniques. Additionally, we introduce the quintic smoothing spline as an alternative interpolation and smoothing technique, compatible with RND-based extrapolation and specifically designed to capture potentially bimodal RNDs.[59]

To provide a comprehensive understanding of our smile construction technique, this chapter is organized as follows: Section 5.1 discusses smile extrapolation. It begins with a brief introduction to the relevant results from extreme value theory and then details our RND tail modeling approach for smile extension. Following that, Section 5.2 presents smile interpolation and smoothing techniques compatible with this RND-based extrapolation method. This section primarily covers the convexity-preserving cubic smoothing spline, which enhances the

[59]In this chapter, parts of the content are derived from my previous work, Albert et al. (2023). Although direct quotations and certain references are not always explicitly indicated, the material partially builds on my prior research.

robustness of the entire smile construction against microstructure noise and ensures accurate risk-measure estimates. Additionally, the quintic smoothing spline is outlined as an alternative technique that does not rely on shape-preserving constraints. This spline offers greater flexibility, particularly in capturing potentially bimodal RNDs, which can arise during times of certain event risk. In contrast to the augmented cubic smoothing spline, the quintic smoothing spline is discussed briefly, as its implementation is typically provided by software, with the details omitted.

5.1 Smile Extrapolation

Our extrapolation approach models the RND tails in an arbitrage-free manner, ensuring that no risk-free profits can be generated through mispricing of the implied volatilities. Since observable option prices do not impose specific distributional assumptions on the underlying RND, it becomes crucial to identify a sufficiently flexible distribution that can accurately capture the various stylized facts observed in financial data, including fat tails, skewness, and kurtosis. Accordingly, and in alignment with the work of Birru and Figlewski (2012), we adopt the General Extreme Value (GEV) distribution, which is widely regarded as a natural candidate for modeling the tails of distributions in this context. This choice is firmly grounded in extreme value theory, particularly the Fisher-Tippet-Gnedenko theorem. Before delving into the detailed implementation of our extrapolation method, we first provide a brief overview of the key properties of the GEV distribution, highlighting its suitability for tail modeling and justifying its selection as the optimal candidate for this purpose, as outlined in McNeil et al. (2015).

5.1.1 Generalized Extreme Value Distribution

The role of the GEV distribution in extreme value theory is comparable to that of the normal distribution in central limit theory. While the latter deals with the convergence of sums of random variables, the former represents the limiting distribution in the convergence of so-called *normalized maxima*, formalized in the Fisher-Tippet-Gnedenko theorem. The GEV distribution is defined as follows:

Definition 42 (GEV Distribution)**.** *The cumulative distribution function of the generalized extreme value distribution is defined as*

$$F_{GEV}(x) = \begin{cases} \exp\left\{-\left(1+\xi\left(\frac{x-\mu}{\sigma}\right)\right)^{-1/\xi}\right\} & \text{for} \quad \xi \neq 0, \\ \exp\left\{-\exp\left\{-\left(\frac{x-\mu}{\sigma}\right)\right\}\right\} & \text{for} \quad \xi = 0, \end{cases} \tag{5.1}$$

where $\mu \in \mathbb{R}$ is the location parameter, $\sigma > 0$ the scale parameter, and $\xi \in \mathbb{R}$ the shape parameter. The corresponding probability density function is given by

$$f_{GEV}(x) = \frac{1}{\sigma} t(x)^{\xi+1} \exp\left\{-t(x)\right\}, \tag{5.2}$$

where

$$t(x) = \begin{cases} 1+\xi\left(\frac{x-\mu}{\sigma}\right)^{-1/\xi} & \text{for} \quad \xi \neq 0, \\ \exp\left\{-\left(\frac{x-\mu}{\sigma}\right)\right\} & \text{for} \quad \xi = 0. \end{cases} \tag{5.3}$$

The support of the distribution depending on ξ follows from

$$supp(X) = \begin{cases} x \in \left[\mu - \frac{\sigma}{\xi}, +\infty\right) & \text{for} \quad \xi > 0, \\ x \in \left(-\infty, +\infty\right) & \text{for} \quad \xi = 0, \\ x \in \left(-\infty, \mu - \frac{\sigma}{\xi}\right] & \text{for} \quad \xi < 0. \end{cases} \tag{5.4}$$

The GEV distribution is called *generalized* since it nests three types of distributions. Depending on the value of shape parameter ξ, it subsumes the reversed Weibull ($\xi < 0$), the Gumbel ($\xi = 0$), and the Fréchet distribution ($\xi > 0$). While the reversed Weibull distribution is short-tailed with a finite right endpoint, the Gumbel and the Fréchet distribution have infinite right endpoints. However, the Fréchet distribution is heavy-tailed compared to the Gumbel distribution as it decays much slower.

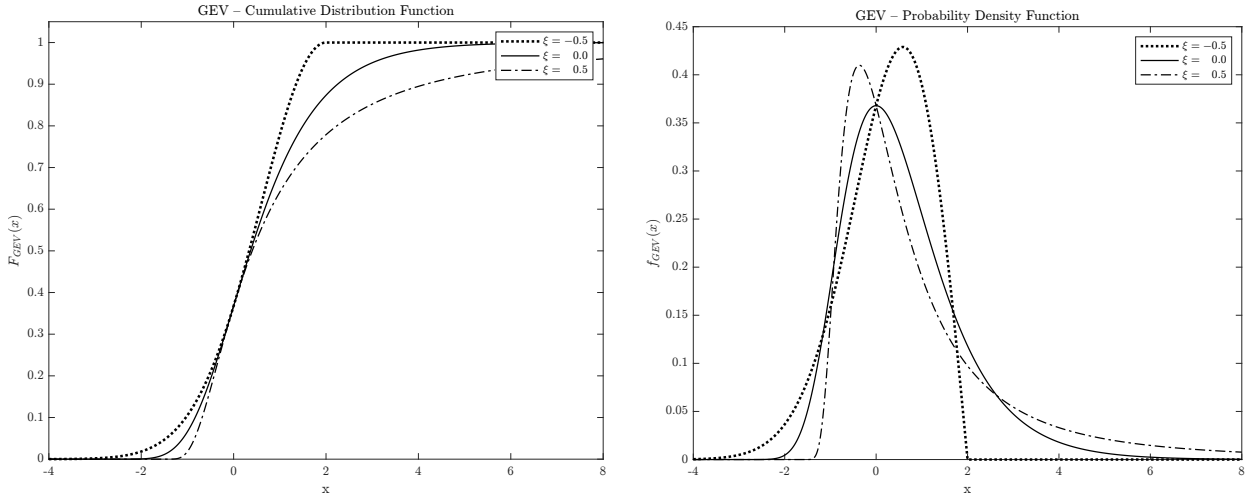

Figure 5.1: GEV Cumulative Distribution and Probability Density Function – The figure plots the cumulative distribution function (left panel) and the probability density function (right panel) of the GEV distribution for three cases: the dotted line corresponds to $\xi = -0.5$ (reversed Weibull), the solid line to $\xi = 0$ (Gumbel), and the dash-dotted line to $\xi = 0.5$ (Fréchet) . In all cases, $\mu = 0$ and $\sigma = 1$.

Figure 5.1 illustrates the aforementioned differences among the three distributions. Apparently, various tail shapes can be produced by modifying the shape parameter ξ. Furthermore, Equations (5.1) and (5.2) are continuous in ξ for a fixed x which facilitates statistical modeling. So, the GEV distribution is highly flexible which leads to the conjecture that is suitable for tail modeling. And indeed, it can be shown that the GEV distribution is not only suitable, but also optimal for tail modeling of an unknown distribution, as formulated in the Fisher-Tippet-Gnedenko Theorem:

Theorem 43 (Fisher-Tippet-Gnedneko Theorem)**.** *Assume that for a sequence of i.i.d. random variables* $(X_i)_{i\in\mathbb{N}}$ *with maximum* $M_n = \max\{X_1, \ldots, X_n\}$ *there exist sequences of real constants* a_n, b_n *with* $a_n > 0$ *such that the normalized maximum converges in distribution to some non-degenerate random variable*

$$\frac{M_n - b_n}{a_n} \xrightarrow{d} X^*. \tag{5.5}$$

Then, this random variable follows the GEV distribution, i.e. $X^* \sim GEV(\mu, \sigma, \xi)$.

Proof. A rigorous proof can be found in De Haan and Ferreira (2006). □

This theorem justifies the use of the GEV distribution for tail modeling, leading to our sophisticated RND tail modeling approach, discussed in the following subsection.

5.1.2 RND Tail Modeling

Our innovative tail modeling approach is based on the premise that deep OTM option prices must be recovered from the tails to be modeled. These tails must also satisfy further properties is a probabilistic sense such that the entire RND represents in fact a probability density function. To explain this nontrivial procedure, we make several assumptions: first, that option prices are available for a dense grid of evenly spaced strike prices $K_1, K_2, , \ldots, K_N$, and second, that the moneyness range is limited. Additionally, we assume that the underlying RND implied by the available option prices is well-behaved. To ensure that extrapolated OTM option prices do not admit arbitrage, we impose no-arbitrage constraints in accordance with Brunner and Hafner (2003), such that the RND satisfies the probability axioms of Kolmogorov as well as the martingale property. Specifically, the risk-neutral density $q(S_T)$ must be non-negative

$$q(S_T) \geq 0 \quad \forall \quad S_T \geq 0 \tag{5.6}$$

and integrate to one

$$\int_0^\infty q(S_T)\,\mathrm{d}S_T = 1. \tag{5.7}$$

Further, the martingale property of the discounted stock price requires that the RND prices options correctly when $K = 0$. This implies that the risk-neutral expectation of S_T equals the current price of a forward contract with maturity in T, i.e.

$$\mathbb{E}^{\mathbb{Q}}(S_T \mid \mathcal{F}_t) = e^{r\tau} S_t, \tag{5.8}$$

where $\tau = T - t$. Considering these contraints, we use the GEV distribution to model the *right* tail of the RND corresponding to OTM call options directly. In particular, the GEV tail is connected to the RND implied by available option prices under two requirements. First, consistent with Birru and Figlewski (2012), PDF and CDF values from the GEV distribution and available option prices must coincide at the connection strike price K_{N-1} to obtain well-behaved RND tails.[60] Second, to satisfy the martingale property, the call option price at the

[60] K_{N-1}, and not K_N, is the connecting strike price for PDF and CDF values due to finite differences approximation, as discussed in Section 3.2.

outermost available strike price K_N computed from the GEV tail $C_{GEV}(t,\tau;K_N)$ must be equal to the outermost available call option price $C(t,\tau;K_N)$. Note, the second requirement ensures that GEV-implied and observed implied volatilities are identical at strike price K_N such that the extrapolated volatility smile is actually continuous. This requirement is a modification of Birru and Figlewski (2012) who impose further restrictions on the PDF, which does not guarantee a continuous volatility smile, as illustrated in Subsection 6.1.5. The optimization problem for the right tail then reads

$$\begin{aligned} \underset{\mu,\sigma,\xi}{\arg\min} \quad & \left(C_{GEV}(t,\tau;K_N) - C(t,\tau;K_N)\right)^2 \\ \text{subject to} \quad & f_{GEV}(K_{N-1}) = \hat{q}(K_{N-1}), \\ & F_{GEV}(K_{N-1}) = \hat{Q}(K_{N-1}), \end{aligned} \tag{5.9}$$

where

$$C_{GEV}(t,\tau;K_N) = e^{-r\tau}\int_{K_N}^{\infty}(S_T - K_N)\, f_{GEV}(S_T)\,\mathrm{d}S_T. \tag{5.10}$$

To model the *left* tail of the RND that corresponds to OTM put options, the GEV must be defined on $-S_T$ and $-\mu$. Analogously, PDF and CDF values from the GEV and available options must coincide at the connecting strike price K_2 and the price of the put option with strike K_1 implied by the GEV tail $P_{GEV}(t,\tau;K_1)$ must equal the outermost available put price $P(t,\tau;K_1)$.[61] The left tail optimization problem reads accordingly

$$\begin{aligned} \underset{-\mu,\sigma,\xi}{\arg\min} \quad & \left(P_{GEV}(t,\tau;K_1) - P(t,\tau;K_1)\right)^2 \\ \text{subject to} \quad & f_{GEV}(-K_2) = \hat{q}(K_2), \\ & 1 - F_{GEV}(-K_2) = \hat{Q}(K_2), \end{aligned} \tag{5.11}$$

where

$$P_{GEV}(t,\tau;K_1) = e^{-r\tau}\int_{0}^{K_1}(K_1 - S_T)\, f_{GEV}(-S_T)\,\mathrm{d}S_T. \tag{5.12}$$

As a result of these optimizations tasks, both RND tails are uniquely characterized by their parameters and thus option prices and implied volatilities outside the given moneyness range

[61] Again, K_2, and not K_1, is the connecting strike price for PDF and CDF values due to the finite differences approximation.

can be computed by (5.10) and (5.12). Nonetheless, this approach is based on the aforementioned strict assumptions on data availability and quality. In practice, option prices are affected by microstructure noise and trading is limited to a discrete grid of unequally spaced and sparsely sampled strikes, though. For such data, the finite-differences approximation of the risk-neutral PDF and CDF values at the connecting strikes K_2 and K_{N-1} is either infeasible or significantly affected by noise. Therefore, we introduce two smile interpolation and smoothing techniques of observed implied volatilities which make our tail modeling applicable to realistic market conditions.

5.2 Smile Interpolation and Smoothing

This section covers two smile interpolation techniques compatible with the RND-based smile extrapolation approach. The first one is the the convexity-preserving cubic smoothing spline, explained in detail in Subsection 5.2.1. This method assumes the observable part of the volatility smile to be purely convex and is distinguished by its robustness with respect to microstructure noise. The second approach is a quintic smoothing spline, addressed in Subsection 5.2.2. This higher order spline ensures smooth RNDs (Figlewski (2010)) and allows for concavity in the central part of the smile. Since the latter does not require a shape-preserving amendment like the former, its methodology will only be discussed briefly. As this technique aims to capture bimodal RNDs rather than estimating option-implied risk measures, we also present the rationale behind bimodal RNDs.

5.2.1 Convexity-Preserving Cubic Smoothing Spline

One of the most popular techniques for interpolation and smoothing raw data is a cubic smoothing spline. While this technique is appropriate for most financial applications in the implied volatility domain, corresponding RNDs can exhibit large spikes and are highly sensitive towards the choice of the smoothing parameter, as described by Figlewski (2018). Along the lines of Fengler (2009), we therefore augment this approach by imposing additional constraints on the smile's shape. In particular, we assume the observable (central) part of the volatility smile to be convex, which is mostly supported by the data. These bounds on the

second-order derivatives act as strong constraints on the spline's roughness, as pointed out by Dole (1999), and ensure suitable estimates of options prices, as wells as PDF and CDF values.

To provide a deeper understanding of this specific spline methodology, we begin with the general definition of a natural cubic spline and justify the need for additional smoothing. Subsequently, we address implementation issues associated with the cubic smoothing spline, with its definition and implementation detailed in the corresponding theorem.

In context of volatility smile interpolation, a natural cubic spline is defined as follows:

Definition 44 (Natural Cubic Spline)**.** *Consider* $i = 1, \ldots, \tilde{N}$ observable *implied volatilities* $\tilde{\sigma}_i$ *with corresponding* observable *strikes* $\tilde{K}_i$ *(knots) where* $\tilde{K}_1 = K_1$ *and* $\tilde{K}_{\tilde{N}} = K_N$*. A function* $g : [\tilde{K}_1, \tilde{K}_{\tilde{N}}] \to \mathbb{R}$ *is called a natural cubic spline if it is a cubic polynomial on every sub-interval* $[\tilde{K}_i, \tilde{K}_{i+1}]$*, if* g*,* g' *and* g'' *are continuous at every knot* $\tilde{K}_i$*, and if* $g'' = g''' = 0$ *at* $\tilde{K}_1$ *and* $\tilde{K}_{\tilde{N}}$ *(natural boundary condition) . Then, in piecewise polynomial representation, the function* g *can be specified as follows*

$$g(K) = a_i + b_i(K - \tilde{K}_i) + c_i(K - \tilde{K}_i)^2 + d_i(K - \tilde{K}_i)^3 \quad \textit{for} \quad \tilde{K}_i \leq K \leq \tilde{K}_{i+1} \tag{5.13}$$

where $a_i, b_i, c_i, d_i \in \mathbb{R}$ *are given constants.*[62]

Since a natural cubic spline incorporates all available data points, it is suitable for smile interpolation in the absence of microstructure noise only. As implied volatilities are frequently distorted, though, smoothing is required. Therefore, a natural cubic smoothing is usually applied. For implementation, one usually switches from the *piecewise polynomial representation* to the so-called *value-second derivative representation*; the interplay of those two will be discussed later. The *value-second derivative representation* facilitates the unique characterization of the spline by solving a single quadratic program. Hence, it allows greater flexibility as additional constraints – in our case convexity constraints – can be added easily. The cubic smoothing spline definition and further technical details, including the *value-second*

[62] This definition implies $g \in \mathcal{C}^2$ on $[\tilde{K}_1, \tilde{K}_{\tilde{N}}]$. Pollock (1999) exploits this continuity condition and provides an implementation based on the *piecewise polynomial representation*.

derivative representation, can be found in Green and Silverman (1994) and are summarized in the following theorem:

Theorem 45 (Cubic Smoothing Spline)**.** *Let g be a cubic spline according to Definition 44. Define*

$$g_i = g(\tilde{K}_i) \qquad \text{and} \qquad \gamma_i = g''(\tilde{K}_i), \tag{5.14}$$

where $\gamma_1 = \gamma_{\tilde{N}} = 0$, $\boldsymbol{g} = (g_1, \ldots, g_{\tilde{N}})^\intercal$ and $\boldsymbol{\gamma} = (\gamma_2, \ldots, \gamma_{\tilde{N}-1})^\intercal$, called the value-second derivative representation. Further, define $h_i = \tilde{K}_{i+1} - \tilde{K}_i$ and let $\boldsymbol{Q}$ be a $\tilde{N} \times (\tilde{N}-2)$ matrix with entries $q_{i,j}$ given by

$$q_{j-1,j} = h_{j-1}^{-1}, \quad q_{j,j} = -h_{j-1}^{-1} - h_j^{-1} \quad \text{and} \quad q_{j+1,j} = h_j^{-1}, \tag{5.15}$$

for $i = 1, \ldots, \tilde{N}$, $j = 2, \ldots, \tilde{N}-1$, and $q_{i,j} = 0$ for $|i-j| \geq 2$. Additionally, let $\boldsymbol{R}$ be a symmetric $(\tilde{N}-2) \times (\tilde{N}-2)$ matrix with entries $r_{i,j}$ given by

$$\begin{aligned} r_{i,i} &= \frac{1}{3}(h_{i-1} + h_i) \quad \text{for} \quad i = 2, \ldots \tilde{N}-1, \\ r_{i,i+1} = r_{i+1,i} &= \frac{1}{6} h_i \quad \text{for} \quad i = 2, \ldots \tilde{N}-2, \end{aligned} \tag{5.16}$$

for $i, j = 2, \ldots, \tilde{N}-1$ and $r_{i,j} = 0$ for $|i-j| \geq 2$. Then, $\boldsymbol{g}$ and $\boldsymbol{\gamma}$ specify a natural cubic spline if and only if

$$\boldsymbol{Q}^\intercal \boldsymbol{g} = \boldsymbol{R}\boldsymbol{\gamma}. \tag{5.17}$$

If (5.17) *holds, the so-called roughness penalty for curvature satisfies*

$$\int_{\tilde{K}_1}^{\tilde{K}_{\tilde{N}}} g''(K)\,\mathrm{d}K = \boldsymbol{\gamma}^\intercal \boldsymbol{R}\boldsymbol{\gamma}. \tag{5.18}$$

Then, for a given smoothing paramter $\lambda > 0$, the cubic smoothing spline results from minimizing

$$\sum_{i=1}^{\tilde{N}} \left(\tilde{\sigma}_i - g(\tilde{K}_i)\right)^2 + \lambda \int_{\tilde{K}_1}^{\tilde{K}_{\tilde{N}}} g''(K)\,\mathrm{d}K \tag{5.19}$$

and can be written – augmented by convexity constraints – as the following quadratic optimization problem

$$\begin{aligned} \underset{\boldsymbol{x}}{\arg\min} \quad & -\boldsymbol{y}^\intercal \boldsymbol{x} + \frac{1}{2}\boldsymbol{x}^\intercal \begin{pmatrix} \boldsymbol{I}_{\tilde{N}} & \boldsymbol{0}_{\tilde{N}\times(\tilde{N}-2)} \\ \boldsymbol{0}_{(\tilde{N}-2)\times\tilde{N}} & \lambda \boldsymbol{R} \end{pmatrix} \boldsymbol{x} \\ \textit{subject to} \quad & \begin{pmatrix} \boldsymbol{Q}^\intercal & -\boldsymbol{R}^\intercal \end{pmatrix} \boldsymbol{x} = \boldsymbol{0}_{(2\tilde{N}-2)\times 1}, \\ & \gamma_2, \ldots, \gamma_{\tilde{N}-1} \geq 0, \end{aligned} \tag{5.20}$$

where $\boldsymbol{y} = (\tilde{\sigma}_1, \ldots, \tilde{\sigma}_{\tilde{N}},\ 0, \ldots, 0)^\intercal$ *and* $\boldsymbol{x} = (g_1, \ldots, g_{\tilde{N}},\ \gamma_2, \ldots, \gamma_{\tilde{N}-1})^\intercal$ *are* $(2\tilde{N}-2)$*-element column vectors.* $\gamma_i \geq 0\ \forall\ i = 2, \ldots, \tilde{N}-1$ *represents the convexity constraints.* $\boldsymbol{I}_n$ *is the identity matrix of dimension* n *and* $\boldsymbol{0}_{k\times l}$ *is a matrix of zeros with* k *rows and* l *columns.*

Proof. Recall the so-called *value-second derivative representation* of the spline, i.e.

$$g_i = g(\tilde{K}_i) \ \text{ and } \ \gamma_i = g''(\tilde{K}_i) \tag{5.21}$$

with $\gamma_1 = \gamma_{\tilde{N}} = 0$ due to the *natural boundary condition*. Now, since g is twice continuously differentiable, g'' is linear. Therefore, for each subinterval $[\tilde{K}_i, \tilde{K}_{i+1}]$ the second derivative $g''(K)$ can be written as

$$\begin{aligned} g''(K) &= \gamma_i + \frac{\gamma_{i+1} - \gamma_i}{\tilde{K}_{i+1} - \tilde{K}_i} \cdot (K - \tilde{K}_i) \\ &= \frac{(\tilde{K}_{i+1} - \tilde{K}_i)\gamma_i + (K - \tilde{K}_i)\gamma_{i+1} - (K - \tilde{K}_i)\gamma_i}{\tilde{K}_{i+1} - \tilde{K}_i} \\ &= \frac{(K - \tilde{K}_i)\gamma_{i+1} + (\tilde{K}_{i+1} - K)\gamma_i}{h_i}, \end{aligned} \tag{5.22}$$

where $h_i = \tilde{K}_{i+1} - \tilde{K}_i$. Integrating $g''(K)$ twice with appropriate additive constants such that $g(\tilde{K}_i) = g_i$ yields

$$\begin{aligned} g(K) =& \frac{(K - \tilde{K}_i)g_{i+1} + (\tilde{K}_{i+1} - K)g_i}{h_i} \\ & - \frac{1}{6}(K - \tilde{K}_i)(\tilde{K}_{i+1} - K_i)\left(\left(1 + \frac{K - \tilde{K}_i}{h_i}\right)\gamma_{i+1} + \left(1 + \frac{\tilde{K}_{i+1} - K}{h_i}\right)\gamma_i\right) \end{aligned} \tag{5.23}$$

for $i = 1, \ldots, \tilde{N} - 1$. This expression represents the cubic spline thoroughly characterized by the values of g_i and γ_i. To determine g_i and γ_i, use the information that g' and g'' must be identical at the knots. The first derivatives at the knots of a subinterval $[K_i, K_{i+1}]$ are given by

$$\begin{aligned} \lim_{K \downarrow K_i} g'(K) &= \frac{g_{i+1} - g_i}{h_i} - \frac{1}{6} h_i (2\gamma_i + \gamma_{i+1}), \\ \lim_{K \uparrow K_{i+1}} g'(K) &= \frac{g_{i+1} - g_i}{h_i} + \frac{1}{6} h_i (\gamma_i + 2\gamma_{i+1}). \end{aligned} \tag{5.24}$$

Hence, for two adjacent polynomial pieces the following condition can be deduced

$$\frac{g_i - g_{i-1}}{h_{i-1}} + \frac{1}{6} h_{i-1} (\gamma_{i-1} + 2\gamma_i) = \frac{g_{i+1} - g_i}{h_i} - \frac{1}{6} h_i (2\gamma_i + \gamma_{i+1}). \tag{5.25}$$

Rearranging the terms yields

$$\frac{g_{i+1} - g_i}{h_i} - \frac{g_i - g_{i-1}}{h_{i-1}} = \frac{1}{6} h_{i-1} \gamma_{i-1} + \frac{1}{3} (h_{i-1} + h_i) \gamma_i + \frac{1}{6} h_i \gamma_{i+1} \tag{5.26}$$

for $i = 2, \ldots, \tilde{N} - 1$. In order to represent (5.26) in matrix notation, recall the definitions of $\boldsymbol{g}$, $\boldsymbol{\gamma}$, $\boldsymbol{Q}$, and $\boldsymbol{R}$ and further note that $\boldsymbol{R}$ is strictly diagonal dominant and thus positive-definite. Then, Equation (5.26), which characterizes the cubic spline uniquely, can be written in matrix notation as follows

$$\boldsymbol{Q}^\intercal \boldsymbol{g} = \boldsymbol{R} \boldsymbol{\gamma}, \tag{5.27}$$

which provides the first result of the theorem. To show the second one, the specification of the *roughness penalty* in *value-second derivative representation*, we first use integration by parts by means of $g''(\tilde{K}_1) = \gamma_1 = 0$ and $g''(K_n) = \gamma_n = 0$, which yields

$$\begin{aligned} \int_{\tilde{K}_1}^{\tilde{K}_{\tilde{N}}} g''(K)^2 \, \mathrm{d}K &= \Big[g''(K) g'(K) \Big]_{\tilde{K}_1}^{\tilde{K}_{\tilde{N}}} - \int_{\tilde{K}_1}^{\tilde{K}_{\tilde{N}}} g'''(K) g'(K) \, \mathrm{d}K \\ &= \Big(g''(\tilde{K}_{\tilde{N}}) g'(\tilde{K}_{\tilde{N}}) - g''(\tilde{K}_1) g'(\tilde{K}_1) \Big) - \int_{K_1}^{K_{\tilde{N}}} g'''(K) g'(K) \, \mathrm{d}K \\ &= - \int_{K_1}^{K_{\tilde{N}}} g'''(K) g'(K) \, \mathrm{d}K. \end{aligned} \tag{5.28}$$

Then, differentiating (5.22) with respect to K gives

$$g'''(K) = \frac{\gamma_{i+1} - \gamma_i}{h_i}, \tag{5.29}$$

which means $g'''(K)$ is constant on each subinterval $[\tilde{K}_i, \tilde{K}_{i+1}]$. Hence, the *roughness penalty* can be expressed in terms of g_i and γ_i by

$$\begin{aligned}
\int_{\tilde{K}_1}^{\tilde{K}_{\tilde{N}}} g''(K)^2 \,\mathrm{d}K &= -\sum_{i=1}^{\tilde{N}-1} g'''(\tilde{K}_i^+) \int_{\tilde{K}_i}^{\tilde{K}_{i+1}} g'(K) \,\mathrm{d}K \\
&= -\sum_{i=1}^{\tilde{N}-1} \frac{\gamma_{i+1} - \gamma_i}{h_i} \cdot \Big(g(\tilde{K}_{i+1}) - g(\tilde{K}_i) \Big) \\
&= -\sum_{i=1}^{\tilde{N}-1} \frac{\gamma_{i+1} - \gamma_i}{h_i} \cdot (g_{i+1} - g_i) \\
&= \sum_{i=1}^{\tilde{N}-1} \frac{\gamma_{i+1} - \gamma_i}{h_i} \cdot (g_i - g_{i+1}) \,,
\end{aligned} \tag{5.30}$$

where $\tilde{K}_i^+$ denotes the right-hand limit of K converging to $\tilde{K}_i$. Since $\gamma_1 = \gamma_{\tilde{N}} = 0$ Equation (5.30) can be rearranged as follows

$$\int_{\tilde{K}_1}^{\tilde{K}_{\tilde{N}}} g''(K)^2 \,\mathrm{d}K = \sum_{i=2}^{\tilde{N}-1} \gamma_i \left(\frac{g_{i+1} - g_i}{h_i} - \frac{g_i - g_{i-1}}{h_{i-1}} \right) = \boldsymbol{\gamma}^\intercal \boldsymbol{Q}^\intercal \boldsymbol{g} = \boldsymbol{\gamma}^\intercal \boldsymbol{R} \boldsymbol{\gamma}, \tag{5.31}$$

which proves the second claim. To show that (5.19) can be formulated as a quadratic optimization program, define $\tilde{\boldsymbol{\sigma}} = (\tilde{\sigma}_1, \cdots, \tilde{\sigma}_{\tilde{N}})^\intercal$ such that the minimization problem reads

$$\begin{aligned}
\sum_{i=1}^{\tilde{N}} \Big(\tilde{\sigma}_i - g(\tilde{K}_i) \Big)^2 + \lambda \int_{\tilde{K}_1}^{\tilde{K}_{\tilde{N}}} g''(K) \,\mathrm{d}K &= (\tilde{\boldsymbol{\sigma}} - \boldsymbol{g})^\intercal (\tilde{\boldsymbol{\sigma}} - \boldsymbol{g}) + \lambda \cdot \boldsymbol{\gamma}^\intercal \boldsymbol{R} \boldsymbol{\gamma} \\
&= \tilde{\boldsymbol{\sigma}}^\intercal \tilde{\boldsymbol{\sigma}} - 2 \tilde{\boldsymbol{\sigma}}^\intercal \boldsymbol{g} + \boldsymbol{g}^\intercal \boldsymbol{g} + \lambda \cdot \boldsymbol{\gamma}^\intercal \boldsymbol{R} \boldsymbol{\gamma}.
\end{aligned} \tag{5.32}$$

Since $\tilde{\boldsymbol{\sigma}}$ is a vector of given constants the following optimization problem is equivalent

$$\begin{aligned}
\underset{\boldsymbol{g}, \boldsymbol{\gamma}}{\arg\min} \quad & -\tilde{\boldsymbol{\sigma}}^\intercal \boldsymbol{g} + \frac{1}{2} \left(\boldsymbol{g}^\intercal \boldsymbol{g} + \lambda \cdot \boldsymbol{\gamma}^\intercal \boldsymbol{R} \boldsymbol{\gamma} \right) \\
\text{subject to} \quad & \boldsymbol{Q}^\intercal \boldsymbol{g} - \boldsymbol{R} \boldsymbol{\gamma} = \boldsymbol{0},
\end{aligned} \tag{5.33}$$

where the constraint ensures the result to be a cubic spline. Finally, by recalling the definitions of $\boldsymbol{y}$ and $\boldsymbol{x}$, (5.33) can be formulated as the desired quadratic program

$$\begin{aligned} \underset{\boldsymbol{x}}{\arg\min} \quad & -\boldsymbol{y}^\intercal \boldsymbol{x} + \frac{1}{2}\boldsymbol{x}^\intercal \begin{pmatrix} \boldsymbol{I}_{\tilde{N}} & \boldsymbol{0}_{\tilde{N}\times(\tilde{N}-2)} \\ \boldsymbol{0}_{(\tilde{N}-2)\times\tilde{N}} & \lambda \boldsymbol{R} \end{pmatrix} \boldsymbol{x} \\ \text{subject to} \quad & \begin{pmatrix} \boldsymbol{Q}^\intercal & -\boldsymbol{R}^\intercal \end{pmatrix} \boldsymbol{x} = \boldsymbol{0}_{(2\tilde{N}-2)\times 1}, \\ & \gamma_2, \ldots, \gamma_{\tilde{N}-1} \geq 0, \end{aligned} \tag{5.34}$$

where $\gamma_i \geq 0 \; \forall \; i = 2, \ldots, \tilde{N} - 1$ represents the additional convexity constraints. □

Solving this quadratic program for a given λ provides the optimal $\boldsymbol{x}$, the elements of which uniquely characterize the cubic smoothing spline in the *value-second derivative representation*. Note that the continuity conditions in Definition 44 lead to the following relation between the two spline representations. Specifically, the coefficients of the *piecewise polynomial representation* in Equation (5.13) can be recovered from the *value-second derivative representation* as follows:[63]

$$\begin{aligned} a_i &= g_i, & b_i &= \frac{g_{i+1} - g_i}{h_i} - \frac{h_i}{6}(2\gamma_i + \gamma_{i+1}), \\ c_i &= \frac{\gamma_i}{2}, & d_i &= \frac{\gamma_{i+1} - \gamma_i}{6h_i}. \end{aligned} \tag{5.35}$$

Therefore, the only remaining task is to find the optimal smoothing parameter λ, which represents a trade-off between closeness to data and degree of curvature. This parameter is typically determined by "leave-one-out" cross-validation.[64] Since this technique represents a standard procedure in many statistical applications, it is not covered here. Instead, compare Green and Silverman (1994), Chapter 3 for additional information.

[63] A detailed derivation can be found in Pollock (1999).

[64] Fengler (2009) states that "leave-one-out" cross-validation is not applicable in his setting. This is mainly due to the focus on the construction of the entire volatility surface. As we limit our analysis to the cross section of strikes for a specific maturity, the parameter λ can be chosen optimally using the aforementioned technique.

5.2.2 Quintic Smoothing Spline

The shape-preserving cubic smoothing spline presented above was designed to stabilize smile extrapolation approach in case of distorted data. As it relies on the convexity assumption of the central part of the smile, it is not compatible with a phenomenon documented in the recent literature, the so-called *concave volatility smile*. This atypical shape of the volatility smile leads to bimodal RNDs, which, while rarely observable on typical trading days, are often detectable several days before specific events (Zhirong and Fong (2012); Alexiou et al. (2023); Kostakis et al. (2023)). While Zhirong and Fong (2012) and Alexiou et al. (2023) identified this feature in connection with financial events, namely the subprime crisis 2008 and earnings announcement dates, Kostakis et al. (2023) focused on a political event instead, in particular the UK referendum on EU membership. All studies came up with the same conclusion, i.e. concave volatility smiles/bimodal RNDs are prevalent at the market only, if short-expiry options cover events relevant to financial markets, on which market participants have diverging jump expectations. In such cases, as argued by Alexiou et al. (2023), the jump component dominates the diffusive one as the time to expiration shrinks such that deviating jump anticipations manifest in a bimodal RND.[65] Then, when information is updated after the event, uncertainty is resolved and the RND becomes unimodal again. Therefore, the occurrence of bimodal RNDs can be seen as a powerful sign of impending event risk (Zhirong and Fong (2012)). Now, in order to extract possibly bimodal RNDs from options prices, an interpolation and smoothing candidate must account for concavity. Both, Alexiou et al. (2023) and Kostakis et al. (2023), use a quintic smoothing spline for this task, as it is perfectly suitable for capturing various smile shapes while producing smooth RNDs (Figlewski (2010)).[66] A quintic spline is defined analogously to the cubic spline of Definition 44, but

[65] The deviating jump expectations of market participants refer to the physical measure rather than to the risk-neutral one extracted from option prices. However, as shown by Kostakis et al. (2023), the change of measure does not affect bimodality in case of short periods of time.

[66] Zhirong and Fong (2012) did not interpolate and smooth implied volatilities. Instead, they used the standard double lognormal approach for extracting the RND from option prices.

with a polynomial order five. Its smoothing variant minimizes the following expression[67]

$$\rho \sum_{i=1}^{\tilde{N}} \left(\tilde{\sigma}_i - g(\tilde{K}_i) \right)^2 + \lambda \int_{\tilde{K}_1}^{\tilde{K}_{\tilde{N}}} g'''(K)^2 \, \mathrm{d}K, \tag{5.36}$$

where $g(.)$ denotes here the quintic spline and ρ is an additional weighting coefficient; otherwise the previous notation applies.[68] In this context, we need to mention the blending approach of Figlewski (2010), which is typically applied before interpolation and smoothing. This blending technique prevents an artifical jump between the implied volatilities of ATM puts and calls from yielding a pseudo-bimodal RND. Mathematically, it reads

$$\tilde{\sigma}_{\text{blend}}(\tilde{K}_i) = \upsilon \cdot \tilde{\sigma}_{i,\text{Put}} + (1 - \upsilon) \cdot \tilde{\sigma}_{i,\text{Call}}, \tag{5.37}$$

where $\tilde{\sigma}_{\text{blend}}$ denotes the blended, $\tilde{\sigma}_{i,\text{Put}}$ the observable put option, and $\tilde{\sigma}_{i,\text{Call}}$ the observable call option implied volatility at strike $\tilde{K}_i$. The weighting scheme is represented by $\upsilon = (\tilde{K}_{\text{high}} - \tilde{K}_i)/(\tilde{K}_{\text{high}} - \tilde{K}_{\text{low}})$, where $\tilde{K}_{\text{high}}$ ($\tilde{K}_{\text{low}}$) is the largest (smallest) strike price in the moneyness range $K/S_0 \in [0.98, 1.02]$. Therefore, when $\tilde{K}_i \approx S_0$, the implied volatilities of the ATM put and call option are equally weighted. For $\tilde{K}_{\text{low}} \leq \tilde{K}_i < S_0$, the put option's implied volatility receives a higher weight, while for the $S_0 < \tilde{K}_i \leq \tilde{K}_{\text{high}}$, the call option's implied volatility is assigned a higher weight.

At this stage, we want to highlight that our RND-based smile extrapolation presented in Subsection 5.1.2 is fully compatible with this type of interpolation and smoothing, as demonstrated in the following illustration, replicated from Alexiou et al. (2023):[69]

[67] Alexiou et al. (2023) and Kostakis et al. (2023) both use the function `spaps` of Matlab's curve-fitting toolbox. The objective function (5.36) corresponds to Matlab's documentation, where ρ represents the smoothing parameter and λ represents the weighting coefficient. To be consistent with previous notation, we reverse the roles of these two parameters.

[68] Please note that here the square of the spline's third-order derivative is used to control its roughness instead of its second-order derivative.

[69] The parameters ρ and λ are determined in accordance with Alexiou et al. (2023), who combined the quintic smoothing spline with the tail modeling approach of Birru and Figlewski (2012), which is similar to but yet distinct from our tail modeling approach.

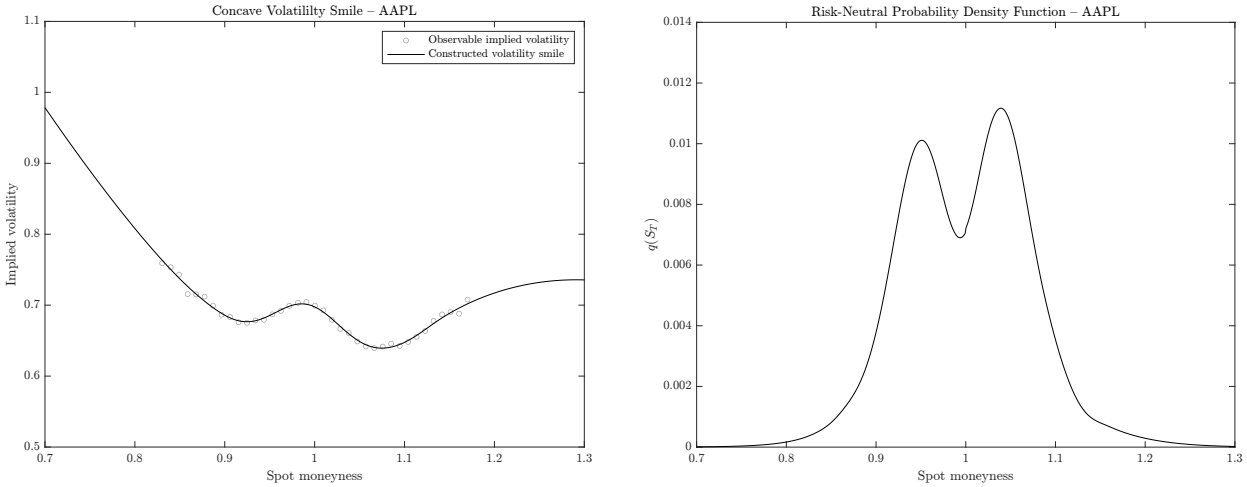

Figure 5.2: Concave Volatility Smile and Bimodal RND – The figure plots Black and Scholes (1973) implied volatilities of option contracts written on Apple (AAPL) stocks with 4 days to expiration, observed on October 28, 2013, along with the constructed volatility smile (left panel) and the corresponding risk-neutral density (right panel). The volatility smile is constructed using the RND-based tail modeling approach of Subsection 5.1.2 for smile extrapolation, combined with a quintic smoothing spline for interpolation and smoothing, incorporating the blending approach of Birru and Figlewski (2012). The risk-neutral density is approximated using finite differences on a fine grid with $\Delta K/S_0 = 0.1\%$. Options data is obtained from OptionMetrics.

Note that this compatibility presents a unique opportunity for future research, as it enables the simultaneous identification of bimodal RNDs alongside accurate risk measure estimation. In contrast, the approach employed by Alexiou et al. (2023) and Kostakis et al. (2023), which combines the quintic smoothing spline with the tail modeling method of Birru and Figlewski (2012), does not offer this capability due to the limitations of the Birru and Figlewski (2012) tail modeling approach, as detailed in Subsection 6.1.5.

Having introduced our sophisticated, arbitrage-free smile construction approach – along with a modified interpolation and smoothing version for RND modeling – we now shift our focus to the comparative analysis of different smile construction methods in the following chapter, which highlights the superiority of the RND-based approach over standard techniques.

Chapter 6

Comparative Analysis

In this chapter, we conduct a comparative analysis of our RND-based smile construction method against conventional techniques – specifically, endpoint volatility and linear regression, both coupled with a cubic smoothing spline – with regard to option-implied risk measure estimates. To demonstrate the superiority of our technique, we structure the analysis within a two-stage framework. First, we perform a numerical analysis following Jiang and Tian (2005), Ammann and Feser (2019), and Aschakulporn and Zhang (2022b). In particular, we deploy an option pricing model to evaluate the accuracy and robustness of risk measure estimates derived from the respective smile construction techniques, while accounting for multiple sources of implementation errors. In addition, we expose the shortcomings of the RND tail modeling approach proposed by Birru and Figlewski (2012). Second, we apply the different smile construction methods to options data, specifically to narrowed moneyness ranges of those data. The exclusion of certain implied volatilities allows us to assess the extrapolation performance of the respective techniques by comparing the reconstructed values to the discarded data. Moreover, it enables us to quantify the impact of different smile extrapolation methods on risk measure estimates, specifically the $\mathbb{RIX}$. In this empirical setting, we focus exclusively on this option-implied risk measure, as it not only partially encompasses the estimation of the BKM variance and $\mathbb{VIX}$, but also serves as an effective indicator of smile extrapolation differences due to its nature of being a tail risk measure.[70]

[70]In this chapter, most of the content is derived from my previous work, Albert et al. (2023). Although direct quotations and certain references are not always explicitly indicated, the material builds extensively on my prior research.

This chapter is structured as follows: Section 6.1 presents the numerical analysis, conducted under two distinct scenarios. First, it outlines the benchmark model and respective parameterizations used to simulate a normal and a volatile trading day – representing the two scenarios – as well as the error metric for risk measure estimates. Next, different sources of implementation errors are addressed. These include truncation alone, truncation combined with discretization, and the combination of all factors with microstructure noise. This successive combination of different error types allows for the analysis of smile construction performance across the full spectrum, from extrapolation errors alone to the complete smile under noise. As a side note, the limitations of the RND tail modeling technique from Birru and Figlewski (2012) are highlighted in this context, demonstrating that their method does not ensure a continuous volatility smile, which can affect risk measure estimates severely. Section 6.2 presents the application of the different smile construction techniques to options written on the set of *FAANG* stocks. Analogous to the numerical analysis, a normal and a volatile trading day are considered, indicated by different levels of the $\mathbb{VIX}$. Then, for three narrowed moneyness ranges, volatility smiles are constructed and $\mathbb{RIX}$ estimates are computed. To quantify the deviation between discarded and extrapolated implied volatilities, the root mean squared error (RMSE) is computed for each combination of underlying asset and moneyness range, respectively.

6.1 Numerical Analysis

In this section, we analyze the different smile construction techniques in terms of their accuracy in risk measure estimation, under both a base case and a crisis scenario. The option-implied risk measures considered are the $\mathbb{RIX}$, along with its components: the non-centered risk-neutral holding period return variance $\mathbb{V}$ and the $\mathbb{VIX}$-type integrated variance $\mathbb{IV}$, all of which, along with their replication portfolios, are presented previously in Subsection 4.4.2. Although only the downside versions are required for the $\mathbb{RIX}$, full-range estimates of $\mathbb{V}$ and $\mathbb{IV}$ are provided, as they are equivalent to the BKM variance and the $\mathbb{VIX}$ such that all risk measures discussed in this thesis are addressed.[71]

[71] Although higher-order BKM moments, such as risk-neutral skewness and kurtosis, are not directly included, they are indirectly addressed from an estimation perspective through the $\mathbb{RIX}$. This is because an

The numerical analysis is structured as follows: Subsection 6.1.1 introduces the benchmark model and scenarios. Subsection 6.1.2 deals with errors from approximating the replication portfolios of $\mathbb{V}, \mathbb{IV}$, and the $\mathbb{RIX}$ – specifically the integrals in Equations (4.64), (4.65), and (4.67) – based on limited ranges of strike prices, with the volatility smile extended by extrapolation. Subsection 6.1.3 considers the combined error from truncation and strike spacing. Section 6.1.4 conducts a simulation study to analyze how random noise in implied volatilities affects the estimation errors. In addition, Subsection 6.1.5 addresses the RND tail modeling approach of Birru and Figlewski (2012) and unveils its shortcomings within the scope of smile extrapolation, i.e. the discontinuous extension of the smile with its potentially large impact on risk measure estimates.

6.1.1 Benchmark Model and Scenarios

Similar to Aschakulporn and Zhang (2022b), we generate option prices using the SVCJ model, which was introduced in Subsection 3.1.3. We choose this explicit model because it is sufficiently rich to produce various shapes of potentially asymmetric volatility smiles, making it appropriate for our numerical analysis.[72] To create a base case and a crisis scenario, we calibrate the SVCJ model on Apple's quarterly stock options with 30 days to expiration on two distinct trading days.[73] The normal trading day (May 22, 2019) is characterized by a $\mathbb{VIX}$-level of 15 and used for the base case scenario, while the volatility trading day (May 20, 2020) exhibits a $\mathbb{VIX}$-level of 28 and refers to the crisis scenario. The calibration is carried out by minimizing the relative root mean square error (RRMSE). Spot price and risk-free interest rate are chosen arbitrarily ($S_0 = 100$, $r = 0.02$). The resulting parameter values are provided in Table 6.1 below:

accurate estimation of the $\mathbb{RIX}$ implies that its underlying drivers, specifically skewness and kurtosis, are also estimated accurately.

[72] Similar models are used in related studies in the literature. For example, Ammann and Feser (2019) use the Bates (1996) model in their comprehensive analysis of different implementation methods.

[73] We calibrate the SVCJ model on individual stock options since corresponding volatility smiles exhibit higher degrees of curvature compared to volatility smirks of index options.

Table 6.1: Parameters of the SVCJ Model in the Benchmark Scenarios

Parameter	*Base Case*	*Crisis*
κ	1.1521	1.4333
θ	0.3437	0.3779
σ	0.6772	0.9892
ρ	-0.5882	-0.6993
V_t	0.0845	0.0669
λ	3.2642	0.1876
μ_X	-0.0318	0.0473
σ_X	0.0273	0.2295
μ_y	0.2245	0.3962
ρ_J	-0.0921	-0.6677

Given the parameterizations, the SVCJ yields the following two volatility smiles (left panel) along with the corresponding risk-neutral densities (right panel):

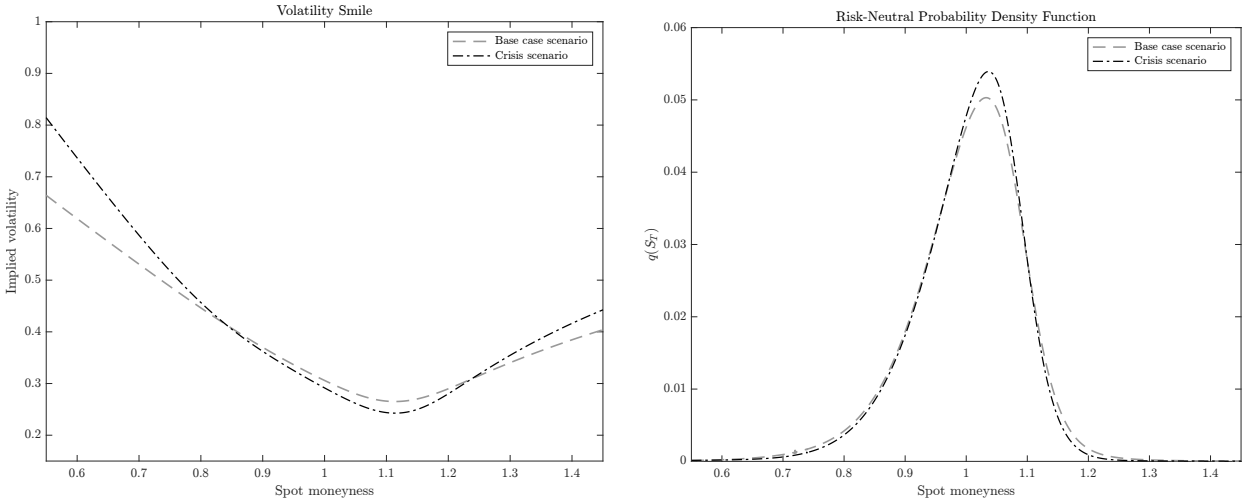

Figure 6.1: Base Case and Crisis Benchmark Scenario – The figure plots Black and Scholes (1973) volatility smiles (left panel) and underlying risk-neutral densities (right panel) implied by the SVCJ model detailed in Subsection 3.1.3. The risk-neutral density is approximated using finite differences with a fine grid of $\Delta K/S_0 = 0.1\%$. The base case scenario emerges for $\kappa = 1.1521$, $\theta = 0.3437$, $\sigma = 0.6772$, $\rho = -0.5882$, $V_t = 0.0845$, $\lambda = 3.2642$, $\mu_X = -0.0318$, $\sigma_X = 0.0273$, $\mu_y = 0.2245$, and $\rho_J = -0.0921$. The crisis scenario differs in that $\kappa = 1.4333$, $\theta = 0.3779$, $\sigma = 0.9892$, $\rho = -0.6993$, $V_t = 0.0669$, $\lambda = 0.1876$, $\mu_X = 0.0473$, $\sigma_X = 0.2295$, $\mu_y = 0.3962$, and $\rho_J = -0.6677$. Dense-grid estimates of the risk-neutral BKM annualized variance, skewness, and kurtosis are $\text{Var}^{\mathbb{Q}}/T = 0.1116$, $\text{Skew}^{\mathbb{Q}} = -1.1993$ and $\text{Kurt}^{\mathbb{Q}} = 6.5872$ in the base case and $\text{Var}^{\mathbb{Q}}/T = 0.1157$, $\text{Skew}^{\mathbb{Q}} = -2.4563$ and $\text{Kurt}^{\mathbb{Q}} = 19.7374$ in the crisis scenario.

As indicated by the wings of the smiles, the two settings differ with respect to higher-order risk-neutral moments. Estimates of BKM risk-neutral moments are $\text{Var}^{\mathbb{Q}}/T = 0.1116$

(annualized), $\text{Skew}^{\mathbb{Q}} = -1.1993$ and $\text{Kurt}^{\mathbb{Q}} = 6.5872$ in the base case and $\text{Var}^{\mathbb{Q}}/T = 0.1157$, $\text{Skew}^{\mathbb{Q}} = -2.4563$ and $\text{Kurt}^{\mathbb{Q}} = 19.7374$ in the crisis scenario.[74] Thus, the crisis scenario implies that the RND has more variance, is more left-skewed, and is more leptokurtic than the one considered in the base case. The implied risk-neutral skewness matches CBOE SKEW Index values during normal and crisis times. Moreover, the skewness is in line with Aschakulporn and Zhang (2022b) in both scenarios. To obtain estimation errors with respect to the benchmark scenarios, we follow Ammann and Feser (2019) and compute percentage errors for different risk-neutral moment-based measures

$$100 \times \frac{\left|\widehat{\mathcal{Y}} - \mathcal{Y}_{\text{dense}}\right|}{\mathcal{Y}_{\text{dense}}}, \qquad \mathcal{Y} = \mathbb{V}, \mathbb{IV}, \mathbb{RIX}, \tag{6.1}$$

where $\widehat{\mathcal{Y}}$ is the candidate estimate and $\mathcal{Y}_{\text{dense}}$ is its benchmark obtained from the full range of SVCJ OTM option prices. In our numerical implementation, we use a grid size of $\Delta K/S_0 = 0.1\%$ and a spot moneyness range of $[0.01, 1.99]$. According to Aschakulporn and Zhang (2022a), skewness approximation errors remain below 10^{-3} for this grid size provided a moneyness range of at least 3/4 to 4/3 of the forward price. Since skewness is a key driver of the $\mathbb{RIX}$, this grid size is chosen accordingly. As defined in Equations (4.64), (4.65), and (4.67), $\mathbb{V}$ and $\mathbb{IV}$ employ OTM put and call options whereas $\mathbb{RIX}$ uses OTM puts only. The following table shows the benchmark estimates:

Table 6.2: Benchmark Scenarios – Model-Free Measures

	Gao et al. (2018)		
	$\mathbb{V}_{\text{dense}}$	$\mathbb{IV}_{\text{dense}}$	$\mathbb{RIX}_{\text{dense}}$
Base Case	0.1117	0.1076	0.0057
Crisis	0.1158	0.1078	0.0095

The table shows dense-grid ($\Delta K/S_0 = 0.1\%$) benchmark estimates of the Gao et al. (2018) model-free measures $\mathbb{V}$, $\mathbb{IV}$, and $\mathbb{RIX}$ for the base case and the crisis scenarios. All estimates are computed from the full range of SVCJ OTM option prices $K_{\text{put}}/S_0 \in [0.01, 1]$, $K_{\text{call}}/S_0 \in (1, 1.99]$ ($\mathbb{RIX}$ from OTM put options only) using trapezoidal integration.

[74] Estimates of BKM risk-neutral moments are obtained from a fine grid ($\Delta K/S_0 = 0.1\%$) of SVCJ OTM option prices across the full moneyness range ($K_{\text{put}}/S_0 \in [0.01, 1]$, $K_{\text{call}}/S_0 \in (1, 1.99]$). Model-generated risk-neutral moments are computed using high-accuracy trapezoidal integration.

6.1.2 Truncation

Having introduced the benchmark model and the two scenarios, we now turn to analyzing the error arising from smile extrapolation, commonly referred to as truncation error. Table 6.3 shows estimation errors when option prices are limited to moneyness ranges of ±25%, ±20%, and ±15% around the spot price and smiles are extended by flat extrapolation (EndPoint), linear extrapolation (LinReg), and RND tail extrapolation (RND), the latter being the technique presented in Subsection 5.1.2.[75] In the available range, benchmark option prices are sampled at a fine grid of $\Delta K/S_0 = 0.1\%$ corresponding to 1981 equally spaced strikes for $\mathbb{V}$ and $\mathbb{IV}$ and 991 for the $\mathbb{RIX}$. Keeping the grid size, the truncated ranges reduce the number of available strikes to 501 for ±25% (251 for $\mathbb{RIX}$), 401 for ±20% (201 for $\mathbb{RIX}$), and 301 for ±15% (151 for $\mathbb{RIX}$). Extrapolation is then used to recover the range of 1981 (991) strikes. All estimates result from trapezoidal integration without interpolation or smoothing.

Table 6.3: Estimation Errors Model-Free Measures – Truncation

	$\mathbb{V}$			$\mathbb{IV}$			$\mathbb{RIX}$		
Obs. range	±25%	±20%	±15%	±25%	±20%	±15%	−25%	−20%	−15%
Panel A: Base Case Scenario									
EndPoint	1.6633	3.2640	5.8731	1.2830	2.6147	4.8715	8.7915	15.5398	24.7732
LinReg	0.0643	0.2564	0.8710	0.0409	0.1980	0.7628	0.4322	1.3784	3.6738
RND	0.0682	0.2000	0.1929	0.0506	0.1552	0.1109	0.4046	1.1134	1.4192
Panel B: Crisis Scenario									
EndPoint	10.0051	12.7714	16.1127	7.1999	9.5510	12.5204	41.4249	48.9764	56.5466
LinReg	2.8324	5.6067	9.1906	1.1288	3.2268	6.7437	15.8089	26.8983	37.1497
RND	0.1001	1.3119	3.9015	0.0666	0.8544	2.8208	2.2844	7.1419	16.3818

The table shows percentage errors $100 \times |\widehat{\mathcal{Y}} - \mathcal{Y}_{\text{dense}}|/\mathcal{Y}_{\text{dense}}$ for $\mathcal{Y} = \mathbb{V}, \mathbb{IV}, \mathbb{RIX}$ using endpoint volatility (EndPoint), linear regression (LinReg), and RND tail (RND) extrapolation for the base case (Panel A) and crisis scenario (Panel B). $\mathcal{Y}_{\text{dense}}$ is the respective benchmark computed from the full range of SVCJ OTM option prices $K_{\text{put}}/S_0 \in [0.01, 1]$, $K_{\text{call}}/S_0 \in (1, 1.99]$ ($\mathbb{RIX}$ from OTM put options only) and $\widehat{\mathcal{Y}}$ is the estimate from the truncated and extrapolated volatility smile. Errors are shown for observable moneyness ranges $[K_{\text{put}}^{\min}/S_0, K_{\text{call}}^{\max}/S_0]$ of $[0.75, 1.25]$ (±25%), $[0.8, 1.2]$ (±20%), $[0.85, 1.15]$ (±15%) where $\mathbb{RIX}$ uses OTM put options only. $\mathcal{Y}_{\text{dense}}$ and $\widehat{\mathcal{Y}}$ follow from trapezoidal integration across dense grids of strikes with $\Delta K/S_0 = 0.1\%$.

[75] Ammann and Feser (2019) show $\mathbb{RIX}$ estimation errors for moneyness ranges ("domain half-width") of -10%, -50% and -80% and report that $\mathbb{RIX}$ estimates become stable at -50%. In contrast, we focus on ranges between -25% and -15% as these more realistic in the light of available data.

Intuitively, errors increase when the observable range of option prices becomes narrower. Without the usual strike spacing and microstructure noise, the results in Table 6.3 confirm that the RND tail extrapolation technique outperforms standard methods in both scenarios. This finding can be attributed to several reasons:

First, *endpoint volatility* extends the truncated smiles using implied volatilities at the outermost strikes K_1 and K_N, only. The narrower the available range of option prices, the larger the error. Deviations from the benchmark smiles are more pronounced in the crisis scenario than in the base case, since the steepness in the former scenario leads to implied volatilities and option prices that are too low. The tails of the underlying RND are underestimated which is more pronounced for the left tail due to negative risk-neutral skewness in the distribution. For $\mathbb{V}$ and $\mathbb{IV}$, the estimation errors reach up to 16.11% and 12.52% in the crisis scenario, compared to 5.87% and 4.87% in the base case. For the $\mathbb{RIX}$, which is computed based solely on OTM put options, the asymmetric smile in the crisis scenario exacerbates the estimation errors, reaching up to 56.55% compared to 24.77% in the base case. With respect to truncation, endpoint volatility has the highest errors when computing risk measure estimates.

Second, *linear extrapolation* determines the slope of the smile outside the available range from the two outermost strikes on each side K_1, K_2, K_{N-1}, and K_N. The bias due to truncation is substantially reduced for all model-free measures in both scenarios. Due to the curvature of the benchmark smiles, errors increase when the moneyness range becomes narrower. The increased convexity of the smile's left wing in the crisis scenario results in higher linear extrapolation errors, reaching 9.19%, 6.74%, and 37.15% for $\mathbb{V}$, $\mathbb{IV}$, and $\mathbb{RIX}$, respectively. In contrast, the base case yields errors of 0.87%, 0.76%, and 3.67%. Linear extrapolation is thus superior to endpoint volatility in the absence of microstructure noise and with densely sampled strikes, but it can still produce sizable errors depending on the degree of smile curvature.

Third, *RND tail modeling* parameterizes the GEV based on the outermost option prices at the strikes K_1 and K_N as well as on the PDF and CDF values of the RND at K_2 and K_{N-1}. In the base case, the GEV tails reproduce the less curved implied volatility smile with small percentage errors. $\mathbb{V}$, $\mathbb{IV}$, and $\mathbb{RIX}$ errors in absolute terms are of similar size or slightly smaller than those from linear extrapolation. In the crisis scenario, the steeper smile with a more pronounced degree of curvature implies higher option prices that are reflected in the PDF and CDF of the RND. Due to its flexibility, the GEV is capable to produce different shapes of the RND and thus accommodate heavier tails. This leads to considerably lower errors and a less severe impact of the truncation range compared to standard extrapolation methods. For the most extreme case – that is $\mathbb{RIX}$ estimation given the narrowest moneyness range – the RND tail modeling approach produces an absolute percentage error that is less than half of the error from linear regression and nearly one-third of that from endpoint volatility.

6.1.3 Strike Spacing

In the next step, we extend the prior analysis to grids with a more realistic strike spacing. In addition to limiting the moneyness range, we assume equally spaced grids with $\Delta K/S_0 = 1\%, 2\%$ and 5%. This further reduces the number of observable contracts for the computation of $\mathbb{V}$ and $\mathbb{IV}$ ($\mathbb{RIX}$) down to $\tilde{N} = 7$ ($\tilde{N} = 4$) for $\pm 15\%$ (-15%) and $\Delta K/S_0 = 5\%$. To approximate the estimators defined in Equations (4.64), (4.65), and (4.67), we apply a natural cubic spline to interpolate the observable implied volatilities. This generates a dense grid of strike prices. Due to the absence of microstructure noise, we omit smoothing.[76] Then, extrapolation is carried out along the lines of Section 6.1.2 and $\mathbb{V}$, $\mathbb{IV}$, and $\mathbb{RIX}$ estimates are computed using trapezoidal integration. The corresponding absolute percentage errors are shown in Table 6.4 on the following page.

[76] As outlined in Subsection 5.2.1, the natural cubic spline arises from Equation (5.19) for $\lambda = 0$.

Table 6.4: Estimation Errors Model-Free Measures – Strike Spacing

	$\mathbb{V}$			$\mathbb{IV}$			$\mathbb{RIX}$		
Obs. range	±25%	±20%	±15%	±25%	±20%	±15%	−25%	−20%	−15%
Panel A: Base Case Scenario									
$\Delta K/S_0 = 1\%$	$\tilde{N} = 51$	$\tilde{N} = 41$	$\tilde{N} = 31$	$\tilde{N} = 51$	$\tilde{N} = 41$	$\tilde{N} = 31$	$\tilde{N} = 26$	$\tilde{N} = 21$	$\tilde{N} = 16$
EndPoint	1.6633	3.2640	5.8730	1.2830	2.6147	4.8714	8.7914	15.5397	24.7731
LinReg	0.0663	0.2705	0.9096	0.0417	0.2111	0.7998	0.4483	1.4320	3.7942
RND	0.0092	0.2456	0.6322	0.0029	0.1974	0.5871	0.0814	1.2084	2.3264
$\Delta K/S_0 = 2\%$	$\tilde{N} = 26$	$\tilde{N} = 21$	$\tilde{N} = 16$	$\tilde{N} = 26$	$\tilde{N} = 21$	$\tilde{N} = 16$	$\tilde{N} = 13$	$\tilde{N} = 11$	$\tilde{N} = 8$
EndPoint	1.6632	3.2638	5.8723	1.2830	2.6145	4.8707	8.7912	15.5392	24.7724
LinReg	0.0695	0.2950	0.9622	0.0440	0.2317	0.8477	0.4672	1.5475	3.9859
RND	0.0247	0.2910	0.7389	0.0138	0.3091	0.6806	0.1767	0.7691	2.7621
$\Delta K/S_0 = 5\%$	$\tilde{N} = 11$	$\tilde{N} = 9$	$\tilde{N} = 7$	$\tilde{N} = 11$	$\tilde{N} = 9$	$\tilde{N} = 7$	$\tilde{N} = 6$	$\tilde{N} = 5$	$\tilde{N} = 4$
EndPoint	1.6631	3.2610	5.8602	1.2830	2.6118	4.8574	8.7869	15.5305	24.7599
LinReg	0.0864	0.3483	1.1026	0.0552	0.2777	0.9750	0.5731	1.7828	4.5043
RND	0.0431	0.2395	0.9310	0.0254	0.2009	0.8484	0.2972	1.1229	3.5479
Panel B: Crisis Scenario									
$\Delta K/S_0 = 1\%$	$\tilde{N} = 51$	$\tilde{N} = 41$	$\tilde{N} = 31$	$\tilde{N} = 51$	$\tilde{N} = 41$	$\tilde{N} = 31$	$\tilde{N} = 26$	$\tilde{N} = 21$	$\tilde{N} = 16$
EndPoint	10.0051	12.7713	16.1125	7.1998	9.5509	12.5202	41.4247	48.9762	56.5464
LinReg	2.9197	5.7738	9.3434	1.1772	3.3819	6.8725	16.2173	27.4580	37.6026
RND	1.0707	4.4211	8.2642	0.6228	2.9938	6.0655	5.2882	19.9643	33.5352
$\Delta K/S_0 = 2\%$	$\tilde{N} = 26$	$\tilde{N} = 21$	$\tilde{N} = 16$	$\tilde{N} = 26$	$\tilde{N} = 21$	$\tilde{N} = 16$	$\tilde{N} = 13$	$\tilde{N} = 11$	$\tilde{N} = 8$
EndPoint	10.0047	12.7706	16.1112	7.1996	9.5502	12.5188	41.4237	48.9748	56.5451
LinReg	3.0473	5.9610	9.5065	1.2484	3.5554	7.0111	16.8278	28.0805	38.0727
RND	1.7007	5.0423	8.7383	1.0153	3.4406	6.4392	8.4553	22.5919	35.1688
$\Delta K/S_0 = 5\%$	$\tilde{N} = 11$	$\tilde{N} = 9$	$\tilde{N} = 7$	$\tilde{N} = 11$	$\tilde{N} = 9$	$\tilde{N} = 7$	$\tilde{N} = 6$	$\tilde{N} = 5$	$\tilde{N} = 4$
EndPoint	9.9999	12.7595	16.0892	7.1961	9.5403	12.4954	41.4049	48.9490	56.5220
LinReg	3.3686	6.4980	9.9807	1.3856	4.0447	7.4078	18.4582	29.8796	39.4845
RND	2.5009	5.9561	9.4676	1.4991	4.1168	7.0251	12.4445	26.2664	37.5623

The table shows percentage errors $100 \times |\widehat{\mathcal{Y}} - \mathcal{Y}_{\text{dense}}|/\mathcal{Y}_{\text{dense}}$ for $\mathcal{Y} = \mathbb{V}, \mathbb{IV}, \mathbb{RIX}$ using endpoint volatility (EndPoint), linear regression (LinReg), and RND tail (RND) extrapolation for the base case (Panel A) and crisis scenario (Panel B). $\mathcal{Y}_{\text{dense}}$ is the respective benchmark computed from the full range of SVCJ OTM option prices $K_{\text{put}}/S_0 \in [0.01, 1]$, $K_{\text{call}}/S_0 \in (1, 1.99]$ ($\mathbb{RIX}$ from OTM put options only) and $\widehat{\mathcal{Y}}$ is the estimate from the truncated and extrapolated volatility smile. Errors are shown for observable moneyness ranges $[K_{\text{put}}^{\min}/S_0, K_{\text{call}}^{\max}/S_0]$ of $[0.75, 1.25]$ (±25%), $[0.8, 1.2]$ (±20%), $[0.85, 1.15]$ (±15%) where $\mathbb{RIX}$ uses OTM put options only. $\mathcal{Y}_{\text{dense}}$ follow from trapezoidal integration across dense grids of strikes with $\Delta K/S_0 = 0.1\%$. $\widehat{\mathcal{Y}}$ are obtained by assuming that options are available for strike grids with $\Delta K/S_0 = 1\%, 2\%, 5\%$ corresponding to $\tilde{N}$ available contracts which are interpolated by a natural cubic spline to achieve $\Delta K/S_0 = 0.1\%$.

For simplicity, we assume that variations in grid size do not affect the outermost strikes $K_1 = \tilde{K}_1$ and $K_N = \tilde{K}_{\tilde{N}}$. Consequently, since the natural cubic spline passes exactly through all observable implied volatilities, the results for *endpoint volatility* are comparable to those in Table 6.3.

For *linear regression*, the impact of coarser strike grids is also limited, due to the following reasons: The slope of the linear extrapolation is derived from the two outermost available strikes on each side of the smile after interpolation. Errors are mainly determined by the interplay between the curvature of the benchmark smile and the width of the observable moneyness range. Further, as the natural cubic spline minimizes the curvature of its piecewise polynomials, this may lead to an underestimation of the curvature of the benchmark smile. As a consequence, the impact of the strike spacing is stronger in the crisis scenario than in the base case.

Errors from *RND tail modeling* are more sensitive with respect to the strike spacing. In the base case, the percentage errors increase slightly but remain smaller than those from linear extrapolation for almost every moneyness range/strike spacing combination. In the crisis scenario, percentage errors are typically considerably lower and tend to increase with the widening strike spacing up to the level of their linear extrapolation counterparts for $\Delta K/S_0 = 5\%$. Errors from linear extrapolation are higher but remain at the same level for differently spaced strikes. This pattern in RND tail modeling errors is due to the technique's reliance on risk-neutral PDF and CDF values. While implied volatilities at $\tilde{K}_1 = K_1$ and $\tilde{K}_{\tilde{N}} = K_N$ are not distorted, PDF and CDF values are highly sensitive to the interpolation procedure at the connecting strikes K_2 and K_{N-1}. Small changes in the slope or curvature of the smile affect the finite differences approximation of the PDF and CDF values which then enter the optimization problem that determines the GEV parameters directly. Thus, RND tail modeling yields different errors in comparison to the dense grid benchmark estimates.

In the absence of noise, linear or RND tail extrapolation should be preferred over endpoint volatility when computing option-implied risk measures, especially for tail risk measures like the $\mathbb{RIX}$. In the crisis scenario, errors from RND extrapolation are smaller than those generated by standard extrapolation methods. As metrics like the $\mathbb{RIX}$ depend strongly on the accuracy of extrapolation to capture jump risk, RND tail modeling yields better results when the RND features negative skewness and excess kurtosis.

6.1.4 Microstructure Noise

An evident drawback of linear extrapolation is its pronounced sensitivity to microstructure noise, as highlighted by Ammann and Feser (2019). Therefore, we conduct a simulation study to shed light on the impact of noise on percentage errors when endpoint volatility, linear, and RND tail extrapolation are applied to estimate $\mathbb{V}$, $\mathbb{IV}$, and $\mathbb{RIX}$. For each moneyness range and strike spacing we generate randomly perturbed implied volatilities $\tilde{\sigma}_{\text{noisy},i}$ according to

$$\tilde{\sigma}_{\text{noisy},i} = \tilde{\sigma}_i \left(1 + \theta\eta\right), \quad i = 1, \ldots, \tilde{N}, \tag{6.2}$$

where $\tilde{\sigma}_i$ are the Black and Scholes (1973) implied volatilities from SVCJ option prices in the base case and crisis scenario, $\eta \sim \mathcal{N}(0,1)$ is a normally distributed random variable, θ controls the amount of noise and $\tilde{\sigma}_{\text{noisy},i}$ are the resulting noisy observations. This approach differs from the existing literature which adds noise to option prices rather than to implied volatilities. The measurement errors generated by Equation (6.2) increase with the level of implied volatility, reflecting the common observation that bid-ask spreads are typically wider for deep OTM contracts. Figure 6.2 depicts the benchmark implied volatility smiles in the base case and the crisis scenario with 95% confidence intervals of noisy observations for $\theta = 2\%$. This implies that, for $\tilde{\sigma}_i = 30\%$, for example, the perturbed $\tilde{\sigma}_{\text{noisy},i}$ will lie within a bid-ask spread of about 2.35% or less with 95% probability ($\leq 1.18\%$ for $\theta = 1\%$ and $\leq 3.53\%$ for $\theta = 3\%$).[77]

[77] For 40%, this spread amounts to ≤ 3.14 for $\theta = 2\%$ ($\leq 1.57\%$ for $\theta = 1\%$ and $\leq 4.70\%$ for $\theta = 3\%$) with 95% probability.

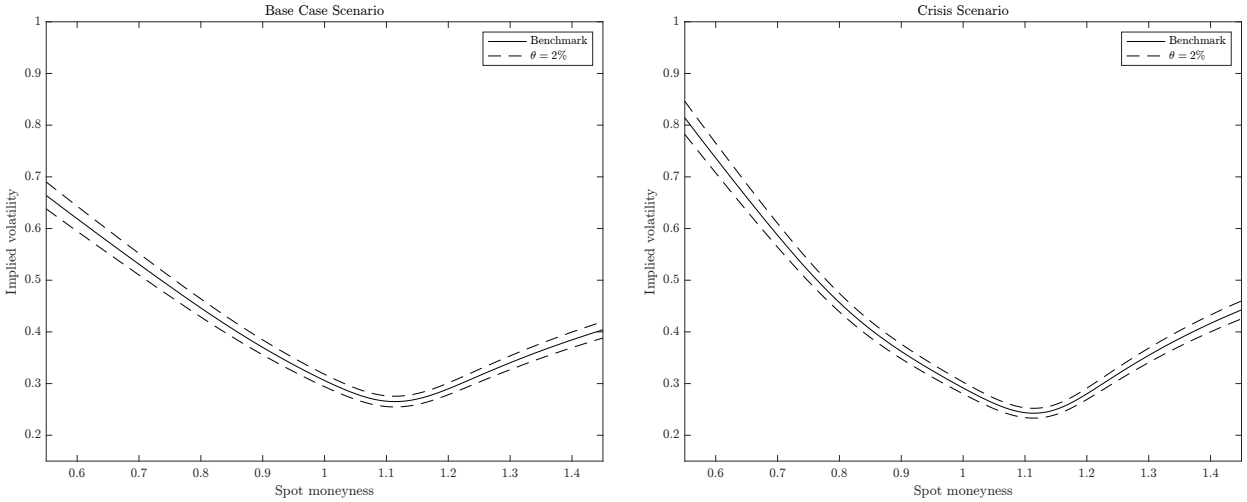

Figure 6.2: Confidence Intervals Simulated Microstructure Noise – The figure plots Black and Scholes (1973) implied volatility smiles in the base case (left panel) and crisis scenario (right panel) alongside with the 95% confidence intervals for randomly perturbed observations $\tilde{\sigma}_{\text{noisy},i} = \tilde{\sigma}_i\,(1+\theta\eta)$, $i = 1, \ldots, \tilde{N}$ where $\tilde{\sigma}_i$ are benchmark implied volatilities generated by the SVCJ model and $\eta \sim \mathcal{N}(0,1)$ for $\theta = 2\%$. The base case scenario emerges for $\kappa = 1.1521$, $\theta = 0.3437$, $\sigma = 0.6772$, $\rho = -0.5882$, $V_t = 0.0845$, $\lambda = 3.2642$, $\mu_X = -0.0318$, $\sigma_X = 0.0273$, $\mu_y = 0.2245$, and $\rho_J = -0.0921$. The crisis scenario differs in that $\kappa = 1.4333$, $\theta = 0.3779$, $\sigma = 0.9892$, $\rho = -0.6993$, $V_t = 0.0669$, $\lambda = 0.1876$, $\mu_X = 0.0473$, $\sigma_X = 0.2295$, $\mu_y = 0.3962$, and $\rho_J = -0.6677$. Dense-grid estimates of the risk-neutral BKM annualized variance, skewness, and kurtosis are $\text{Var}^{\mathbb{Q}}/T = 0.1116$, $\text{Skew}^{\mathbb{Q}} = -1.1993$ and $\text{Kurt}^{\mathbb{Q}} = 6.5872$ in the base case and $\text{Var}^{\mathbb{Q}}/T = 0.1157$, $\text{Skew}^{\mathbb{Q}} = -2.4563$ and $\text{Kurt}^{\mathbb{Q}} = 19.7374$ in the crisis scenario.

Table 6.5 on the following page shows average estimation errors for $\mathbb{V}$, $\mathbb{IV}$, and $\mathbb{RIX}$ based on 1000 sets of perturbed implied volatilities with microstructure noise when $\theta = 2\%$. Tables 6.6 and 6.7 at the subsection's end report the results for $\theta = 1\%$ to 3%. Error standard deviations are given in parentheses. As before, we vary the moneyness range and the strike spacing to examine how the interplay between different sources of error affects estimates obtained from endpoint volatility, linear regression, and RND tail extrapolation. Cubic spline smoothing is applied to recover a dense grid of strikes with $\Delta K/S_0 = 0.1\%$ from the perturbed implied volatilities. For endpoint volatility and linear regression, the standard spline version is used, while for RND tail modeling, the additional convexity preserving constraints are enforced. The benchmark estimates $\mathcal{Y}_{\text{dense}}$ remain unchanged.

Table 6.5: Average Estimation Errors $\mathbb{V}$, $\mathbb{IV}$, $\mathbb{RIX}$ – Microstructure Noise ($\theta = 2\%$)

	$\mathbb{V}$			$\mathbb{IV}$			$\mathbb{RIX}$		
Obs. range	±25%	±20%	±15%	±25%	±20%	±15%	−25%	−20%	−15%
Panel A: Base Case Scenario									
$\Delta K/S_0 = 1\%$									
EndPoint	1.7245	3.2877	5.9337	1.3490	2.6371	4.9308	8.8799	15.5541	24.9031
	(0.7460)	(0.7601)	(0.8481)	(0.6949)	(0.7281)	(0.8034)	(1.6524)	(1.7527)	(2.0070)
LinReg	0.9436	2.1004	3.3834	0.8441	1.6344	2.7139	4.1488	12.1014	17.3491
	(1.0575)	(7.3974)	(10.4656)	(1.3565)	(4.6544)	(6.8053)	(5.4505)	(60.3711)	(83.3280)
RND	0.7662	1.1462	2.0278	0.6740	0.9419	1.6808	3.0339	5.3631	9.1444
	(0.6299)	(1.2992)	(2.0306)	(0.5375)	(0.9245)	(1.4893)	(3.0201)	(8.7003)	(12.2417)
$\Delta K/S_0 = 2\%$									
EndPoint	1.7788	3.2987	5.9019	1.4277	2.6477	4.8977	8.9102	15.6057	24.8691
	(0.9631)	(1.0605)	(1.2002)	(0.8755)	(1.0158)	(1.1445)	(2.2484)	(2.2933)	(2.6485)
LinReg	1.4303	2.6492	3.4581	1.2488	2.0618	2.8319	6.7282	16.5746	16.5630
	(2.7344)	(20.3827)	(5.2640)	(2.0027)	(10.7220)	(3.8991)	(20.2345)	(200.9856)	(33.4848)
RND	1.0566	1.3959	2.4659	0.9341	1.1659	2.0152	4.2326	6.4565	11.4825
	(0.9705)	(1.3217)	(2.7167)	(0.7778)	(1.0112)	(1.9238)	(5.5587)	(7.6908)	(17.5472)
$\Delta K/S_0 = 5\%$									
EndPoint	2.0388	3.3801	5.9434	1.7509	2.7699	4.9194	9.0061	15.5989	25.1786
	(1.3825)	(1.6539)	(1.7790)	(1.2689)	(1.5424)	(1.7348)	(3.2634)	(3.3998)	(3.3091)
LinReg	1.6892	2.1283	2.8492	1.5738	1.8471	2.3821	6.2011	9.5201	12.4604
	(1.4931)	(1.9624)	(2.4454)	(1.3518)	(1.6141)	(1.9505)	(8.4019)	(11.0144)	(12.5932)
RND	1.5129	1.8935	2.5271	1.3856	1.6249	2.1231	5.3290	8.2590	11.2687
	(1.2010)	(1.5731)	(2.2236)	(1.0865)	(1.3023)	(1.7610)	(5.4967)	(8.0713)	(12.0881)
Panel B: Crisis Scenario									
$\Delta K/S_0 = 1\%$									
EndPoint	10.1264	12.8370	16.1891	7.3151	9.6159	12.5958	41.5612	49.0403	56.6415
	(0.7565)	(0.7359)	(0.7966)	(0.7355)	(0.7179)	(0.7751)	(1.2707)	(1.1748)	(1.2229)
LinReg	5.5353	9.3647	11.7996	3.3473	6.4165	8.7549	27.8110	42.8380	47.6512
	(15.6522)	(18.8217)	(17.2233)	(8.3927)	(11.1471)	(10.5816)	(99.1038)	(108.0739)	(94.4738)
RND	4.5607	6.8721	9.7103	3.0284	4.8884	7.2571	20.9241	29.1939	37.9253
	(2.1024)	(2.8439)	(3.7165)	(1.4859)	(2.0446)	(2.6680)	(9.4762)	(12.3837)	(16.1471)
$\Delta K/S_0 = 2\%$									
EndPoint	10.1405	12.8401	16.1573	7.3334	9.6192	12.5632	41.5029	49.0343	56.6007
	(1.0207)	(1.0119)	(1.1160)	(0.9953)	(0.9975)	(1.0953)	(1.6892)	(1.5094)	(1.5849)
LinReg	7.3170	9.3258	10.7803	4.6906	6.5702	8.0290	36.7359	43.4754	42.2453
	(18.2264)	(34.6330)	(6.4968)	(10.5451)	(18.2972)	(4.7217)	(109.5680)	(223.6443)	(27.8208)
RND	4.7910	6.9982	9.4720	3.2182	4.9696	7.0668	21.7683	29.7649	37.0732
	(2.3549)	(3.1150)	(3.7455)	(1.6966)	(2.2556)	(2.8052)	(10.4324)	(13.5568)	(15.1840)
$\Delta K/S_0 = 5\%$									
EndPoint	10.1426	12.8611	16.1838	7.3377	9.6483	12.5722	41.4850	48.9443	56.7468
	(1.6413)	(1.5928)	(1.6389)	(1.6317)	(1.5876)	(1.6504)	(2.3303)	(2.1869)	(1.9497)
LinReg	5.3366	6.9507	10.0354	3.7445	4.7684	7.5110	25.7046	30.4975	38.9435
	(4.7442)	(4.0461)	(3.6064)	(3.6374)	(3.0914)	(2.9649)	(22.4480)	(16.7320)	(11.3941)
RND	5.0353	6.8641	9.7635	3.4331	4.9098	7.3054	22.8725	28.8523	37.9672
	(2.7462)	(3.5065)	(3.3383)	(2.0259)	(2.5905)	(2.7144)	(11.9799)	(14.7157)	(11.2561)

The table shows simulation-based averages (1000 runs) of percentage errors $100 \times |\widehat{\mathcal{Y}} - \mathcal{Y}_{\text{dense}}|/\mathcal{Y}_{\text{dense}}$ for $\mathcal{Y} = \mathbb{V}, \mathbb{IV}, \mathbb{RIX}$ using endpoint volatility (EndPoint), linear regression (LinReg), and RND tail (RND) extrapolation for the base case (Panel A) and crisis scenario (Panel B) with error standard deviation in parentheses. $\mathcal{Y}_{\text{dense}}$ is the respective benchmark computed from the full range of SVCJ OTM option prices $K_{\text{put}}/S_0 \in [0.01, 1]$, $K_{\text{call}}/S_0 \in (1, 1.99]$ ($\mathbb{RIX}$ OTM put options only) using trapezoidal integration over dense grids of strikes with $\Delta K/S_0 = 0.1\%$. Estimates $\widehat{\mathcal{Y}}$ are obtained from randomly perturbed implied volatility smiles $\tilde{\sigma}_{\text{noisy},i} = \tilde{\sigma}_i\,(1 + 0.02\eta)$, $i = 1, \ldots, \tilde{N}$ where $\tilde{\sigma}_i$ are Black and Scholes (1973) implied volatilities computed from SVCJ option prices and $\eta \sim \mathcal{N}(0, 1)$. $\widehat{\mathcal{Y}}$ are computed from extrapolated moneyness ranges $[K_{\text{put}}^{\min}/S_0, K_{\text{call}}^{\max}/S_0]$ of $[0.75, 1.25]$ (±25%), $[0.8, 1.2]$ (±20%), and $[0.85, 1.15]$ (±15%) ($\mathbb{RIX}$: OTM put options only) based on cubic spline smoothing (RND: with convexity constraints) of strike grids with $\Delta K/S_0 = 1\%, 2\%, 5\%$.

The results show that without noise, estimation errors from endpoint volatility are generally higher than those from the other extrapolation techniques. With noise, they increase only slightly and error standard deviations grow moderately with θ. Simulated microstructure noise mainly affects linear regression and RND tail extrapolation. In the base case, estimation errors from LinReg rise considerably on average compared to their RND counterparts, even though they do not exceed those from endpoint volatility. Smiles based on linear regression generate the least stable results. In terms of the errors' standard deviation, values are up to 201% for $\Delta K/S_0 = 2\%$ and 20% moneyness range in case of the $\mathbb{RIX}$, while RND values are moderate. Differences in extrapolation techniques are even more pronounced in the crisis scenario. $\mathbb{V}$, $\mathbb{IV}$, and $\mathbb{RIX}$ estimation errors from EndPoint remain stable but are considerably larger than their LinReg and RND counterparts. LinReg again generates the least stable results now with a standard deviation up to 224% for $\Delta K/S_0 = 2\%$ and 20% moneyness range in case of the $\mathbb{RIX}$.

The large variations in LinReg error standard deviations in the presence of microstructure noise are due to two contrary effects. First, an unfavorably perturbed implied volatility near the spline's boundary can have a substantial impact on the slope between its outermost knots. Large deviations in this slope and thus estimation errors become more likely. Second, the larger the strike spacing is, the more pronounced is the impact of smoothing. The influence of a single unfavorably perturbed implied volatility near the boundary of the spline can be dampened by the roughness penalty term. As implied volatilities are perturbed randomly, it is difficult to assess which effect will eventually prevail. With the noise level increasing, extreme LinReg errors and error standard deviations become more likely. As already stated by Ammann and Feser (2019), for example, linear extrapolation must be considered as highly unreliable in the presence of microstructure noise. As this technique may yield misleading results, we conclude that it should not be used in smile construction for the estimation of option-implied risk measures.

The numbers confirm that RND tail extrapolation is considerably more robust with respect to microstructure noise than linear extrapolation which can be attributed to its construction based on option prices and risk-neutral PDF and CDF values. This approach prevents large errors by ensuring that the underlying RND is well-behaved in the sense that it is positive and continuous. Average risk measure estimation errors and standard deviations are generally low. In line with intuition, they increase with the level of the noise. For high microstructure noise and a narrow moneyness range of -15% – as shown in Table 6.7 – the advantage of RND tail modeling over endpoint volatility vanishes with coefficients of variation around 1. In these limiting cases, endpoint volatility may be preferable as it represents the best estimate in the absence of reliable information (the number of contracts available to smile construction is limited to 7 for $\Delta K/S_0 = 5\%$). This may explain why endpoint volatility is often considered as the method of choice in smile construction. In the crisis scenario, average estimation errors from RND tail extrapolation are considerably smaller than those from endpoint volatility and error standard deviations remain moderate. RND tail extrapolation can mitigate the bias induced by endpoint volatility and is – at the same time – considerably more stable than linear extrapolation. Hence, we conclude that, in particular when event risk is high, it is the superior approach to obtain accurate estimates of $\mathbb{V}$, $\mathbb{IV}$, and especially the $\mathbb{RIX}$.

Having confirmed the superiority of the arbitrage-free RND-based smile construction approach within this numerical analysis, we now turn to the tail modeling approach proposed by Birru and Figlewski (2012), which, while similar to yet distinct from our technique, exhibits considerable limitations in smile extrapolation. To illustrate these drawbacks, the following subsection uses this model-based setting to address the issue of smile discontinuity and its implications for risk measure estimates, with particular emphasis on the $\mathbb{RIX}$, which is most affected.

Table 6.6: Average Estimation Errors $\mathbb{V}$, $\mathbb{IV}$, $\mathbb{RIX}$ – Low Microstructure Noise ($\theta = 1\%$)

	$\mathbb{V}$			$\mathbb{IV}$			$\mathbb{RIX}$		
Obs. range	±25%	±20%	±15%	±25%	±20%	±15%	−25%	−20%	−15%
Panel A: Base Case Scenario									
$\Delta K/S_0 = 1\%$									
EndPoint	1.7012	3.2864	5.9121	1.3159	2.6366	4.9115	8.8509	15.5648	24.8266
	(0.3801)	(0.3839)	(0.4335)	(0.3664)	(0.3673)	(0.4093)	(0.8363)	(0.8944)	(1.0497)
LinReg	0.5183	0.9857	2.0870	0.4419	0.7885	1.7341	2.4604	4.9550	9.5963
	(0.7701)	(1.3968)	(3.3704)	(0.6094)	(1.0190)	(2.3628)	(5.1290)	(8.7475)	(22.8086)
RND	0.4123	0.6915	1.4286	0.3558	0.5650	1.2120	1.7428	3.2716	6.1905
	(0.3304)	(0.5847)	(1.0567)	(0.2825)	(0.4532)	(0.8200)	(1.4922)	(3.2506)	(5.6731)
$\Delta K/S_0 = 2\%$									
EndPoint	1.7170	3.2932	5.9010	1.3314	2.6424	4.8997	8.8637	15.5833	24.8071
	(0.5159)	(0.5332)	(0.6073)	(0.4953)	(0.5142)	(0.5782)	(1.1316)	(1.1621)	(1.3563)
LinReg	0.6942	1.1152	2.1505	0.5966	0.9211	1.7618	3.1795	5.6135	9.7631
	(0.8312)	(2.0274)	(1.9692)	(0.6537)	(1.4344)	(1.5122)	(5.1509)	(14.2492)	(10.4508)
RND	0.5560	0.8201	1.5849	0.4858	0.6770	1.3205	2.2690	3.8600	7.0678
	(0.4622)	(0.7235)	(1.1855)	(0.3870)	(0.5610)	(0.9155)	(2.2955)	(3.9959)	(6.4612)
$\Delta K/S_0 = 5\%$									
EndPoint	1.7478	3.3239	5.9260	1.3869	2.6752	4.9158	8.9049	15.5652	24.9322
	(0.8303)	(0.8479)	(0.8923)	(0.7700)	(0.8257)	(0.8713)	(1.6443)	(1.7054)	(1.6556)
LinReg	0.8359	1.1701	1.8271	0.7695	0.9844	1.5431	3.1140	5.4102	7.8458
	(0.6438)	(0.8974)	(1.2811)	(0.5949)	(0.7387)	(1.0707)	(2.7168)	(4.3407)	(5.6660)
RND	0.7811	1.0207	1.5716	0.7133	0.8731	1.3390	2.7483	4.4782	6.7538
	(0.6009)	(0.7929)	(1.1224)	(0.5469)	(0.6638)	(0.9549)	(2.4890)	(3.7654)	(5.0169)
Panel B: Crisis Scenario									
$\Delta K/S_0 = 1\%$									
EndPoint	10.0786	12.8149	16.1582	7.2686	9.5933	12.5665	41.5253	49.0340	56.5959
	(0.3820)	(0.3735)	(0.4062)	(0.3707)	(0.3634)	(0.3941)	(0.6498)	(0.6058)	(0.6360)
LinReg	4.1408	7.1081	10.0933	2.1732	4.8478	7.4814	21.3348	31.3431	40.0307
	(3.1412)	(3.8905)	(5.9449)	(2.0832)	(2.7409)	(3.9039)	(16.0767)	(18.5504)	(28.7684)
RND	3.7016	6.3486	9.2301	2.3872	4.4774	6.8945	17.4203	27.3164	36.1922
	(1.6437)	(2.1569)	(2.3762)	(1.1273)	(1.5495)	(1.8345)	(7.3540)	(9.2560)	(8.4998)
$\Delta K/S_0 = 2\%$									
EndPoint	10.0857	12.8109	16.1429	7.2786	9.5902	12.5513	41.4899	49.0188	56.5702
	(0.5139)	(0.5100)	(0.5656)	(0.5008)	(0.5020)	(0.5539)	(0.8540)	(0.7677)	(0.8174)
LinReg	4.3964	6.9066	9.6942	2.4957	4.6650	7.2166	22.1814	30.7372	37.9981
	(3.5282)	(4.7953)	(3.2668)	(2.5525)	(3.3163)	(2.5085)	(17.1683)	(23.7228)	(11.8234)
RND	3.8484	6.2174	8.9844	2.5062	4.3853	6.7070	17.9930	26.6793	35.2845
	(1.8467)	(2.3825)	(2.7854)	(1.2749)	(1.7273)	(2.1484)	(8.3838)	(9.9900)	(10.0058)
$\Delta K/S_0 = 5\%$									
EndPoint	10.0717	12.8128	16.1551	7.2676	9.5973	12.5570	41.4615	48.9577	56.6189
	(0.8215)	(0.7967)	(0.8201)	(0.8169)	(0.7940)	(0.8248)	(1.1681)	(1.0969)	(0.9783)
LinReg	3.7330	6.2552	9.9318	2.1068	3.9585	7.4021	19.3556	28.3534	38.9690
	(2.0138)	(2.4416)	(2.3826)	(1.4431)	(1.9045)	(1.9460)	(8.6599)	(9.1856)	(7.3694)
RND	3.9071	6.1680	9.6527	2.5752	4.3571	7.2166	18.1399	26.2519	37.6687
	(2.0457)	(2.4098)	(2.2106)	(1.4387)	(1.8090)	(1.7746)	(9.1690)	(9.4911)	(7.3631)

The table shows simulation-based averages (1000 runs) of percentage errors $100 \times |\widehat{\mathcal{Y}} - \mathcal{Y}_{\text{dense}}|/\mathcal{Y}_{\text{dense}}$ for $\mathcal{Y} = \mathbb{V}, \mathbb{IV}, \mathbb{RIX}$ using endpoint volatility (EndPoint), linear regression (LinReg), and RND tail (RND) extrapolation for the base case (Panel A) and crisis scenario (Panel B) with error standard deviation in parentheses. $\mathcal{Y}_{\text{dense}}$ is the respective benchmark computed from the full range of SVCJ OTM option prices $K_{\text{put}}/S_0 \in [0.01, 1]$, $K_{\text{call}}/S_0 \in (1, 1.99]$ ($\mathbb{RIX}$ OTM put options only) using trapezoidal integration over dense grids of strikes with $\Delta K/S_0 = 0.1\%$. Estimates $\widehat{\mathcal{Y}}$ are obtained from randomly perturbed implied volatility smiles $\tilde{\sigma}_{\text{noisy},i} = \tilde{\sigma}_i\,(1 + 0.01\eta)$, $i = 1, \ldots, \tilde{N}$ where $\tilde{\sigma}_i$ are Black and Scholes (1973) implied volatilities computed from SVCJ option prices and $\eta \sim \mathcal{N}(0, 1)$. $\widehat{\mathcal{Y}}$ are computed from extrapolated moneyness ranges $[K^{\min}_{\text{put}}/S_0, K^{\max}_{\text{call}}/S_0]$ of $[0.75, 1.25]$ (±25%), $[0.8, 1.2]$ (±20%), and $[0.85, 1.15]$ (±15%) ($\mathbb{RIX}$: OTM put options only) based on cubic spline smoothing (RND: with convexity constraints) of strike grids with $\Delta K/S_0 = 1\%, 2\%, 5\%$.

Table 6.7: Average Estimation Errors $\mathbb{V}$, $\mathbb{IV}$, $\mathbb{RIX}$ – High Microstructure Noise ($\theta = 3\%$)

	$\mathbb{V}$			$\mathbb{IV}$			$\mathbb{RIX}$		
Obs. range	±25%	±20%	±15%	±25%	±20%	±15%	−25%	−20%	−15%
Panel A: Base Case Scenario									
$\Delta K/S_0 = 1\%$									
EndPoint	1.7811	3.2744	5.9319	1.4364	2.6265	4.9255	8.8964	15.5455	24.9815
	(1.0372)	(1.1321)	(1.2582)	(0.9450)	(1.0729)	(1.1942)	(2.4616)	(2.6138)	(2.9313)
LinReg	1.4662	3.9642	4.9204	1.3481	2.8912	3.9267	6.4855	26.7617	27.4641
	(2.3413)	(22.9979)	(20.5245)	(3.3078)	(12.9801)	(13.6706)	(13.4823)	(214.3320)	(174.9337)
RND	1.1256	1.5935	2.6546	0.9933	1.3158	2.1586	4.4013	7.4327	12.5426
	(1.0173)	(1.9345)	(3.7510)	(0.8302)	(1.3569)	(2.5380)	(5.6708)	(13.2398)	(26.5127)
$\Delta K/S_0 = 2\%$									
EndPoint	1.9378	3.2944	5.8813	1.6274	2.6660	4.8721	8.9502	15.6349	24.9766
	(1.2815)	(1.5433)	(1.7813)	(1.1629)	(1.4402)	(1.6974)	(3.3668)	(3.4085)	(3.9027)
LinReg	2.3895	3.4638	4.7285	2.0274	2.7937	3.9262	12.4619	20.6339	23.5885
	(6.6998)	(21.4363)	(10.2468)	(4.2360)	(11.7641)	(7.1874)	(57.7489)	(209.4360)	(77.6022)
RND	1.5312	2.0469	3.4770	1.3589	1.7011	2.7862	6.0691	9.5897	16.9315
	(1.3476)	(2.4093)	(4.8093)	(1.1047)	(1.7103)	(3.2289)	(7.4576)	(16.4170)	(34.2856)
$\Delta K/S_0 = 5\%$									
EndPoint	2.4981	3.5683	5.9276	2.2571	3.0338	4.9014	9.2839	15.6582	25.4695
	(1.8474)	(2.2205)	(2.6359)	(1.7211)	(2.0363)	(2.5499)	(4.5248)	(5.0581)	(4.9632)
LinReg	2.6574	3.1201	3.9295	2.4814	2.7955	3.2886	10.1788	13.6906	17.7699
	(3.2213)	(3.1532)	(4.4319)	(2.6196)	(2.8309)	(3.2895)	(24.0340)	(18.7345)	(26.8616)
RND	2.2781	2.7757	3.5752	2.0729	2.3866	2.9950	8.3156	12.1442	16.4955
	(1.8947)	(2.4722)	(3.7677)	(1.6572)	(1.9887)	(2.7489)	(10.2811)	(13.9707)	(24.5172)
Panel B: Crisis Scenario									
$\Delta K/S_0 = 1\%$									
EndPoint	10.1588	12.8446	16.2009	7.3469	9.6234	12.6032	41.5716	49.0304	56.6937
	(1.1290)	(1.0972)	(1.1717)	(1.0981)	(1.0707)	(1.1433)	(1.8899)	(1.7465)	(1.7696)
LinReg	8.7758	15.1291	13.5901	5.3931	9.7540	9.9695	47.1965	78.2070	56.8042
	(62.5362)	(70.2588)	(34.1502)	(28.9650)	(36.3139)	(19.9224)	(440.2742)	(455.7391)	(201.2402)
RND	5.1005	7.3219	10.1877	3.4458	5.2289	7.6042	23.0896	30.8821	39.8171
	(2.5112)	(3.2555)	(4.1925)	(1.8123)	(2.3522)	(2.9795)	(11.0520)	(14.3327)	(18.7555)
$\Delta K/S_0 = 2\%$									
EndPoint	10.1751	12.8503	16.1430	7.3671	9.6273	12.5422	41.4998	49.0391	56.6489
	(1.5225)	(1.5097)	(1.6552)	(1.4849)	(1.4895)	(1.6267)	(2.5150)	(2.2428)	(2.3341)
LinReg	13.3271	15.4141	12.5762	8.2689	9.9186	9.4182	73.4822	83.7409	50.7033
	(66.5418)	(148.9089)	(17.5108)	(32.8188)	(65.7805)	(11.4687)	(450.4826)	(1085.8793)	(91.3701)
RND	5.4608	7.6316	10.2239	3.7321	5.4401	7.5951	24.4190	32.3435	40.2989
	(2.8070)	(3.7293)	(5.0016)	(2.0733)	(2.6680)	(3.5361)	(12.2218)	(16.8888)	(22.6497)
$\Delta K/S_0 = 5\%$									
EndPoint	10.1768	12.8832	16.1581	7.3696	9.6688	12.5250	41.4812	48.9300	56.9045
	(2.4568)	(2.3914)	(2.4630)	(2.4399)	(2.3841)	(2.4865)	(3.4929)	(3.2731)	(2.9312)
LinReg	7.8106	8.2221	10.6668	5.8368	6.0722	7.9760	37.2716	35.4562	41.4469
	(12.4583)	(7.8450)	(5.3707)	(8.2431)	(5.5818)	(4.1756)	(68.9000)	(38.6688)	(20.0501)
RND	5.8443	7.6818	10.0315	4.0681	5.5237	7.4869	26.4100	32.2697	39.2160
	(3.3941)	(4.4302)	(4.4810)	(2.5800)	(3.2397)	(3.5726)	(14.3142)	(19.4865)	(16.6956)

The table shows simulation-based averages (1000 runs) of percentage errors $100 \times |\widehat{\mathcal{Y}} - \mathcal{Y}_{\text{dense}}|/\mathcal{Y}_{\text{dense}}$ for $\mathcal{Y} = \mathbb{V}, \mathbb{IV}, \mathbb{RIX}$ using endpoint volatility (EndPoint), linear regression (LinReg), and RND tail (RND) extrapolation for the base case (Panel A) and crisis scenario (Panel B) with error standard deviation in parentheses. $\mathcal{Y}_{\text{dense}}$ is the respective benchmark computed from the full range of SVCJ OTM option prices $K_{\text{put}}/S_0 \in [0.01, 1]$, $K_{\text{call}}/S_0 \in (1, 1.99]$ ($\mathbb{RIX}$ OTM put options only) using trapezoidal integration over dense grids of strikes with $\Delta K/S_0 = 0.1\%$. Estimates $\widehat{\mathcal{Y}}$ are obtained from randomly perturbed implied volatility smiles $\tilde{\sigma}_{\text{noisy},i} = \tilde{\sigma}_i\,(1 + 0.03\eta)$, $i = 1, \ldots, \tilde{N}$ where $\tilde{\sigma}_i$ are Black and Scholes (1973) implied volatilities computed from SVCJ option prices and $\eta \sim \mathcal{N}(0, 1)$. $\widehat{\mathcal{Y}}$ are computed from extrapolated moneyness ranges $[K^{\min}_{\text{put}}/S_0, K^{\max}_{\text{call}}/S_0]$ of $[0.75, 1.25]$ (±25%), $[0.8, 1.2]$ (±20%), and $[0.85, 1.15]$ (±15%) ($\mathbb{RIX}$: OTM put options only) based on cubic spline smoothing (RND: with convexity constraints) of strike grids with $\Delta K/S_0 = 1\%, 2\%, 5\%$.

6.1.5 Tail Modeling Approach of Birru and Figlewski (2012)

Finally, we contrast the RND tail modeling technique from Birru and Figlewski (2012) with our tail construction methodology. The key difference between these approaches lies in how they parameterize the GEV distribution to model the RND tails. Birru and Figlewski (2012) model the right (left) tail of the RND by parameterizing the GEV according to the CDF at strike price K_{N-1} (K_2). For the PDF, they choose the same options and another one with K_n, $2 < n < N-1$.

When choosing $n = N-2$, right tail optimization problem of Birru and Figlewski (2012) reads

$$\begin{aligned} \underset{\mu,\sigma,\xi}{\arg\min} \quad & \Big(F_{GEV}(K_{N-1}) - \hat{Q}(K_{N-1})\Big)^2 \\ \text{subject to} \quad & f_{GEV}(K_{N-1}) = \hat{q}(K_{N-1}), \\ & f_{GEV}(K_{N-2}) = \hat{q}(K_{N-2}). \end{aligned} \tag{6.3}$$

Similarly, when choosing $n = 3$, their left tail optimization problem reads

$$\begin{aligned} \underset{-\mu,\sigma,\xi}{\arg\min} \quad & \Big(1 - F_{GEV}(-K_2) - \hat{Q}(K_2)\Big)^2 \\ \text{subject to} \quad & f_{GEV}(-K_2) = \hat{q}(K_2), \\ & f_{GEV}(-K_3) = \hat{q}(K_3). \end{aligned} \tag{6.4}$$

In addition to the degrees of freedom in selecting K_n, the technique used by Birru and Figlewski (2012) does not consider the martingale property. Thus, in comparison to our approach, it does not ensure that the outermost option prices at strikes K_1 and K_N are accurately recovered by the modeled tails. As a result, implied volatilities may not match at the connecting strikes K_1 and K_N, leading to a discontinuous volatility smile and RND tails that violate no-arbitrage constraints. This discontinuity can significantly affect the accuracy of risk measure estimates, with the impact being most pronounced for tail risk measures like the $\mathbb{RIX}$.

To demonstrate this, we evaluate the tail modeling approach of Birru and Figlewski (2012) relative to our RND tail extrapolation, with a focus on the modeled RND tails, the continuity of the volatility smile, and the $\mathbb{RIX}$ estimates. In this context, we use the crisis scenario and a spot moneyness range of $[0.8, 1.2]$ ($\pm 20\%$), extending the RND implied by available option prices using both tail modeling approaches, and extracting the fitted GEV parameters. Figure 6.3 shows the RND with tails modeled by both techniques, while Table 6.8 indicates deviating GEV parameters.

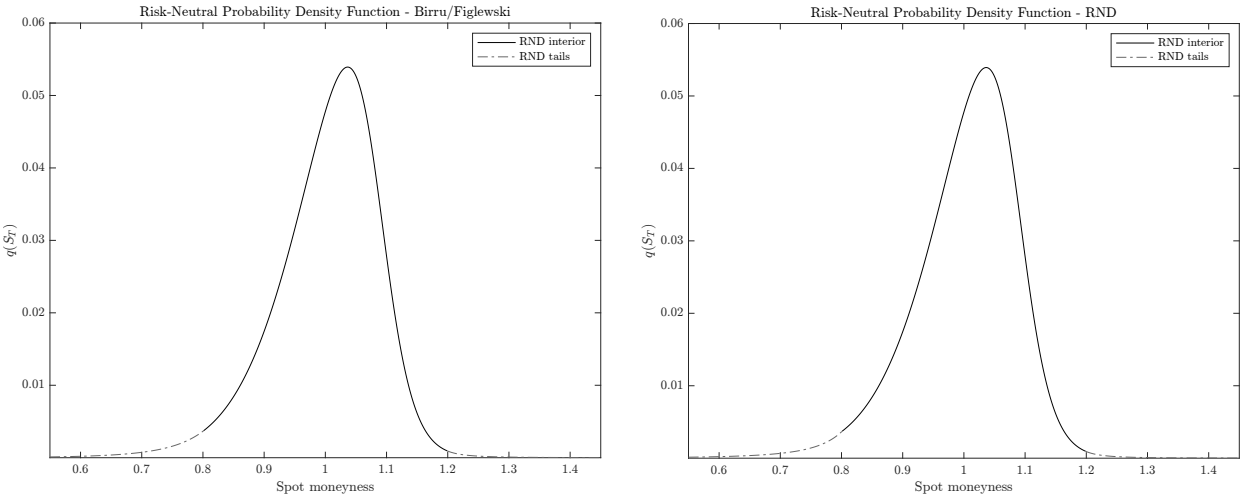

Figure 6.3: Modeled RND Tails – The figure plots risk-neutral probability densities with tails modeled according to Birru and Figlewski (2012) (Birru/Figlewski-RND, left panel) and RND tail extrapolation (RND, right panel). Based on benchmark option prices (crisis scenario) generated by the SVCJ model, the risk-neutral probability density inside the spot moneyness range of $[0.8, 1.2]$ ("RND interior") is approximated using finite differences with a fine grid of $\Delta K/S_0 = 0.1\%$, while tails follow from the respective tail modeling approaches ("RND tails").

Table 6.8: GEV Parameters

	Birru/Figlewski-RND		RND	
	Left Tail	Right Tail	Left Tail	Right Tail
μ	98.4106	113.1404	92.1554	114.3723
σ	3.7050	0.1571	1.3680	0.0735
ξ	0.1477	0.5930	0.4102	0.7234

The table shows fitted location (μ), scale (σ), and shape (ξ) parameter of the GEV distribution resulting from tail modeling according to Birru and Figlewski (2012) and the RND tail extrapolation for the left and the right tail, respectively.

Although the tails seem to be equivalent at a first glance, it is striking that the RND tail extrapolation yields higher values for the shape parameter ξ than the proposed method of Birru and Figlewski (2012). As a consequence, it assigns more probability mass to the RND tails which translates into higher option prices and implied volatilities, as depicted in Figure 6.4:

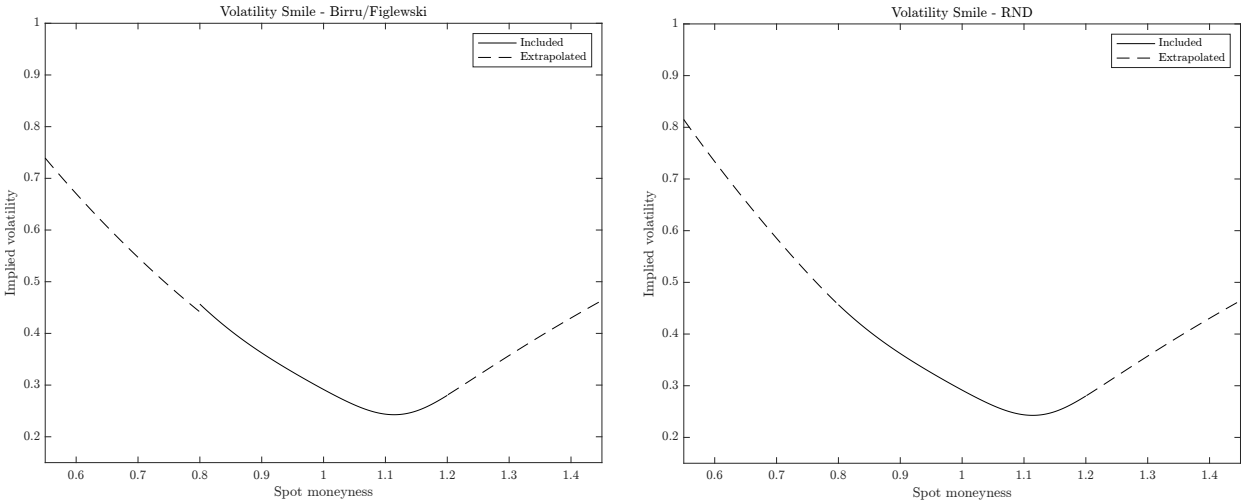

Figure 6.4: Extrapolated Volatility Smiles – The figure plots extrapolated Black and Scholes (1973) implied volatility smiles resulting from RND tail modeling according to Birru and Figlewski (2012) (Volatility Smile-Birru/Figlewski, left panel) and the RND tail extrapolation (Volatiliy Smile - RND, right panel). Implied volatilities inside the spot moneyness range of $[0.8, 1.2]$ ("Included") result from a dense grid ($\Delta K/S_0 = 0.1\%$) of benchmark option prices (crisis scenario) generated by the SVCJ model detailed in 3.1.3. Extrapolated implied volatilities follow from RND tail modeling according to the respective approaches ("Extrapolated").

While the higher extrapolated implied volatilities of the RND tail extrapolation concatenate the smile perfectly, the lower volatilities of Birru and Figlewski (2012) introduce discontinuities at the outermost strikes which is not admissible under considerations of no-arbitrage. The higher option prices generated by the RND tail extrapolation lead to a percentage error of 7.14% with respect to the $\mathbb{RIX}$, relative to the benchmark value of 0.0095. In contrast, the error from Birru and Figlewski (2012) reaches 32.84% due to tail underestimation. Hence, incorporating the martingale property in tail modeling is crucial for accurate smile extrapolation and option-implied risk measure estimation, especially for tail risk measures such as the $\mathbb{RIX}$. This makes our RND-based technique superior to the tail modeling approach proposed by Birru and Figlewski (2012).

6.2 Empirical Application

This section outlines the application of the RND-based smile construction technique to real-world financial data, including the analysis of its impact on $\mathbb{RIX}$ estimates for both a normal and a volatile trading day.[78] First, similar to the numerical analysis, the RND-based technique's efficiency is compared to that of standard approaches by constructing volatility smiles based on narrowed moneyness ranges. To assess the accuracy of the different smile construction approaches, discarded contracts are used to compute RMSE of extrapolated implied volatilities. Second, the $\mathbb{RIX}$ is estimated based on the full set of observable and constructed OTM put options. Details regarding the data are provided in Subsection 6.2.1, while the main results are presented in Subsection 6.2.2.

6.2.1 Data and Summary Statistics

Analogous to the base case and crisis scenario in the numerical analysis, the previously identified normal and volatile trading days are applied for the empirical examination as well. Specifically, May 22, 2019 represents the normal trading day, while May 20, 2020 corresponds to the volatile trading day, based on the $\mathbb{VIX}$ levels observed on those dates. To obtain a sufficient number of observable contracts for the empirical analysis, we focus on 30-day quarterly options written on the highly liquid stocks of Facebook (Meta), Amazon, Apple, Netflix, and Google (Alphabet), collectively known as the *FAANG* stocks.[79] The choice of these underlyings ensures that the number of OTM option contracts is sufficiently large and of high quality, allowing for the computation of meaningful RMSE. Raw options data are obtained from the OptionMetrics database, which also provides European options calculated from American options using an algorithm based on the binomial tree model of Cox et al. (1979).

[78] Since the differences between the smile construction techniques are most pronounced for the $\mathbb{RIX}$, as indicated by results in Section 6.1, and given that $\mathbb{V}^-$ and $\mathbb{IV}^-$ are included by construction, $\mathbb{V}$ and $\mathbb{IV}$ are not analyzed separately.

[79] *FAANG* stocks did not pay any dividends within the periods under consideration.

Table 6.9 shows summary statistics for implied volatilities of *FAANG* individual stock options for both observation dates. In line with intuition, almost all moments exhibit higher values on the volatile day. The increases in mean and median indicate a level effect, while sharp increases in the maximum values, such as for Apple or Netflix, reflect higher prices for deep OTM put options.[80] This is natural, as deep OTM puts often serve as "crash insurance" during periods of heightened volatility.

Table 6.9: Summary Statistics – Implied Volatilities

	Mean	SD	Median	Min	Max
Panel A: May 22, 2019 (Normal)					
AAPL	0.4380	0.1337	0.4377	0.2656	0.8937
AMZN	0.4003	0.2477	0.2915	0.2205	1.3737
FB	0.4538	0.2707	0.3435	0.2160	1.2937
GOOG	0.3410	0.1893	0.2763	0.1840	1.0376
NFLX	0.5360	0.2945	0.3991	0.2855	1.4177
Panel B: May 20, 2020 (Volatile)					
AAPL	0.5939	0.3758	0.4500	0.2379	1.7140
AMZN	0.5380	0.2767	0.4429	0.2850	1.4074
FB	0.5693	0.2556	0.4594	0.3387	1.2458
GOOG	0.5330	0.2917	0.4320	0.2190	1.2514
NFLX	0.8303	0.6023	0.5682	0.3759	2.8537

The table shows mean, standard deviation (SD), median, minimum (Min), and maximum (Max) for implied volatilities of 30-day quarterly options written on the *FAANG* stocks (Facebook (Meta), Amazon, Apple, Netflix, Google (Alphabet)) on May 22, 2019 (Panel A, normal) and May 20, 2020 (Panel B, volatile). Data is retrieved from OptionMetrics and individual stocks are identified by their ticker symbols.

Table 6.10 on the following page conveys information about the number of OTM contracts available in moneyness intervals of 0.05. The number of OTM put options with a spot moneyness less than 0.75 is substantially higher on the volatile than on the normal day. Similar to the previous observation, this reflects the fact that these contracts are often used as "crash insurance" in volatile market conditions.

[80] Figure 6.5 in the subsequent subsection indicates that, in line with economic intuition, maximum implied volatility values correspond to deep OTM put options.

Table 6.10: Summary Statistics – Number of OTM Option Contracts

	OTM Put Options						OTM Call Options					
Moneyness	0 – 0.75	0.75 – 0.80	0.80 – 0.85	0.85 – 0.90	0.90 – 0.95	0.95 – 1.00	1.00 – 1.05	1.05 – 1.10	1.10 – 1.15	1.15 – 1.20	1.20 – 1.25	1.25 – ∞
Panel A: May 22, 2019 (Normal)												
AAPL	18	9	6	3	4	4	3	4	4	2	2	19
AMZN	84	15	13	18	19	26	37	19	18	15	13	35
FB	17	2	2	3	4	4	3	4	3	2	2	12
GOOG	30	12	11	12	11	22	23	13	6	6	5	25
NFLX	35	4	4	3	6	7	8	5	3	4	3	25
Panel B: May 20, 2020 (Volatile)												
AAPL	33	4	3	4	7	6	5	3	3	3	3	12
AMZN	135	25	25	25	25	22	13	8	6	6	8	30
FB	21	3	5	4	5	4	3	2	2	3	2	8
GOOG	102	9	14	14	14	14	14	14	7	7	7	15
NFLX	60	4	5	4	5	4	5	4	4	5	4	27

The table shows the number of out-of-the-money (OTM) 30-day quarterly option contracts written on the *FAANG* stocks (Facebook (Meta), Amazon, Apple, Netflix, Google (Alphabet)) on May 22, 2019 (Panel A, normal) and May 20, 2020 (Panel B, volatile) for moneyness intervals of 0.05. Data is obtained from OptionMetrics and individual stocks are identified by their ticker symbols.

6.2.2 Results

We apply RND tail extrapolation, endpoint volatility, and linear regression combined with cubic spline smoothing (RND with convexity constraints) to construct full volatility smiles for moneyness ranges around the spot of ±25%, ±20%, and ±15%, respectively. For OTM put options, we compute RMSE of extrapolated implied volatilities with respect to their observable counterparts located outside the respective moneyness range. To evaluate how the accuracy of different smile extrapolation techniques translates into risk measure estimates, we then compute $\mathbb{RIX}$ estimates from the set of observable and constructed OTM put option prices. This procedure is repeated for both trading days. The results are summarized in Table 6.11 on the next page.

Table 6.11: RMSE and $\mathbb{RIX}$ Estimates

	Panel A: May 22, 2019 (Normal)						*Panel B: May 20, 2020 (Volatile)*					
	RMSE			$\widehat{\mathbb{RIX}}$			RMSE			$\widehat{\mathbb{RIX}}$		
Obs. range	−25%	−20%	−15%	−25%	−20%	−15%	−25%	−20%	−15%	−25%	−20%	−15%
AAPL												
EndPoint	.1631	.1585	.1757	.0052	.0048	.0041	.5489	.5822	.6050	.0063	.0051	.0041
LinReg	.0471	.0382	.0492	.0058	.0058	.0053	.1729	.1862	.1932	.0100	.0091	.0086
RND	.0383	.0295	.0389	.0058	.0059	.0053	.0906	.0858	.0809	.0118	.0114	.0113
AMZN												
EndPoint	.3925	.3981	.4108	.0026	.0023	.0020	.4103	.4246	.4361	.0037	.0032	.0028
LinReg	.1634	.1492	.1558	.0029	.0029	.0027	.1205	.1269	.1628	.0051	.0047	.0040
RND	.0927	.0786	.0851	.0030	.0030	.0028	.0526	.0646	.0769	.0084	.0058	.0049
FB												
EndPoint	.4231	.4452	.4695	.0029	.0025	.0021	.4249	.4318	.4249	.0064	.0059	.0052
LinReg	.1542	.1234	.1632	.0033	.0035	.0030	.1612	.1826	.2459	.0076	.0072	.0063
RND	.0791	.0533	.0783	.0035	.0037	.0031	.1136	.1276	.2331	.0078	.0074	.0064
GOOG												
EndPoint	.3178	.3102	.3129	.0017	.0015	.0013	.3861	.4180	.4416	.0042	.0036	.0030
LinReg	.0944	.0894	.0919	.0022	.0021	.0020	.1330	.1186	.1424	.0057	.0059	.0050
RND	.0643	.0545	.0584	.0025	.0024	.0022	.0898	.0682	.0856	.0066	.0077	.0061
NFLX												
EndPoint	.4693	.4944	.5109	.0050	.0044	.0037	.9903	.9967	.9968	.0072	.0065	.0056
LinReg	.1535	.1880	.2433	.0063	.0057	.0050	.5626	.6122	.7448	.0097	.0086	.0068
RND	.0815	.1128	.1796	.0066	.0058	.0050	.3303	.3806	.7436	.0106	.0091	.0068

The table shows RMSE of extrapolated implied volatilities with respect to observable discarded OTM put options written on the *FAANG* stocks (Facebook (Meta), Amazon, Apple, Netflix, Google (Alphabet)) for May 22, 2019 (Panel A, normal) and May 20, 2020 (Panel B, volatile). Volatility smiles are constructed using endpoint volatility (EndPoint), linear regression (LinReg), and RND tail (RND) extrapolation combined with cubic spline smoothing (RND with convexity constraints) based on narrowed moneyness ranges $[K_{\text{put}}^{\min}/S_0, K_{\text{call}}^{\max}/S_0]$ of $[0.75, 1.25]$ ($\pm 25\%$), $[0.8, 1.2]$ ($\pm 20\%$), and $[0.85, 1.15]$ ($\pm 15\%$). RMSE and $\widehat{\mathbb{RIX}}$ follow from OTM put options only which is indicated by the negative sign of the underlying moneyness range. We compute $\widehat{\mathbb{RIX}}$ from a dense grid of observable *and* constructed OTM put option prices using trapezoidal integration. ΔK is chosen such that observable strikes are included as knots while ensuring $\Delta K/S_0 \leq 0.1\%$. Individual stocks are identified by their ticker symbols.

First, the RMSE of implied volatilities derived from the RND approach are substantially smaller than those obtained from standard techniques. This holds for all *FAANG* stocks and all three moneyness ranges on both trading days. On average, RMSE of extrapolated volatilities differ between the RND approach and endpoint volatility (linear regression) by 0.27 (0.05) for the normal and 0.37 (0.07) for the volatile day. Furthermore, RMSE are robust with respect to the size of the available moneyness range with similar orders of

magnitude. This indicates that RND tail extrapolation is superior to endpoint volatility and linear regression when brought to the data. Figure 6.5 illustrates the differences in smile construction for Apple and Google on the normal and the volatile trading day. Discarded implied volatilities from OTM put options are more accurately matched by the RND-based approach than by its competitors. The improvement is even more pronounced for the volatile trading day indicating that RND-based smile construction is particularly advantageous when rare disaster concerns may be present.

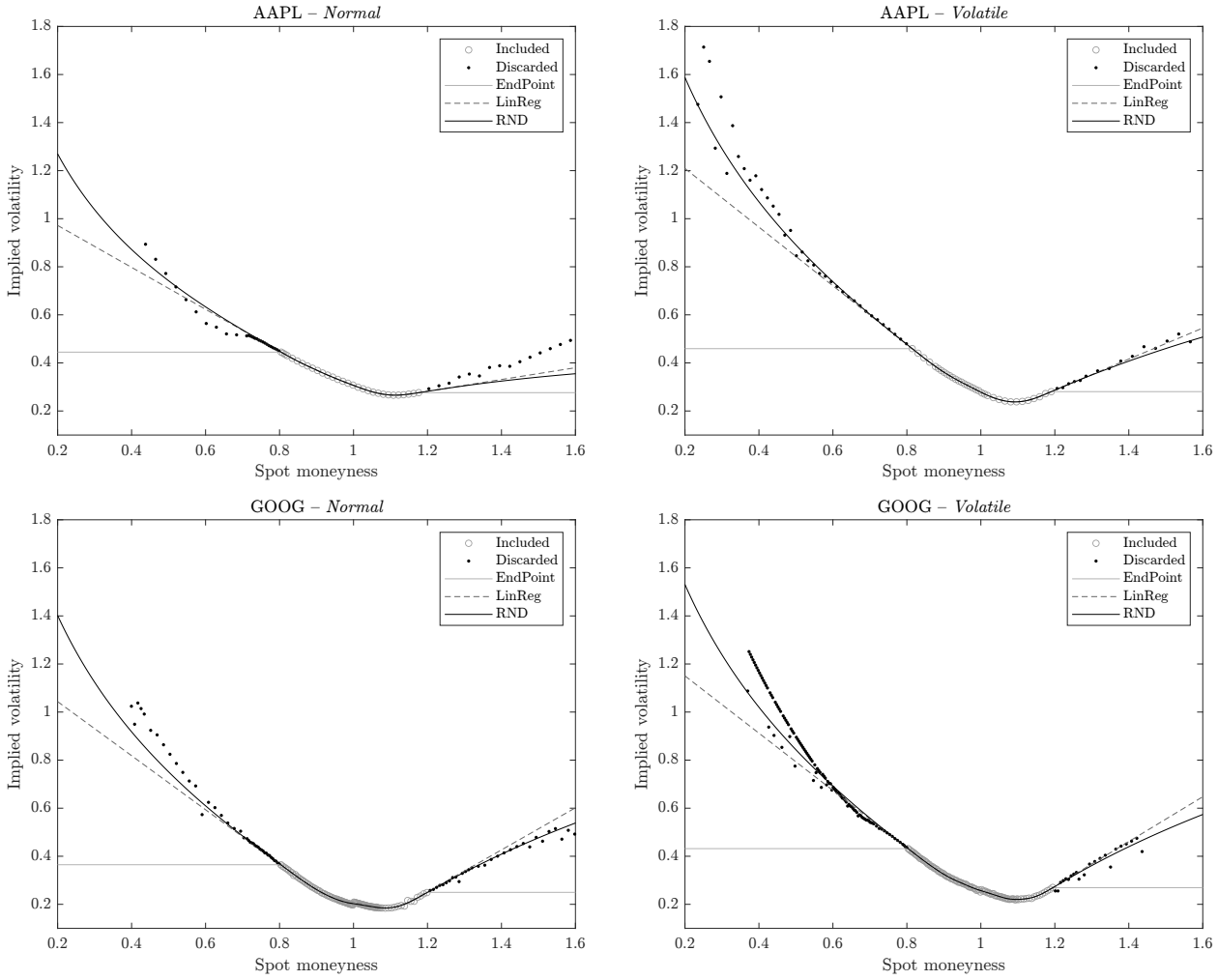

Figure 6.5: Empirical Extrapolated Volatility Smiles – The figure plots extrapolated Black and Scholes (1973) implied volatility smiles for option contracts on Apple (AAPL, top panels) and Google (GOOG, bottom panels) on the normal (left panels) and the volatile observation day (right panels). Based on implied volatilities of observable contracts in an narrowed spot moneyness range of $[0.8, 1.2]$ ("Included"), volatility smiles are extrapolated by endpoint volatility (EndPoint), linear regression (LinReg), and RND tail (RND) extrapolation after cubic spline smoothing (RND with convextiy constraints). Implied volatilities of observable contracts outside the moneyness range ("Discarded") are plotted against extrapolated volatility smiles. Options data is obtained from OptionMetrics.

Second, RND-based $\mathbb{RIX}$ estimates on the volatile day are considerably higher than those from standard techniques. This holds across all *FAANG* stocks and all three moneyness ranges. On average, estimates using the RND approach exceed those from endpoint volatility (linear regression) by 0.0033 (0.0012) in absolute and 73.97% (18.29%) in relative terms on that day. For the normal day, the differences are less pronounced. On average, RND-based $\mathbb{RIX}$ estimates still exceed those from endpoint volatility (linear regression) by 0.0010 (0.0001) in absolute and 35.59% (4.87%) in relative terms. Given the higher accuracy of RND tail extrapolation, we conclude that corresponding $\mathbb{RIX}$ estimates are superior to their counterparts from standard techniques. Endpoint volatility and linear regression tend to underestimate rare disaster concerns when jump and tail risks are prevalent.

This is further illustrated by aligning the volatility smiles of Apple and Google in Figure 6.5 with the corresponding $\mathbb{RIX}$ estimates in Table 6.11. On both observation days, RND-based extrapolated volatility smiles exhibit curvature and clearly differ from those using endpoint volatility and linear regression. This only translates to substantial differences in $\mathbb{RIX}$ estimates on the volatile day, though. RND tail modeling takes curvature into account explicitly. This additional flexibility allows to incorporate higher implied volatilities of deep OTM put options. When market volatility is high, these contracts tend to be more expensive than on days with moderate volatility. As deep OTM puts influence $\mathbb{RIX}$ estimates substantially due to the implicit weighting scheme in (4.67), small changes in their prices have a comparably large impact.

As a result, and consistent with the numerical analysis in Section 6.1, the empirical application confirms the superiority of the RND-based smile construction approach over standard techniques. Notably, when options data are sparsely sampled and distorted, this method is the only reliable choice for constructing volatility smiles and ensuring accurate risk measure estimates.

Chapter 7

Conclusion and Outlook

In this thesis, we focus on estimating option-implied risk measures through volatility smile construction. By combining and enhancing existing techniques for smile construction and RND modeling, we propose the arbitrage-free RND-based smile construction approach, which ensures accurate and robust risk measure estimates. This method uses RND tail modeling for smile extrapolation and a convexity-preserving cubic smoothing spline for interpolation. Our analysis shows that this approach provides more reliable option-implied risk measure estimates than standard methods, establishing it as the superior technique.

Building on the foundational concepts of stochastic processes discussed in Chapter 2, with particular emphasis on quadratic variation, Chapter 3 delves into the fundamentals of option pricing theory. This includes an exploration of pricing models and methods for extracting the RND from options. Following this, we provide a comprehensive review of the most relevant option-implied risk measures in Chapter 4. These measures encompass the BKM risk-neutral moments of the holding period log-return, the CBOE $\mathbb{VIX}$, and jump and tail index $\mathbb{RIX}$. For all of these measures, we provide the underlying mathematics in depth as well as the corresponding replication portfolios, which are constructed based on the generic spanning concept. Within this context, we also address practical issues related to estimation via volatility smile construction.

In Chapter 5 we detail the arbitrage-free RND-based smile construction approach. First, we present the RND tail modeling methodology for smile extrapolation, which uses the GEV distribution under no-arbitrage constraints to offer high tail flexibility. Additionally, we provide the shape-preserving cubic smoothing spline as a compatible interpolation and smoothing technique, which ensures robustness of the entire smile construction method. In the context of pure RND modeling, we also introduce a quintic smoothing spline as an additional interpolation technique that complements the RND-based extrapolation.

In Chapter 6, the sophisticated smile construction technique is then benchmarked against standard methods – specifically endpoint volatility and linear regression, both combined with a cubic smoothing spline – through a two-stage analysis. In the first stage, a numerical analysis is conducted using an option pricing model to assess the robustness of option-implied risk measure estimates derived from different smile construction techniques, in relation to various sources of implementation errors. In the second stage, the different smile construction techniques are applied to financial data and evaluated based on $\mathbb{RIX}$ estimates, which, by construction, partially encompass the BKM risk-neutral variance and the $\mathbb{VIX}$. In both analysis, the arbitrage-free RND-based smile construction technique outperforms standard approaches, demonstrating its superiority.

The clear advantage of this smile construction technique over standard approaches lies in its ability to estimate risk measures even when options data are limited and/or distorted. This opens up a broad spectrum of future research opportunities. First, it facilitates the estimation of option-implied risk measures across a wide range of underlying assets, not limited to indices. The forward-looking nature of these measures can serve as valuable predictors in various empirical studies. Second, its modified version offers the unique opportunity to capture bimodal RNDs while accurately estimating option-implied risk measures, further enhancing its empirical applicability. Third, and perhaps most notably, there is potential to extend the arbitrage-free RND-based smile construction method to cover the entire volatility surface. In the context of the $\mathbb{RIX}$, this would enable to describe the RND left-tail behavior across different maturities through a straightforward sequence of corresponding estimates.

Due to these and related research questions, estimating option-implied risk measures via volatility smile construction remains a dynamic field of study. I hope that the ideas presented will contribute to both current and future advancements in this area.

Appendix A

Basics of Stochastic Calculus

Stochastic calculus provides the mathematical framework for analyzing and manipulating stochastic processes, offering the tools necessary to rigorously handle the randomness inherent in asset price dynamics. The fundamentals of stochastic calculus include the Itô integral, the most widely used stochastic integral in finance, and Itô's formulae. These formulae form a set of results that provide the stochastic differential of a function for various classes of stochastic processes. Both concepts are discussed in the following, starting with the Itô integral in Appendix A.1 and continuing with Itô's formulae in Appendix A.2.

A.1 The Itô Integral

The Itô integral is widely regarded as the most well-known and fundamental type of stochastic integral. Of paramount importance in the context of finance, the Itô integral is driven by Brownian motion, which serves as the integrator. It is defined as follows:

Definition 46. *Let* $(\Omega, \mathcal{F}, \mathbb{P})$ *be a probability space equipped with filtration* $\{\mathcal{F}_t\}$, $(W_t)_t$ *be a Brownian motion, and* $(\sigma_t)_t$ *be an adapted process satisfying the square-integrability condition, i.e.* $\mathbb{E}\int_0^T \sigma_t^2 \mathrm{d}t < \infty$. *Further, let* Π_n *be a partition of the time interval* $[0, T]$ *and* $(\sigma_{n,t})_t$ *be a simple process, i.e.* $\sigma_{n,t}$ *is constant on each subinterval* $[t_i, t_{i+1})$, $i = 0, \ldots, n-1$. *Then,*

for any $t_k \leq \bar{t} \leq t_{k+1}$, the Itô integral $I_{n,\bar{t}}$ of the simple process $(\sigma_{n,t})_t$ is defined as

$$I_{n,\bar{t}} = \int_0^{\bar{t}} \sigma_{n,t} \, \mathrm{d}W_t = \sum_{i=0}^{k-1} \sigma_{n,t_i} \cdot \left(W_{t_{i+1}} - W_{t_i} \right) + \sigma_{n,t_k} (W_{\bar{t}} - W_{t_k}). \tag{A.1}$$

For non-simple processes $(\sigma_t)_t$, which are allowed to vary continuously and potentially jump, choose a sequence of simple processes such that

$$\lim_{n \to \infty} \mathbb{E} \left(\int_0^{\bar{t}} \left| \sigma_{n,t} - \sigma_t \right|^2 \mathrm{d}t \right) = 0. \tag{A.2}$$

Then, for any $\bar{t} \in [0, T]$, the Itô integral $I_{\bar{t}}$ is defined as the limit of $I_{n,\bar{t}}$

$$I_{\bar{t}} = \int_0^{\bar{t}} \sigma_t \mathrm{d}W_t = \lim_{n \to \infty} \int_0^{\bar{t}} \sigma_{n,t} \, \mathrm{d}W_t. \tag{A.3}$$

It is crucial to emphasize that the square-integrability condition is fundamental for the Itô integral. Specifically, this condition ensures not only the existence of the Itô integral but also guarantees that the integral satisfies the martingale property and that the integral converges appropriately. Further details on this topic can be found for example in Shreve (2004).

A.2 Itô's Formulae

Having established the Itô integral in Appendix A.1, we now focus on the fundamental aspects of stochastic calculus, particularly Itô's formulae. These formulae provide a method to compute the differential of functions of stochastic processes. Given their importance in mathematical finance, we will consider two specific instances. The first is Itô's formula for Itô processes, applicable to pure diffusion processes driven by Brownian motion. The second is Itô's formula for jump-diffusion processes, which, as its name suggests, is designed for processes that combine an Itô process with a (compensated) compound Poisson process. Commencing with the simpler case, the formula for Itô processes is given by:

Theorem 47 (Itô's Formula for Itô Processes)**.** *Let X be an Itô process defined as*

$$X_{\bar{t}} = X_0 + \int_0^{\bar{t}} \mu_t \mathrm{d}t + \int_0^{\bar{t}} \sigma_t \mathrm{d}W_t, \quad \bar{t} \in [0, T], \tag{A.4}$$

where $(\mu_t)_t$ and $(\sigma_t)_t$ are adapted processes. Further assume that $(\sigma_t)_t$ satisfies the square-integrability condition, i.e. $\mathbb{E}\int_0^T \sigma_t \mathrm{d}t < \infty$. Then, for any $\mathcal{C}^{1,2}$ function $f : [0, T] \times \mathbb{R} \to \mathbb{R}$, it holds

$$\begin{aligned} f(\bar{t}, X_{\bar{t}}) = f(0, X_0) &+ \int_0^{\bar{t}} \left(\frac{\partial f}{\partial t}(t, X_t) + \frac{\partial f}{\partial x}(t, X_t)\mu_t + \frac{1}{2}\frac{\partial^2 f}{\partial x^2}(t, X_t)\sigma_t^2 \right) \mathrm{d}t \\ &+ \int_0^{\bar{t}} \frac{\partial f}{\partial x}(t, X_t))\sigma_t \mathrm{d}W_t. \end{aligned} \tag{A.5}$$

Partial Proof. We only proof the case where $f(t, X_t)$ is sufficiently "smooth", i.e. when the partial derivatives $\frac{\partial^2 f}{\partial x \partial t}(t, X_t)$ and $\frac{\partial^2 f}{\partial t^2}(t, X_t)$ are also defined and continuous. This additional assumption enables us to prove the theorem quite intuitively using a Taylor series expansion of second order.[81] First, fix some $\bar{t} \in [0, T]$ and let $(\Pi_n)_n$ be a sequence of partitions of the time interval $[0, \bar{t}]$ such that $\|\Pi_n\| \to 0$ as $n \to \infty$. Then, for some partition Π_n, the difference between $f(0, X_0)$ and $f(\bar{t}, X_{\bar{t}})$ can be written as the sum of changes on each subinterval $[t_i, t_{i+1})$. This can be achieved by performing a Taylor series expansion of second order on each subinterval and then aggregating the respective terms as follows

$$\begin{aligned} f(\bar{t}, X_{\bar{t}}) - f(0, X_0) &= \sum_{i=0}^{n-1} \Big(f(t_{i+1}, X_{t_{i+1}}) - f(t_i, X_{t_i}) \Big) \\ &= \sum_{i=0}^{n-1} \frac{\partial f}{\partial t}(t_i, X_{t_i})(t_{i+1} - t_i) + \sum_{i=0}^{n-1} \frac{\partial f}{\partial x}(t_i, X_{t_i})(X_{t_{i+1}} - X_{t_i}) \\ &\quad + \frac{1}{2}\sum_{i=0}^{n-1} \frac{\partial^2 f}{\partial x^2}(t_i, X_{t_i})(X_{t_{i+1}} - X_{t_i})^2 \\ &\quad + \sum_{i=0}^{n-1} \frac{\partial^2 f}{\partial x \partial t}(t_i, X_{t_i})(t_{i+1} - t_i)(X_{t_{i+1}} - X_{t_i}) \\ &\quad + \frac{1}{2}\sum_{i=0}^{n-1} \frac{\partial^2 f}{\partial t^2}(t_i, X_{t_i})(t_{i+1} - t_i)^2 + \text{higher-order terms}. \end{aligned} \tag{A.6}$$

[81] The complete proof relies on the d-dimensional Itô's formula, which is not covered in this thesis. Formula (A.4) represents a special case of this formula, where the first dimension pertains to time t and the second dimension corresponds to the Itô process X.

Then, when taking the limit, the left-hand side remains unaffected, while for the right-hand side is evaluated term by term. For the first sum, we obtain an ordinary Lebesgue integral

$$\lim_{n\to\infty} \sum_{i=0}^{n-1} \frac{\partial f}{\partial t}(t_i, X_{t_i})(t_{i+1} - t_i) = \int_0^{\bar{t}} \frac{\partial f}{\partial t}(t, W_t)\mathrm{d}t. \tag{A.7}$$

For the second sum, we can write

$$\lim_{n\to\infty} \sum_{i=0}^{n-1} \frac{\partial f}{\partial x}(t_i, X_{t_i})(X_{t_{i+1}} - X_{t_i}) = \int_0^{\bar{t}} \frac{\partial f}{\partial x}(t, X_t))\mathrm{d}X_t, \tag{A.8}$$

which can be decomposed in an ordinary Lebesgue integral and an Itô integral

$$\int_0^{\bar{t}} \frac{\partial f}{\partial x}(t, X_t)\mathrm{d}X_t = \int_0^{\bar{t}} \frac{\partial f}{\partial x}(t, X_t)\mu_t\mathrm{d}t + \int_0^{\bar{t}} \frac{\partial f}{\partial x}(t, X_t)\mathrm{d}W_t. \tag{A.9}$$

To evaluate the third sum, recall the definition of quadratic variation (Definition 23), i.e.

$$\lim_{n\to\infty} \sum_{i=0}^{n-1} \frac{\partial^2 f}{\partial x^2}(t_i, X_{t_i})(X_{t_{i+1}} - X_{t_i})^2 = \int_0^{\bar{t}} \frac{\partial^2 f}{\partial x^2}(t, X_t))\mathrm{d}[X, X]_t. \tag{A.10}$$

As X accumulates quadratic variation at rate σ_t^2 per unit of time, as stated in Proposition 28, we obtain

$$\int_0^{\bar{t}} \frac{\partial^2 f}{\partial x^2}(t, X_t)\mathrm{d}[X, X]_t = \int_0^{\bar{t}} \frac{\partial^2 f}{\partial x^2}(t, X_t)\sigma_t^2\mathrm{d}t, \tag{A.11}$$

which is again an ordinary Lebesgue integral. The fourth and the fifth sum do not contribute because

$$\begin{aligned}
&\lim_{n\to\infty} \left| \frac{1}{2} \sum_{i=0}^{n-1} \frac{\partial^2 f}{\partial x \partial t}(t_i, X_{t_i})(t_{i+1} - t_i)(X_{t_{i+1}} - X_{t_i}) \right| \\
&\qquad \leq \frac{1}{2} \lim_{n\to\infty} \sum_{i=0}^{n-1} \left| \frac{\partial^2 f}{\partial x \partial t}(t_i, X_{t_i}) \right| (t_{i+1} - t_i) \left| (X_{t_{i+1}} - X_{t_i}) \right| \\
&\qquad \leq \frac{1}{2} \lim_{n\to\infty} \max_i \left| X_{t_{i+1}} - X_{t_i} \right| \cdot \lim_{n\to\infty} \sum_{i=0}^{n-1} \left| \frac{\partial^2 f}{\partial x \partial t}(t_i, X_{t_i}) \right| (t_{i+1} - t_i) \\
&\qquad = \frac{1}{2} \cdot 0 \cdot \int_0^{\bar{t}} \left| \frac{\partial^2 f}{\partial x \partial t}(t, X_t)) \right| \mathrm{d}t,
\end{aligned} \tag{A.12}$$

and similarly

$$\begin{aligned}\lim_{n\to\infty}\left|\frac{1}{2}\sum_{i=0}^{n-1}\frac{\partial^2 f}{\partial t^2}(t_i,X_{t_i})(t_{i+1}-t_i)(X_{t_{i+1}}-X_{t_i})\right| \\ &\leq \frac{1}{2}\lim_{n\to\infty}\sum_{i=0}^{n-1}\left|\frac{\partial^2 f}{\partial t^2}(t_i,X_{t_i})\right|(t_{i+1}-t_i)^2 \\ &\leq \frac{1}{2}\lim_{n\to\infty}\max_i(t_{i+1}-t_i)\cdot\lim_{n\to\infty}\sum_{i=0}^{n-1}\left|\frac{\partial^2 f}{\partial x\partial t}(t_i,X_{t_i})\right|(t_{i+1}-t_i) \\ &= \frac{1}{2}\cdot 0\cdot\int_0^{\bar{t}}\left|\frac{\partial^2 f}{\partial t^2}(t,X_t))\right|\mathrm{d}t, \end{aligned} \tag{A.13}$$

where we used the fact that X is continuous in the last step for both sums, which implies $\lim_{n\to\infty}\max_i\left|X_{t_{i+1}}-X_{t_i}\right|=0$. Likewise, higher-order terms do not contribute. □

In the presence of jumps, Itô's formula for Itô processes is augmented by an additional term corresponding to the compound Poisson process. The resulting formula for jump-diffusion processes is given in the following theorem:

Theorem 48 (Itô's Formula for Jump-Diffusion Processes)**.** *Let X be a jump diffusion process composed of an Itô process and a compound Poisson process*

$$X_{\bar{t}} = X_0 + \int_0^{\bar{t}}\mu_t\mathrm{d}t + \int_0^{\bar{t}}\sigma_t\mathrm{d}W_t + \sum_{t\in[0,\bar{t}]}^{\Delta X_t\neq 0}\Delta X_t, \quad \bar{t}\in[0,T], \tag{A.14}$$

where $\Delta X_t = X_t - X_{t-}$ represents the jump size, and $(\mu_t)_t$ and $(\sigma_t)_t$ are adapted processes. Further assume that $(\sigma_t)_t$ satisfies the square-integrability condition, i.e. $\mathbb{E}\int_0^T\sigma_t\mathrm{d}t<\infty$. Then, for any $\mathcal{C}^{1,2}$ function $f:[0,T]\times\mathbb{R}\to\mathbb{R}$, it holds

$$\begin{aligned} f(\bar{t},X_{\bar{t}}) = f(0,X_0) &+ \int_0^{\bar{t}}\left(\frac{\partial f}{\partial t}(t,X_t)+\frac{\partial f}{\partial x}(t,X_t)\mu_t+\frac{1}{2}\frac{\partial^2 f}{\partial x^2}(t,X_t)\sigma_t^2\right)\mathrm{d}t \\ &+ \int_0^T\frac{\partial f}{\partial x}(t,X_t)\sigma_t\mathrm{d}W_t + \sum_{t\in[0,\bar{t}]}^{\Delta X_t\neq 0}\Big(f(t,X_{t-}+\Delta X_t)-f(t,X_{t-})\Big). \end{aligned} \tag{A.15}$$

Proof. See Øksendal (2003). □

Appendix B

Option Pricing via Fourier Transform

Fourier transform techniques provide an elegant approach to pricing options. For sophisticated stock price dynamics, the conditional risk-neutral densities applied in (3.3) and (3.4) are typically intricate, often defying analytical formulation. In such cases, it is usually easier to operate in the Fourier space using characteristic functions. The characteristic function of a random variable is the Fourier transform of its density, provided it exists. Leveraging Lévy's inversion theorem (Lévy (1925)) allows non-tractable densities to be expressed in terms of characteristic functions. Therefore, if the characteristic function is known and of analytical nature, option prices can be readily computed through integral evaluation in a Black-Scholes style pricing formula.[82] Prior to deriving this pricing formula, the required definitions and theorems will be introduced first.

B.1 Characteristic Functions and Fourier Inversion Theorem

As its name suggests, the characteristic function of a random variable uniquely characterizes its distribution. This means that, in addition to facilitating the derivation of distribution moments – akin to moment-generating functions – it also allows the expression of both the CDF and the PDF. The characteristic function of a random variable is defined as follows:

[82] Characteristic functions are typically derived from the dynamics of the underlying stochastic process. For further details, see, for example, Cont (2004).

Definition 49 (Characteristic Function)**.** *Let* $(\Omega, \mathcal{F}, \mathbb{P})$ *be a probability space and* X *be a real-valued random variable. Then, the complex-valued function* $\varphi_X : \mathbb{R} \to \mathbb{C}$ *defined as*

$$\varphi_X(u) = \mathbb{E}\left(e^{\mathrm{i}uX}\right) \tag{B.1}$$

is called the characteristic function of X*. If* X *has a density* f_X*, then* (B.1) *simplifies to*

$$\varphi_X(u) = \int_{-\infty}^{\infty} e^{\mathrm{i}ux} f_X(x)\mathrm{d}x, \tag{B.2}$$

where φ_X *is the Fourier transform of* f_X*.*

Therefore, in contrast to the PDF, the characteristic function of a random variable always exists. An exceedingly valuable theorem within the domain of characteristic functions is the inversion formula, which enables the expression of the CDF and the PDF of a random variable in terms of its characteristic function:

Theorem 50 (Inversion Formula)**.** *Let* $(\Omega, \mathcal{F}, \mathbb{P})$ *be a probability space and* X *is a real-valued random variable. If* φ_X *is the characteristic function of* X*, then the distribution function* F_X *is given by*

$$F_X(x) = \frac{1}{2} - \frac{1}{2\pi}\int_{-\infty}^{\infty} \frac{e^{-\mathrm{i}ux}\varphi_X(u)}{\mathrm{i}u}\mathrm{d}u. \tag{B.3}$$

The corresponding density function f_X*, if it exists, is obtained by*

$$f_X(x) = \frac{1}{2\pi}\int_{-\infty}^{\infty} e^{-\mathrm{i}ux}\varphi_X(u)\mathrm{d}u. \tag{B.4}$$

Partial Proof. Here we only give the proof for the simpler case where the density exists, following Carr (2003). Let $\delta(.)$ denote the Dirac's delta function. Then, f_X can be expressed as follows

$$f_X(x) = \int_{-\infty}^{\infty} f_X(y)\,\delta(y-x)\,\mathrm{d}y. \tag{B.5}$$

The Fourier integral representation of Dirac's delta function is given by

$$\delta(y-x) = \frac{1}{2\pi}\int_{-\infty}^{\infty} e^{\mathrm{i}u(y-x)}\mathrm{d}u. \tag{B.6}$$

Substituting (B.6) in (B.5) yields

$$\begin{aligned} f_X(x) &= \int_{-\infty}^{\infty} f_X(y)\cdot\frac{1}{2\pi}\int_{-\infty}^{\infty} e^{\mathrm{i}u(y-x)}\mathrm{d}u\,\mathrm{d}y \\ &= \frac{1}{2\pi}\int_{-\infty}^{\infty} e^{-\mathrm{i}ux}\int_{-\infty}^{\infty} e^{\mathrm{i}uy} f_X(y)\mathrm{d}y\,\mathrm{d}u. \end{aligned} \tag{B.7}$$

Recall Equation (B.2) of Definition 49. Then, f_X can be rewritten as

$$f_X(x) = \frac{1}{2\pi}\int_{-\infty}^{\infty} e^{-\mathrm{i}ux}\varphi_X(u)\mathrm{d}u. \tag{B.8}$$

Since F_X is the antiderivative of f_X and F_X is a cumulative distribution function, the additive constant $\frac{1}{2}$ in (B.3) follows directly. □

In the context of option pricing, one typically encounters an alternative formulation of the inversion formula, which exploits the symmetry observed in the real and imaginary components of the characteristic function. This modified formulation, derived from the original theorem of Lévy (1925), is provided by Gil-Pelaez (1951):

Theorem 51 (Gil-Pelaez (1951) Inversion Formula)**.** *Let $(\Omega, \mathcal{F}, \mathbb{P})$ be a probability space and X a real-valued random variable. If φ_X is the characteristic function of X and x is a continuity point of F_X, then*

$$F_X(x) = \frac{1}{2} - \frac{1}{\pi}\int_{-\infty}^{\infty} \Re\left(\frac{e^{-\mathrm{i}ux}\varphi_X(u)}{iu}\right)\mathrm{d}u. \tag{B.9}$$

The corresponding density function f_X, if it exists, is given by

$$f_X(x) = \frac{1}{\pi}\int_{0}^{\infty} \Re\left(e^{-\mathrm{i}ux}\varphi_X(u)\right)\mathrm{d}u. \tag{B.10}$$

Partial Proof. Again, we only proof the case where the density exists. For the full proof, we

refer to Gil-Pelaez (1951). First, note that for φ_X the following property holds

$$\varphi_X(-u) = \mathbb{E}\left(e^{-\mathrm{i}uX}\right) = \mathbb{E}\left(\cos(-uX) + \mathrm{i}\cdot\sin(-uX)\right) = \mathbb{E}\left(\cos(uX) - \mathrm{i}\cdot\sin(uX)\right) = \overline{\varphi_X(u)}\,, \tag{B.11}$$

where $\overline{\varphi_X(u)}$ denotes the complex conjugate of $\varphi_X(u)$. Thus, $\varphi(u)$ is even in its real part and odd in its imaginary part. Since f_X is real-valued, (B.4) can be written as

$$\begin{aligned}
f_X(x) &= \frac{1}{2\pi}\Re\left(\int_{-\infty}^{\infty} e^{-\mathrm{i}ux}\varphi_X(u)\mathrm{d}u\right) \\
&= \frac{1}{2\pi}\Re\left(\int_{-\infty}^{0} e^{-\mathrm{i}ux}\varphi_X(u)\mathrm{d}u\right) + \frac{1}{2\pi}\Re\left(\int_{0}^{\infty} e^{-\mathrm{i}ux}\varphi_X(u)\mathrm{d}u\right) \\
&= \frac{1}{2\pi}\Re\left(\int_{0}^{\infty} \overline{e^{-\mathrm{i}ux}\varphi_X(u)}\mathrm{d}u\right) + \frac{1}{2\pi}\Re\left(\int_{0}^{\infty} e^{-\mathrm{i}ux}\varphi_X(u)\mathrm{d}u\right) \\
&= \frac{1}{2\pi}\Re\left(\int_{0}^{\infty} e^{\mathrm{i}ux}\varphi_X(-u)\mathrm{d}u\right) + \frac{1}{2\pi}\Re\left(\int_{0}^{\infty} e^{-\mathrm{i}ux}\varphi_X(u)\mathrm{d}u\right) \\
&= \frac{1}{2\pi}\Re\left(\int_{0}^{\infty} e^{-\mathrm{i}ux}\varphi_X(u)\mathrm{d}u\right) + \frac{1}{2\pi}\Re\left(\int_{0}^{\infty} e^{-\mathrm{i}ux}\varphi_X(u)\mathrm{d}u\right) \\
&= \frac{1}{\pi}\int_{0}^{\infty} \Re\left(e^{-\mathrm{i}ux}\varphi_X(u)\right)\mathrm{d}u,
\end{aligned} \tag{B.12}$$

where the symmetry property is used in the penultimate step. Similarly, as F_X is real-valued, (B.3) can be written as

$$\begin{aligned}
F_X(x) &= \frac{1}{2} - \frac{1}{2\pi}\Re\left(\int_{-\infty}^{\infty} \frac{e^{-\mathrm{i}ux}\varphi_X(u)}{\mathrm{i}u}\mathrm{d}u\right) \\
&= \frac{1}{2} - \frac{1}{2\pi}\Re\left(\int_{-\infty}^{0} \frac{e^{-\mathrm{i}ux}\varphi_X(u)}{\mathrm{i}u}\mathrm{d}u\right) - \frac{1}{2\pi}\Re\left(\int_{0}^{\infty} \frac{e^{-\mathrm{i}ux}\varphi_X(u)}{\mathrm{i}u}\mathrm{d}u\right) \\
&= \frac{1}{2} - \frac{1}{2\pi}\Re\left(\int_{0}^{\infty} \overline{\left(\frac{e^{-\mathrm{i}ux}\varphi_X(u)}{\mathrm{i}u}\right)}\mathrm{d}u\right) - \frac{1}{2\pi}\Re\left(\int_{0}^{\infty} \frac{e^{-\mathrm{i}ux}\varphi_X(u)}{\mathrm{i}u}\mathrm{d}u\right) \\
&= \frac{1}{2} - \frac{1}{2\pi}\Re\left(\int_{0}^{\infty} \frac{e^{\mathrm{i}ux}\varphi_X(-u)}{-\mathrm{i}u}\mathrm{d}u\right) - \frac{1}{2\pi}\Re\left(\int_{0}^{\infty} \frac{e^{-\mathrm{i}ux}\varphi_X(u)}{\mathrm{i}u}\mathrm{d}u\right) \\
&= \frac{1}{2} - \frac{1}{2\pi}\Re\left(\int_{0}^{\infty} \frac{e^{-\mathrm{i}ux}\varphi_X(u)}{\mathrm{i}u}\mathrm{d}u\right) - \frac{1}{2\pi}\Re\left(\int_{0}^{\infty} \frac{e^{-\mathrm{i}ux}\varphi_X(u)}{\mathrm{i}u}\mathrm{d}u\right) \\
&= \frac{1}{2} - \frac{1}{\pi}\int_{0}^{\infty} \Re\left(\frac{e^{-\mathrm{i}ux}\varphi_X(u)}{\mathrm{i}u}\right)\mathrm{d}u,
\end{aligned} \tag{B.13}$$

where the symmetry property is used again in the penultimate step. □

B.2 Black-Scholes Style Pricing Formula

Initially proposed by Heston (1993), Bakshi and Madan (2000) present a generalized option pricing formula that is reminiscent in style of Black and Scholes (1973) . Leveraging the outcomes of the preceding section, we now derive this formula along the lines of Schmelzle (2010):[83]

Define X as the log-return, i.e. $X \equiv \ln\left(\frac{S_T}{S_0}\right)$. Then, $S_T = S_0 e^X$ such that (3.3) can be rewritten as

$$\begin{aligned} C(0,T;K) &= e^{-rT}\mathbb{E}^{\mathbb{Q}}\left(\left(S_0 e^X - K\right)^+\right) \\ &= e^{-rT}\int_{-\infty}^{\infty}(S_0 e^x - K)\,\mathbb{1}_{\{S_0 e^x > K\}}\,q(x)\mathrm{d}x \\ &= e^{-rT}\int_{\ln(K/S_0)}^{\infty}(S_0 e^x - K)q(x)\mathrm{d}x \\ &= S_0\int_{\ln(K/S_0)}^{\infty} e^{-rT}e^x q(x)\mathrm{d}x - e^{-rT}K\int_{\ln(K/S_0)}^{\infty} q(x)\mathrm{d}x \\ &= S_0\Pi_1 - e^{-rT}K\Pi_2, \end{aligned} \tag{B.14}$$

where now $q(.)$ denotes the risk-neutral density of the log-return rather than that of S_T. Π_1 and Π_2 are the conditional probabilities that the option expires ITM. Due to simplicity, we start with the computation of Π_2:

$$\begin{aligned} \Pi_2 &\equiv \int_{\ln(K/S_0)}^{\infty} q(x)\mathrm{d}x \\ &= 1 - \int_{-\infty}^{\ln(K/S_0)} q(x)\mathrm{d}x \\ &= 1 - Q_X(\ln(K/S_0)) \\ &= 1 - \left(\frac{1}{2} - \frac{1}{\pi}\int_{-\infty}^{\infty}\Re\left(\frac{e^{-\mathrm{i}u\ln(K/S_0)}\varphi_X(u)}{\mathrm{i}u}\right)\mathrm{d}u\right) \\ &= \frac{1}{2} + \frac{1}{\pi}\int_{-\infty}^{\infty}\Re\left(\frac{e^{-\mathrm{i}u\ln(K/S_0)}\varphi_X(u)}{\mathrm{i}u}\right)\mathrm{d}u, \end{aligned} \tag{B.15}$$

[83] Schmelzle (2010) present the derivation utilizing the characteristic function of the logarithmic stock price instead of the log-return. For completeness, we adopt the log-return approach to provide the reader with a choice between both methodologies.

where we used the inversion formula (B.9) in the penultimate step. For evaluating Π_1, things are slightly more subtle. First, we perform a change of measure along the lines of Geman et al. (1995)

$$\frac{\mathrm{d}\widetilde{\mathbb{Q}}}{\mathrm{d}\mathbb{Q}} = \frac{e^X}{\mathbb{E}^{\mathbb{Q}}\left(e^X\right)}, \tag{B.16}$$

where $\mathbb{E}^{\mathbb{Q}}\left(e^X\right) = \mathbb{E}^{\mathbb{Q}}\left(S_T/S_0\right) = e^{rT}$ such that the new density $\widetilde{q}(x)$ is given by

$$\widetilde{q}(x) = e^{x-rT} q(x). \tag{B.17}$$

Therefore, the characteristic function of X under the new measure $\widetilde{\mathbb{Q}}$ can be expressed as

$$\widetilde{\varphi}_X(u) = \int_{-\infty}^{\infty} e^{\mathrm{i}ux}\widetilde{q}(x)\mathrm{d}x = e^{-rT}\int_{-\infty}^{\infty} e^{\mathrm{i}ux}e^x q(x)\mathrm{d}x = \frac{\mathbb{E}^{\mathbb{Q}}\left(e^{\mathrm{i}uX+X}\right)}{\mathbb{E}^{\mathbb{Q}}\left(e^X\right)} = \frac{\varphi_X(u-\mathrm{i})}{\varphi_X(-\mathrm{i})}. \tag{B.18}$$

Considering (B.9), (B.17), and (B.18), Π_1 can be transformed to

$$\begin{aligned}
\Pi_1 &\equiv \int_{\ln(K/S_0)}^{\infty} e^{-rT}e^x q(x)\mathrm{d}x \\
&= \int_{\ln(K/S_0)}^{\infty} e^{-rT}e^x e^{-(x-rT)}\widetilde{q}(x)\mathrm{d}x \\
&= \int_{\ln(K/S_0)}^{\infty} \widetilde{q}(x)\mathrm{d}x \\
&= 1 - \int_{-\infty}^{\ln(K/S_0)} \widetilde{q}(x)\mathrm{d}x \\
&= 1 - \widetilde{Q}_X(\ln(K/S_0)) \\
&= 1 - \left(\frac{1}{2} - \frac{1}{\pi}\int_{-\infty}^{\infty} \Re\left(\frac{e^{-\mathrm{i}u\ln(K/S_0)}\widetilde{\varphi}_X(u)}{\mathrm{i}u}\right)\mathrm{d}u\right) \\
&= \frac{1}{2} + \frac{1}{\pi}\int_{-\infty}^{\infty} \Re\left(\frac{e^{-\mathrm{i}u\ln(K/S_0)}\varphi_X(u-\mathrm{i})}{\mathrm{i}u\,\varphi_X(-\mathrm{i})}\right)\mathrm{d}u,
\end{aligned} \tag{B.19}$$

which completes the derivation of (B.14). Applying put-call parity, as detailed in Theorem 38, yields the equivalent put option pricing formula

$$P(0,T;K) = e^{-rT}K(1-\Pi_2) - S_0(1-\Pi_1). \tag{B.20}$$

It is essential to note that in this derivation, X denotes the log-return, as it does in Aschakulporn and Zhang (2022b). Some authors, such as Heston (1993) or Branger (2004), price options via Fourier transform by the characteristic function of the logarithmic stock price.[84] In such cases, small modifications of Π_1 and Π_2 are required.

[84]Branger (2004) employed the Fourier transform of the state-price density associated with the logarithmic stock price as the characteristic function, leading to slightly different formulas for Π_1 and Π_2.

Bibliography

Albert, P., Herold, M., Muck, M., 2023. Estimation of rare disaster concerns from option prices — An arbitrage-free RND-based smile construction approach. Journal of Futures Markets 43, 1807–1835.

Alexiou, L., Goyal, A., Kostakis, A., Rompolis, L., 2023. Pricing Event Risk: Evidence from Concave Implied Volatility Curves. Unpublished Working Paper .

Ammann, M., Feser, A., 2019. Robust estimation of risk–neutral moments. Journal of Futures Markets 39, 1137–1166.

Aschakulporn, P., Zhang, J. E., 2022a. Bakshi, Kapadia, and Madan (2003) risk-neutral moment estimators: A Gram–Charlier density approach. Review of Derivatives Research 25, 233–281.

Aschakulporn, P., Zhang, J. E., 2022b. Bakshi, Kapadia, and Madan (2003) risk-neutral moment estimators: An affine jump-diffusion approach. Journal of Futures Markets 42, 365–388.

Bahra, B., 1997. Implied risk-neutral probability density functions from option prices: Theory and application. Unpublished Working Paper.

Bakshi, G., Cao, C., Chen, Z., 1997. Empirical Performance of Alternative Option Pricing Models. The Journal of Finance 52, 2003–2049.

Bakshi, G., Kapadia, N., Madan, D., 2003. Stock return characteristics, skew laws, and the differential pricing of individual equity options. Review of Financial Studies 16, 101–143.

Bakshi, G., Madan, D., 2000. Spanning and derivative-security valuation. Journal of Financial Economics 55, 205–238.

Bates, D. S., 1996. Jumps and stochastic volatility: Exchange rate processes implicit in Deutsche Mark options. Review of Financial Studies 9, 69–107.

Bates, D. S., 2000. Post-'87 crash fears in the S&P 500 futures option market. Journal of Econometrics 94, 181–238.

Bingham, N. H., Kiesel, R., 2004. Risk-Neutral Valuation. Springer Finance, Springer, second ed.

Birru, J., Figlewski, S., 2012. Anatomy of a meltdown: The risk neutral density for the S&P 500 in the fall of 2008. Journal of Financial Markets 15, 151–180.

Björk, T., 2009. Arbitrage Theory in Continuous Time. Oxford university press.

Black, F., Scholes, M., 1973. The pricing of options and corporate liabilities. The Journal of Political Economy 81, 637–654.

Bliss, R. R., Panigirtzoglou, N., 2002. Testing the stability of implied probability density functions. Journal of Banking & Finance 26, 381–422.

Bliss, R. R., Panigirtzoglou, N., 2004. Option-Implied Risk Aversion Estimates. The Journal of Finance 59, 407–446.

Bollerslev, T., Gibson, M., Zhou, H., 2011. Dynamic estimation of volatility risk premia and investor risk aversion from option-implied and realized volatilities. Journal of Econometrics 160, 235–245.

Branger, N., 2004. An Anatomy of Option Pricing Models. Unpublished Working Paper .

Breeden, D. T., Litzenberger, R. H., 1978. Prices of state-contingent claims implicit in option prices. The Journal of Business 51, 621–651.

Britten-Jones, M., Neuberger, A., 2000. Option prices, implied price processes, and stochastic volatility. The Journal of Finance 55, 839–866.

Brunner, B., Hafner, R., 2003. Arbitrage-free estimation of the risk-neutral density from the implied volatility smile. The Journal of Computational Finance 7, 75–106.

Campa, J. M., Chang, P. H. K., Reider, R. L., 1998. Implied exchange rate distributions: Evidence from OTC option markets. Journal of International Money and Finance 17, 117–160.

Campbell, J. Y., Lo, A. W., MacKinlay, A., 1997. The Econometrics of Financial Markets. Princeton University Press.

Carr, P., 2003. Option pricing using integral transforms. Presentation. http://www. math. nyu. edu/research/carrp/papers/pdf/integtransform. pdf .

Carr, P., Madan, D., 1998. Towards a theory of volatility trading. In: Jarrow, R. A. (ed.), *Volatility*, Risk Books, London 417–427.

Carr, P., Madan, D., 2001. Optimal positioning in derivative securities. Quantitative Finance 1, 19–37.

Carr, P., Wu, L., 2006. A Tale of Two Indices. The Journal of Derivatives 13, 13–29.

Carr, P., Wu, L., 2009. Variance risk premiums. Review of Financial Studies 22, 1311–1341.

CBOE, 2019. Cboe Volatillity Index - White Paper .

Cont, R., 2001. Empirical properties of asset returns: stylized facts and statistical issues. Quantitative finance 1, 223.

Cont, R., 2004. Financial Modelling with Jump Processes. Chapman & Hall/CRC Financial Mathematics Series, Chapman & Hall/CRC.

Cox, J. C., Ingersoll, J. E., Ross, S. A., 1985. A theory of the term structure of interest rates. Econometrica 53, 385–407.

Cox, J. C., Ross, S. A., Rubinstein, M., 1979. Option pricing: A simplified approach. Journal of Financial Economics 7, 229–263.

De Haan, L., Ferreira, A., 2006. Extreme Value Theory. Springer Series in Operations Research and Financial Engineering, Springer.

Delbaen, F., Schachermayer, W., 1994. A general version of the fundamental theorem of asset pricing. Mathematische Annalen 300, 463–520.

Demeterfi, K., Derman, E., Kamal, M., Zou, J., 1999a. A guide to volatility and variance swaps. The Journal of Derivatives 6, 9.

Demeterfi, K., Derman, E., Kamal, M., Zou, J., 1999b. More than you ever wanted to know about volatility swaps. Goldman Sachs quantitative strategies research notes 41, 1–56.

Dole, D., 1999. CoSmo: A constrained scatterplot smoother for estimating convex, monotonic transformations. Journal of Business & Economic Statistics 17, 444–455.

Duffie, D., Pan, J., Singleton, K., 2000. Transform analysis and asset pricing for affine jump-diffusions. Econometrica 68, 1343–1376.

Fengler, M. R., 2009. Arbitrage-free smoothing of the implied volatility surface. Quantitative Finance 9, 417–428.

Figlewski, S., 2010. Estimating the implied risk neutral density for the US market portfolio. In: Bollerslev, T., Russell, J., Watson, M. (eds.), *Volatility and Time Series Econometrics: Essays in Honor of Robert Engle*, Oxford University Press, Advanced Texts in Econometrics 323–353.

Figlewski, S., 2018. Risk-neutral densities: A review. Annual Review of Financial Economics 10, 329–359.

Frey, R., 2017. Lecture notes continuous-time finance. Vienna University of Economics and Business .

Gao, G. P., Gao, P., Song, Z., 2018. Do hedge funds exploit rare disaster concerns? Review of Financial Studies 31, 2650–2692.

Gao, G. P., Lu, X., Song, Z., 2019. Tail risk concerns everywhere. Management Science 65, 3111–3130.

Geman, H., Karoui, N. E., Rochet, J.-C., 1995. Changes of numéraire, changes of probability measure and option pricing. Journal of Applied Probability 32, 443–458.

Gil-Pelaez, J., 1951. Note on the inversion theorem. Biometrika 38, 481–482.

Green, P. J., Silverman, B. W., 1994. Nonparametric regression and generalized linear models: A roughness penalty approach, vol. 58 of *Monographs on statistics and applied probability*. Chapman & Hall, London, first ed.

Harrison, J., Pliska, S. R., 1981. Martingales and stochastic integrals in the theory of continuous trading. Stochastic Processes and their Applications 11, 215–260.

Heston, S. L., 1993. A closed-form solution for options with stochastic volatility with applications to bond and currency options. Review of Financial Studies 6, 327–343.

Jackwerth, J. C., 2004. Option-Implied Risk-Neutral Distributions and Risk Aversion. Research Foundation of AIMR.

Jacod, J., Shiryaev, A., 2013. Limit Theorems for Stochastic Processes. Springer Science & Business Media.

Jiang, G. J., Tian, Y. S., 2005. The model-free implied volatility and its information content. Review of Financial Studies 18, 1305–1342.

Jiang, G. J., Tian, Y. S., 2007. Extracting model-free volatility from option prices. The Journal of Derivatives 14, 35–60.

Kapadia, N., Du, J., 2012. The tail in the volatility index. Unpublished Working Paper.

Karatzas, I., Shreve, S. E., 1998. Brownian Motion and Stochastic Calculus, vol. 113 of *Graduate Texts in Mathematics*. Springer.

Kostakis, A., Mu, L., Otsubo, Y., 2023. Detecting political event risk in the option market. Journal of Banking & Finance 146, 106624.

Lévy, P., 1925. Calcul des Probabilités. Gauthier-Villars, Paris.

Lewis, A., 2002. Fear of jumps. Wilmott magazine 1, 60.

Malz, A. M., 1997. Estimating the Probability Distribution of the Future Exchange Rate from Option Prices. The Journal of Derivatives 5, 18–36.

McNeil, A. J.-G., Frey, R.-G., Embrechts, P.-G.-n., 2015. Quantitative Risk Management: Concepts, Techniques and Tools. Princeton Series in Finance, Princeton University Press, revised ed.

Merton, R. C., 1976. Option pricing when underlying stock returns are discontinuous. Journal of Financial Economics 3, 125–144.

Muck, M., 2022. Arbitrage-free smile construction on FX option markets using Garman-Kohlhagen deltas and implied volatilities. Review of Derivatives Research 25, 293–314.

Øksendal, B., 2003. Stochastic Differential Equations. Universitext, Springer, sixth ed.

Pagan, A., 1996. The econometrics of financial markets. Journal of Empirical Finance 3, 15–102.

Pollock, D., 1999. Smoothing with Cubic Splines. In: Nguyen, T., Pollock, D., Green, R. C. (eds.), *Handbook of Time Series Analysis, Signal Processing, and Dynamics*, Elsevier professional, Signal Processing and Its Applications 293–322, first ed.

Privault, N., 2013. Stochastic Finance: An Introduction with Market Examples. Chapman & Hall/CRC Financial Mathematics Series, Chapman & Hall/CRC.

Rosenberg, J., 2000. Implied volatility functions. The Journal of Derivatives 7, 51–64.

Schmelzle, M., 2010. Option pricing formulae using fourier transform: Theory and application. Preprint, http://pfadintegral. com .

Shimko, D., 1993. Bounds of probability. Risk 6, 33–37.

Shreve, S., 2004. Stochastic Calculus for Finance II: Continuous-Time Models. Springer, first ed.

Ulrich, M., Walther, S., 2020. Option-implied information: What's the vol surface got to do with it? Review of Derivatives Research 23, 323–355.

Whaley, R. E., 2000. The investor fear gauge. Journal of portfolio management 26, 12.

Zhirong, C., Fong, W.-M., 2012. Was the Writing on the Wall? An Options Analysis of the 2008 Lehman Brothers Crisis. Journal of Investment Management 10, 91–102.